PLANT ARCHITECTURE AND THE ALLOMETRY OF HYDRAULIC TRANSPORT, LIGHT INTERCEPTION AND GROWTH

by

Duncan D. Smith

A dissertation submitted to the faculty of
The University of Utah
in partial fulfillment of the requirements for the degree of

Doctor of Philosophy

Department of Biology

The University of Utah

August 2015

The University of Utah Graduate School

STATEMENT OF DISSERTATION APPROVAL

The dissertation of **Duncan D. Smith**

has been approved by the following supervisory committee members:

John S. Sperry	, Chair	**April 30, 2015** Date Approved
Frederick R. Adler	, Member	**April 30, 2015** Date Approved
David R. Bowling	, Member	**April 30, 2015** Date Approved
Brian J. Enquist	, Member	Date Approved
Thomas A. Kursar	, Member	**April 30, 2015** Date Approved

and by **M. Denise Dearing**, Chair/Dean of

the Department/College/School of **Biology**

and by David B. Kieda, Dean of The Graduate School.

ABSTRACT

The metabolic scaling theory identifies network architecture as a major predictor of whole plant metabolism via hydraulic conductance of the xylem and the shared stomatal pathway for water loss and carbon gain. To predict hydraulic properties, this theory utilizes the West, Brown, Enquist (WBE) architectural model, which is based on principles of space-filling, biomechanical stability, and optimality of hydraulic transport and it is meant to be generally representative of plants. However, plants are highly diverse in their network architecture. Does this diversity matter or does it represent different ways of accomplishing the same task? This dissertation addresses that question by extending WBE to include architectural variation and by testing model predictions and assumptions.

The model predicts the scaling exponent between hydraulic conductance and plant size. This exponent depends on the "bottleneck" effect, where greater hydraulic resistance in leaves and twigs steepens the exponent. The bottleneck effect was greater when xylem conduits were much larger or more abundant in the trunk than in the twigs. Observed diversity in xylem properties predicted that different functional groups had substantial overlap in hydraulic transport and its scaling. Branching architecture did not influence the bottleneck effect. However, deviating from WBE increased hydraulic conductance and biomechanical stability while requiring less tissue but reducing light interception. Branching could alter hydraulic scaling if architecture changed ontogenetically, which data suggested.

MST assumes direct proportionality between sapflow and growth. This was supported in five of six tested species. However, tree species grew more per water use than shrubs, likely reflecting differential allocation. Differences between species were partially attributable to xylem anatomy and plant size.

Among this variation in xylem anatomy, branching architecture, and plant stature, the dimensions of leaves and twigs also vary with thicker twigs curiously tending to support few large leaves instead of many small leaves (Corner's rule). Why do plants coordinate leaf and twig size? Corner's rule was recast as the prediction that larger twig leaf areas are composed of larger leaves. Species supported this prediction and had highly convergent

scaling. A model predicted that Corner's rule exists to optimize the return on investment in leaves.

CONTENTS

LIST OF FIGURES

LIST OF TABLES

ACKNOWLEDGMENTS

Above all others, I would like to thank Dr. John Sperry who introduced me to research as an undergraduate and was the first person to encourage me to pursue a PhD. Throughout my graduate career, he was my biggest supporter and provided invaluable assistance and advice that made the contents herein possible.

I would also like to thank my committee, Fred Adler, Dave Bowling, Brian Enquist and Tom Kursar, for their insight and for keeping my view broad and asking tough questions when needed.

A portion of this dissertation was a product of or was inspired by collaboration with Brian Enquist, Lisa Bentley, Van Savage and Peter Reich. I am thankful to them for including me in their meetings and research.

Thank you to the Biology Department for funding much of my time as a student through teaching assistantships and to NSF for funding the remainder.

Thank you to Shannon Nielsen for help with all administrative details.

CHAPTER 1

INTRODUCTION

Land plants are modular and indeterminate organisms. Variation in modules and how they are arranged has led to great architectural diversity (Hallé et al. 1978) as lineages adapted to fill different niches. Yet among this diversity, plant networks function to address similar requirements: they physically support the arrangement of photosynthetic and reproductive tissues in space and they provide transport between spatially separated resources. Water and nutrients must move from the soil to sites of photosynthesis where light and CO_2 are available and the carbon and energy captured in the form of photosynthate must move from these sites to growing and respiring tissues. The transport of water is especially important because water is often lost to the atmosphere when plants open their stomata to take in CO_2. If this water is not replaced, stomata will shut to avoid water stress but consequently reduce carbon uptake. Thus, there is a direct link between water transport and carbon fixation (Hubbard et al. 2001). Water transport is a physical process dependent on the architecture network. To a large extent, the dimensions and numbers of functional xylem conduits determine a plant's hydraulic conductance. Hydraulic conductance and the pressure difference between soil and leaf determine the rate of sapflow. Therefore, plant architecture, through its effect on water transport, is a major determinant of carbon gain.

The importance of hydraulic architecture and its link to carbon has long been recognized (Yang & Tyree 1993), though increased attention followed introduction of the model by West, Brown & Enquist (WBE; Enquist et al. 1998; West et al. 1999) as part of metabolic scaling theory. The WBE model simplifies and generalizes plant architecture as symmetrically branching networks of tapering stems plumbed with tapering xylem conduits (further details in Chapter 2). This model predicts hydraulic conductance and how it scales with network size and then assumes how hydraulic conductance scales with sapflow and growth. The scaling of hydraulic conductance is particularly important because plant growth leads to longer path lengths, which can reduce the hydraulic conductance supplying each leaf. The scaling exponent indicates how effective plants are at overcoming the consequence of longer

path lengths. The model predicts the maximum exponent (full compensation for longer paths), which agrees with observations across species (Niklas & Enquist 2001). However, while the model may predict the general trend across species, it does not address individual variation within and between species. Are there consequences to the architectural diversity of plants or does this diversity represent different ways of achieving the same result? This dissertation seeks to determine the impact of architectural variation on plant function, including: hydraulic transport and its scaling with plant size and growth; biomechanics and safety from buckling; and light interception at the whole plant and individual twig levels. These questions are addressed through a combination of empirical measurements and modelling, including extensions to the WBE model.

1.1 The chapters

Chapter 2 extends a version of the WBE model recently updated by Savage et al. (2010) to more explicitly define the hydraulic network by including leaves, roots and non-conducting tissues: pith; heartwood and bark. This extended version is used to ask how variation in hydraulic architecture may affect whole plant physiology and, in effect, how broadly species may differ. The model is assessed using: (1) the sapflow (Q) by trunk diameter (D_{B0}) scaling exponent, q (i.e. $Q \propto D_{B0}^{q}$) and (2) the sapflow rate at a reference trunk diameter, Q_{ref}. It is emphasized that the value of q depends largely on the "bottleneck effect". That is, q is maximized when the greatest hydraulic impediment is at the end of the transport path (i.e., in the twigs or leaves). A sensitivity analysis was conducted to see how model parameters affect q and Q_{ref}. Then, "species" in different functional groups were created by combining model parameters from the literature to predict the "scaling space" of q and Q_{ref} for each functional group. Considerable scaling space overlap existed between groups with contrasting anatomy such as conifers and diffuse-porous tropical angiosperms. Results from the scaling space were used to show that intraspecific q may differ from interspecific q if larger-statured species (e.g., trees) are systematically different from smaller-statured species (e.g, shrubs) This prediction was revisited with Chapter 4. Chapter 2 represents a major stride from using the model as a general predictor of scaling exponents to a parameterizable model to predict Q and q in actual plants. This chapter was published in *Functional Ecology* (Sperry, Smith, Savage, Enquist, McCulloh, Reich, Bentley & von Allmen 2012).

Chapter 3 extends the model further by relaxing the external branching architecture. Empirical measurements and evidence of apical control via hormones (Cline 1997) suggest

that symmetric branching used in the WBE model is not representative of most plants. Therefore, the model was used to ask how branching architecture affects hydraulic conductance, stem biomass, mechanical stability and light interception. Notably, these last two had not been previously assessed in the WBE framework although both were invoked as principles of architecture. Perfect symmetry will make all trunk-to-twig path lengths the same. Whereas empirical measurements and initial modeling showed that any deviation from symmetry led to a nonuniform distribution of path lengths. This observation prompted the "path fraction" to quantify branching architecture. The model was extended to be compatible with WBE architecture and followed the same principles of area-preserving branching and elastic similarity (McMahon & Kronauer 1976). Measurements and estimations of branching architecture suggested ontogenetic trends in the path fraction, which had implications for q. This chapter was published in *New Phytologist* (Smith, Sperry, Enquist, Savage, McCulloh & Bentley 2014).

Chapter 4 addresses two main hypotheses: 1) growth and water transport are isometrically related (as assumed in metabolic scaling theory) and 2) larger statured species have steeper hydraulic and metabolic scaling (as proposed in Chapter 2). The argument for the first hypothesis can be made by assuming that within species, water use efficiency is constant over time (making assimilation isometric with sapflow) and a constant fraction of assimilate is devoted to growth (making assimilation and growth isometric). However, species may differ in the how much sapflow increases with each increase in mass (i.e., the metabolic scaling exponent). By virtue of their small stature, shrub species were expected to have shallower metabolic scaling than co-occurring tree species. If both hypotheses are correct then the difference between shrubs and trees should be reflected in their xylem anatomy — shrubs having less conduit taper and/or a smaller fraction of trunk sapwood. Xylem properties from each species were used in the model presented in Chapter 3. Emphasis is placed on the importance of understanding intraspecific relationships before explaining interspecific relationships. This chapter appeared in *Plant, Cell and Environment* (Smith & Sperry 2014).

Chapter 5 addresses how leaves might be more accurately modeled. In Chapter 2, leaf hydraulic conductance was shown to have a strong influence on sapflow and how it scales. However, the link between leaf and twig hydraulic conductance was based on a limited data set. It has long been recognized that thicker twigs support larger leaves (Corner 1949), but the lack of a mechanistic explanation for this trend has prevented its incorporation into the model. Most data testing "Corner's rule" have been interspecific, which may confound the

underlying reason why thicker twigs have larger leaves. In this chapter, Corner's rule was revisited with an intraspecific data set, which led to a reformulation of the rule as: twigs with larger leaf areas also have larger individual leaves. Furthermore, species increased the number of leaves in a similar manner, which suggests a common response to some external variable. A model was developed to ask if Corner's rule results from optimal light gap filling to maximize the benefit of absorbing light minus the cost of leaves. This chapter is being prepared for submission to *Ecology Letters*.

1.2 References

Cline M.G. (1997) Concepts and terminology of apical dominance. *American Journal of Botany* 84, 1064–1069.

Corner E.J.H. (1949) The durian theory of the origin of the modern tree. *Annals of Botany* 13, 368–414.

Enquist B.J., Brown J.H. & West G.B. (1998) Allometric scaling of plant energetics and population density. *Nature* 395, 163–165.

Hallé F., Oldeman R.A.A. & Tomlinson P.B. (1978) *Tropical trees and forests: an architectural analysis*. Springer-Verlag, Berlin, Heidelberg, New York.

Hubbard R.M., Stiller V., Ryan M.G. & Sperry J.S. (2001) Stomatal conductance and photosynthesis vary linearly with plant hydraulic conductance in ponderosa pine. *Plant Cell and Environment* 24, 113–121.

McMahon T.A. & Kronauer R.E. (1976) Tree structures: deducing the principle of mechanical design. *Journal of Theoretical Biology* 59, 443–466.

Niklas K.J. & Enquist B.J. (2001) Invariant scaling relationships for interspecific plant biomass production rates and body size. *Proceedings of the National Academy of Sciences of the United States of America* 98, 2922–2927.

Savage V.M., Bentley L.P., Enquist B.J., Sperry J.S., Smith D.D., Reich P.B. & von Allmen E.I. (2010) Hydraulic trade-offs and space filling enable better predictions of vascular structure and function in plants. *Proceedings of the National Academy of Sciences of the United States of America* 107, 22722–22727.

Smith D.D. & Sperry J.S. (2014) Coordination between water transport capacity, biomass growth, metabolic scaling and species stature in co-occurring shrub and tree species. *Plant, Cell and Environment* 37, 2679–2690.

Smith D.D., Sperry J.S., Enquist B.J., Savage V.M., McCulloh K.A. & Bentley L.P. (2014) Deviation from symmetrically self-similar branching in trees predicts altered hydraulics, mechanics, light interception and metabolic scaling. *New Phytologist* 201, 217–229.

Sperry J.S., Smith D.D., Savage V.M., Enquist B.J., McCulloh K.A., Reich P.B., Bentley L.P. & von Allmen E.I. (2012) A species-level model for metabolic scaling in trees I. boundaries to scaling space within and across species. *Functional Ecology* 26, 1054–1065.

West G.B., Brown J.H. & Enquist B.J. (1999) A general model for the structure and allometry of plant vascular systems. *Nature* 400, 664–667.

Yang S. & Tyree M.T. (1993) Hydraulic resistance in *Acer saccharum* shoots and its influence on leaf water potential and transpiration. *Tree Physiology* 12, 231–242.

CHAPTER 2

A SPECIES-LEVEL MODEL FOR METABOLIC SCALING IN TREES I. EXPLORING BOUNDARIES TO SCALING SPACE WITHIN AND ACROSS SPECIES

2.1 Summary

1. Metabolic scaling theory predicts how tree water flow rate (Q) scales with tree mass (M) and assumes identical scaling for biomass growth rate (G) with M. Analytic models have derived general scaling expectations from proposed optima in the rate of axial xylem conduit taper (taper function) and the allocation of wood space to water conduction (packing function). Recent predictions suggest G and Q scale with M to the 0.7 power with 0.75 as an upper bound.

2. We complement this *a priori* optimization approach with a numerical model that incorporates species-specific taper and packing functions, plus additional empirical inputs essential for predicting Q (effects of gravity, tree size, heartwood, bark, and hydraulic resistance of leaf, root and interconduit pits). Traits are analysed individually, and in ensemble across tree types, to define a 2D "scaling space" of absolute Q vs. its scaling exponent with tree size.

3. All traits influenced Q and many affected its scaling with M. Constraints driving the optimization of taper or packing functions, or any other trait, can be relaxed via compensatory changes in other traits.

Reprinted with permission from John Wiley & Sons. Sperry J.S., Smith D.D., Savage V.M., Enquist B.J., McCulloh K.A., Reich P.B., Bentley L.P. & von Allmen E.I. (2012) A species-level model for metabolic scaling in trees I. Exploring boundaries to scaling space within and across species. *Functional Ecology* 26, 1054–1065.

4. The scaling space of temperate trees overlapped despite diverse anatomy and winter-adaptive strategies. More conducting space in conifer wood compensated for narrow tracheids; extensive sapwood in diffuse-porous trees compensated for narrow vessels; and limited sapwood in ring-porous trees negated the effect of large vessels. Tropical trees, however, achieved the greatest Q and steepest size-scaling by pairing large vessels with extensive sapwood, a combination compatible with minimal water stress and no freezing-stress.

5. Intraspecific scaling across all types averaged $Q \propto M^{0.63}$ (maximum = $Q \propto M^{0.71}$) for size-invariant root-shoot ratio. Scaling reached $Q \propto M^{0.75}$ only if conductance increased faster in roots than in shoots with size. Interspecific scaling could reach $Q \propto M^{0.75}$, but this may require the evolution of size-biased allometries rather than arising directly from biophysical constraints.

6. Our species-level model is more realistic than its analytical predecessors and provides a tool for interpreting the adaptive significance of functional trait diversification in relation to whole tree water use and consequent metabolic scaling.

2.2 Introduction

How does tree water use scale with tree size, and how does it differ across species? Given the essential role of water, this question is fundamental to understanding the metabolic scaling of individual trees, species, forest communities and ecosystems. Predicting the answer from vascular anatomy is the subject of this study. Modeling water use from vascular properties has a long history dating at least to da Vinci's rule of area-preserving branching (Richter 1970), continuing with the Ohm's law analogy of van den Honert (1948; Richter 1973) and culminating in the concept of "hydraulic architecture" (Zimmermann 1978) represented in contemporary models (e.g., Tyree 1988; Sperry et al. 2002; Macinnis-Ng et al. 2011). At the heart of these complex models is a simple relationship for whole-tree sap flow at steady state (Q):

$$Q = K(\Delta P - \rho g H) \tag{2.1}$$

where K is tree hydraulic conductance, ΔP is soil to canopy pressure drop, and $\rho g H$ is the pressure required to offset the force of gravity on the water column (ρ = density of water; g, acceleration of gravity; H, tree height). Canopy xylem pressure regulation (via stomatal control of Q) constrains the $(\Delta P - \rho g H)$ term, and most of the uncertainty in hydraulic

modeling lies in representing K, which depends mostly on the complex anatomy of the flow path from soil to leaf.

Until the revolutionary approach of West, Brown and Enquist (WBE; West et al. 1997, 1999; Enquist et al. 2000), most hydraulic modeling was based on specifying what K is from empirical inputs. In contrast, the WBE model derives what the allometric scaling of K should be by assuming a universal set of optimization criteria and an intentionally minimalist representation of plant vasculature. The WBE goal is to predict universal expectations for how K, and hence Q, and all dependent metabolic processes, should scale with plant size. The focus is on predicting the power function scaling exponent (b):

$$Y \propto M^b \tag{2.2}$$

where Y is the variable of interest (K, Q, rates of metabolism or growth) and M is plant mass.

The result is a metabolic scaling theory that emphasizes the unifying consequences of selection for optimal vascular transport under overarching constraints. Savage et al. (2010) have recently extended the theory with important improvements in how it represents vascular architecture.

In this study, we present a model that strikes a middle ground between the structure-to-function optimization approach of Savage et al. (and its WBE predecessors) and the descriptive-empirical approach of more complex numerical models. We add a minimal set of hydraulic inputs to the Savage et al. analytical model with the goal of predicting the actual value of K and Q rather than proportional proxies that are sufficient for predicting scaling exponents. Our species-level model turns the proportionality in Eqn. 2.2 ($Y \propto M^b$) into an equality ($Y = k_0 M^b$) by specifying scaling multipliers (k_0). The additional complexity requires a numerical approach, but is justified because selection for optimal vascular function should concern traits underlying the multiplier as well as the exponent. Furthermore, variation in scaling multipliers across species could influence interspecific exponents (b) independently of the intraspecific value of b. We relax any *a priori* optimization criteria and allow key hydraulic inputs to be empirical, so that we can predict the "scaling space" defined by variation in k_0 and b across species. Figure 2.1 provides a roadmap of the Savage et al. (2010) model. The branching architecture component (Fig. 2.1, left) specifies that the tree has symmetric, self-similar branching architecture that preserves the cross-sectional area of branches across each branching junction (da Vinci's rule; Horn 2000). Hence, the tree can be represented by a column (Fig. 2.1, center). The mass allometry module predicts

the best-fit power-law scaling between trunk diameter (D_{B0}; 0 denotes trunk branch rank; symbols in Table 2.1) and tree mass (M):

$$D_{B0} = k_1 M^c \tag{2.3}$$

where k_1 is the scaling multiplier and c the scaling exponent. The value of the exponent c is derived from well tested theory that H must scale with $D_{B0}^{2/3}$ for trees to maintain a constant safety margin from buckling under their own weight ("elastic similarity"; McMahon 1973). An elastically similar column has a mass exponent of $c = 3/8$ in Eqn. 2.3 (West et al. 1997, 1999; Enquist et al. 2000; Savage et al. 2010).

The water use allometry module predicts how the steady-state rate of midday xylem transport (Q) scales with trunk diameter:

$$Q = k_2 D_{B0}^q \tag{2.4}$$

with multiplier k_2 and water use exponent, q. To obtain Q, the Hagen-Poiseuille equation (Zimmermann 1983) is used to calculate tree hydraulic conductance (K) from the number and dimensions of the xylem conduits in the tree sapwood, given by the xylem architecture module (Fig. 2.1, right). The prediction of K yields Q by Eqn. 2.1, and the scaling of Q with tree size yields the water use allometry of Eqn. 2.4. Previous derivations of the water use exponent q in Eqn. 2.4 have assumed that selection for transport efficiency has driven it to its theoretical maximum of $q = 2$ (for the assumed xylem architecture; West et al. 1999; Enquist et al. 2000; Savage et al. 2010). At this point, the rate of whole-tree water transport depends solely on its trunk basal area and is not negatively influenced by tree height or transport distance ($Q \propto D_{B0}^2/H^0$).

The fifth metabolic isometry component of the Savage et al. model is a fundamental assumption of metabolic scaling theory: because photosynthetic CO_2 flux and transpirational water flux are both limited by stomatal diffusion, gross photosynthesis and potential isometric surrogates such as total respiration and growth rate (G) should scale proportionally with Q (Enquist et al. 2007a). Combining metabolic isometry with the mass and water use allometries predicts metabolic scaling: $G \propto Q \propto M^{cq}$, where the metabolic scaling exponent is the product of the exponents for mass (c; Eqn. 2.3) and water use (q; Eqn. 2.4) scaling.

If $c = 3/8$ (from elastic similarity) and $q = 2$ (the theoretical Savage et al. maximum), the metabolic exponent $cq = 3/4$ (West et al. 1999; Enquist et al. 2000). This prediction has provoked debate, partly over the validity of metabolic isometry and partly regarding q (e.g., Meinzer et al. 2005; Reich et al. 2006; Enquist et al. 2007a; Sperry et al. 2008).

Metabolic isometry is addressed in the second paper of this series (von Allmen et al. 2012). Here, we focus on the derivation of q.

For $q = 2$ the negative effects of tree height and distance on Q must be eliminated. Height is negated if the drop in xylem pressure from soil to canopy (ΔP) compensates for gravity ($\rho g H$), making the driving force ($\Delta P - \rho g H$; Eqn. 2.1) height-invariant. However, the ($\Delta P - \rho g H$) term often declines with height (Mencuccini 2003; Ryan et al. 2006).

Transport distance can be negated by the "bottleneck effect" where high flow resistance at the end of the xylem pipeline restricts the flow rate regardless of pipeline length. A bottleneck effect is consistent with the tapering of xylem conduits from trunk to terminal twig (West et al. 1999; Enquist et al. 2000; Sperry et al. 2008). This narrowing is captured in the Savage et al. model by a "taper function": the conduit diameter inside the terminal twigs is assumed size-invariant and conduits widen proximally as the stems themselves widen across branch ranks (Fig. 2.1, downward "axial taper" arrow).

The bottleneck effect is also influenced by how the number of conduits running in parallel changes across branch ranks. The Savage et al. model uses a "packing function" (Sperry et al. 2008) to govern the number of conduits that fit in a specified portion of wood space. Consequently, as conduits become narrower towards the twigs, their number per wood area increases (Fig. 2.1, upward "conduit packing" arrow). To optimize space-filling, Savage et al. assume a universal packing function that allocates a constant fraction of wood space to transport vs. across all branch ranks. Savage et al. then solve for optimal conduit taper on the basis of an efficiency vs. safety trade-off (see also Enquist et al. 2000). Taper is increased just enough to yield $q = 2$ (to maximize transport efficiency), but no more. Excessive taper would continue to widen conduits proximally, but to no effect other than to compromise safety from cavitation (larger conduits tend to be more vulnerable; Hacke et al. 2006).

Is the bottleneck effect enough to yield $q = 2$? Savage et al. recognize that not all species have identical taper and packing functions (McCulloh et al. 2010), suggesting that the space-filling and efficiency vs. safety trade-offs they invoke may have diverse context-dependent optima (Price et al. 2007). The intentional simplicity of the Savage et al. model also excluded additional variables that potentially influence the bottleneck effect such as the terminal resistance of leaves and the presence of nonconducting heartwood and bark.

The Savage et al. model also considers a basic issue in the derivation of q: the water use allometry only becomes a pure power function (e.g., Eqn. 2.4) at the limit of infinite tree size (Mencuccini et al. 2007). Thus, best-fit power functions across different size ranges

yield different q (and c) exponents. For example, Savage et al. solve for the rate of conduit taper that is just sufficient to make $q = 2$ at the limit of infinite tree size, while the same taper yields only $q = 1.86$ for finite-sized trees. This leads to their prediction of a metabolic scaling exponent of $cq = 0.70$ $(3/8 \cdot 1.86)$ in trees of actual size, with $cq = 0.75$ as an upper bound (Savage et al. 2010).

Our species model attempts to clarify some of the uncertainty in metabolic scaling theory by revisiting the derivation of the water use allometry component (Eqns. 2.1 and 2.4). New inputs of xylem architecture and function (asterisks in Fig. 2.1, see Model Description) are added to the Savage et al. framework to improve q estimation and to enable the prediction of the k_2 multiplier so that actual flow rates, Q, can be estimated. We focus on how specific hydraulic traits can effect the scaling of water use. For simplicity, we do not alter the branching architecture of the Savage et al. model (2010). We apply the new model to four objectives. (i) Using the simpler Savage et al. parameterization, we quantify the effects of finite tree size and gravity (i.e., the $[\Delta P - \rho g H]$ term) on intraspecific scaling. (ii) We determine the influence of new inputs and variable taper and packing on the water use exponent (q) and multiplier (k_2). (iii) We translate how interspecific variation in wood traits translates into a map of "scaling space" — defined by all possible combinations of multipliers (k_2) and the exponents (q) across species. The scaling space was simulated for four major functional tree types: conifers, ring-porous- and tropical and temperate diffuse-porous-angiosperms. (iv) Ecological drivers of scaling diversity are discussed, as are the implications for three-fourth power metabolic scaling within vs. across species. The second paper tests the model against empirical measurements (von Allmen et al. 2012).

2.3 Model description

The model has 17 inputs, with default values listed in Table 2.2. The model was written as a macro in Microsoft Excel using Visual Basic for Applications and is available from the senior author.

2.3.1 Branching architecture and mass allometry

Trees are represented as a symmetrically self-similar structure shown in Fig. 2.1 (left). Branches at level i (counting from $i = 0$ at the trunk) are identical in length and diameter. Area-preservation (da Vinci's rule; Horn 2000) sets the ratio of daughter/mother branch diameter (β) at $\beta = n^{1/2}$, where n is the daughter/mother branch number ratio (Table 2.1 defines all symbols). Elastic similarity, which requires $H \propto D_{B0}^{2/3}$ (McMahon 1973), sets the

daughter/ mother branch length ratio (γ) at $\gamma = n^{1/3}$. Modeled trees converge on elastic similarity with size as observed (Niklas & Spatz 2004).

Dimensions of the terminal branch rank (twigs) are assumed constant regardless of tree size. Twig diameter was set to 2 mm. Twig length was selected to yield convergence in large trees on the desired safety factor from buckling (H_B/H). The height at elastic buckling (H_B) was calculated according to Niklas (1994). Simulated "species" had identical branch architecture inputs (default β, γ, n, H_B/H, twig diameter, twig length; Table 2.2). The mass scaling exponent (c) was obtained from the slope of log-log plots of D_{B0} vs. tree volume ($V = \pi D_{B0}^2 H/4$) across networks of different size. We did not specify the multiplier k_1 for intraspecific scaling. However, for simulations of interspecific scaling, k_1 across species was specified by assuming branch tissue density equalled wood density (Supporting information, S2.3).

2.3.2 Xylem architecture and water use allometry ($Q = k_2 D_{B0}^q$)

The "taper function" describes how xylem conduit diameter (D_C, μm) increases with stem diameter (D_{Bi} mm):

$$D_C = k_3 D_{Bi}^p \tag{2.5}$$

where p is the "taper exponent" and k_3 (μm mm^{-p})the multiplier. The default $p = 1/3$ is the smallest p yielding $q = 2$ at the limit of infinite tree size in the Savage et al. model (2010). The choice of the minimum D_C in the terminal twigs dictated k_3 (default $D_C\ twig = 10$ μm, Table 2.2). When the model was run with axial taper alone (as in the Savage et al. model), D_C narrows as D_{Bi} narrows, but is constant from pith to cambium at a given branch level (Fig. 2.1, downward "axial taper" arrow). When radial taper is added, D_C increases from pith to cambium, starting from $D_C = D_C\ twig$ and increasing with the taper function as branch diameter is incremented (in 100 μm steps) to D_{Bi} (Fig. 2.1, enlarged cross-section). To avoid unrealistically large D_C, a maximum (Table 2.2, $D_C\ max$) was set. Default $D_C\ max$ was set to 240 μm because this was the greatest D_C in our functional type survey (Table 2.3; Supporting information, S2.2).

The number of xylem conduits per xylem area (F, mm^{-2}) was calculated from conduit diameter (D_C, μm) using the "packing function" (Sperry et al. 2008):

$$F = k_4 D_C^d \tag{2.6}$$

where d is the packing exponent (a negative number) and k_4 (mm^{-2} μm^{-d}) the multiplier. The choice of k_4 dictated the fraction of the total wood area occupied by xylem conduits

($C_F < 1$). For square packing (one conduit per square of space), maximum $F = 10^6 D_C^{-2}$ and $C_F = [k_4/10^6] D_C^{(d+2)}$. Savage et al. assumed an optimal d= -2 (our default), such that C_F is constant from twig to trunk (or pith to cambium). The default k_4 (Table 2.2) was chosen to yield $C_F = 0.1$, a typical hardwood value (McCulloh et al. 2010). If d was less negative than 2, then C_F increased from twig to trunk and vice-versa for d more negative than 2.

Xylem cross-sectional area was obtained by subtracting the bark and pith area from total branch area. Pith diameter (D_P, mm) was invariant within a tree, with a default of 1 mm. The bark thickness at level i (T_{Bi}, mm) was calculated from branch diameter (D_{Bi}, mm) as:

$$T_{Bi} = k_5 D_{Bi}^a \tag{2.7}$$

where a is the bark exponent and k_5 ($\text{mm}^{(1-a)}$) the multiplier. For simplicity, we restricted the analysis of bark thickness to the two bark functions used to test the model in the companion paper (von Allmen et al. 2012). These were from a relatively thin-barked maple (*Acer grandidentatum*) and a thicker-barked oak (*Quercus gambelii*). Maple served as the default (Table 2.2).

Total xylem area was divided into nonconducting heartwood and conducting sapwood. The sapwood area (A_{Si}, mm^2) at level i from branch diameter (D_{Bi}, mm) is given by:

$$A_{Si} = k_6 D_{Bi}^s \tag{2.8}$$

where s is the sapwood exponent and k_6 ($\text{mm}^{(2-s)}$) the multiplier. The exponent s has a maximum of $s = 2$ to avoid sapwood area from exceeding xylem area and a minimum of $s = 1$ for thin sapwood of approximately constant depth. Values of k_6 and s were obtained from the companion paper on oak and maple (von Allmen et al. 2012) and the sapflux literature. Sapwood functions were adjusted to have heartwood first appear at $D_{Bi} = 2.2$ cm and expand to reduce sapwood to varying percentages of total basal area at $D_{B0} = 72$ cm. The default percentage was 74%. This corresponded to a default sapwood depth from the cambium of 18.9 cm. Power functions for Eqns. 2.5-2.8 were chosen because of their convenience and good fit to empirical trends. The hydraulic conductance of a branch (K_{Bi}) was calculated from branch length (L_i, μm), and the number (N_C) and diameter (D_C, μm) of xylem conduits, using the Hagen-Poiseuille equation. Conduit number was obtained from the packing function and the sapwood area. When the model was run with radial D_C taper,

we integrated the Hagen-Poiseuille equation from the inner sapwood boundary ($x = 0$) to the cambium ($x = rc$) to yield the K_{Bi}:

$$K_{Bi} = C \int_{x=0}^{x=rc} N_c(x)\pi[D_C(x)]^4/(128\eta L_i)dx \tag{2.9}$$

where $N_C(x)$ and $D_C(x)$ are functions of the radial distance x across the sapwood according to the packing and taper functions. The integral was solved numerically by 100 μm increments in x (smaller increments were unnecessary). The viscosity, η, was set at 0.001 Pa s for 20 °C. The dimensionless constant C is an empirical correction factor ($0 < C < 1$) that accounts for interconduit flow resistance. The literature yielded default correction factors of $C = 0.44$ (angiosperms; Hacke et al. 2006) and $C = 036$ (conifers; Pittermann et al. 2005). Branch K_{Bi} was multiplied by the number of branches in level i to yield the parallel conductance of rank i. Rank conductances in series gave the hydraulic conductance of the stem network.

Leaf and root system conductances were extrapolated from the branch network conductance. Leaf conductance was given by ratio of leaf conductance per twig conductance (K_L/K_T), which was assumed to be size-invariant. This ratio is not often measured, but values from *Acer grandidentatum* and *Quercus gambelii* cited in the companion paper (von Allmen et al. 2012) provided a range. A similar approach was used to incorporate root system conductance. The shoot conductance (K_S, all branches plus leaves) was multiplied by the ratio of tree-shoot conductance (K/K_S) to obtain the whole-tree (root plus shoot) conductance. The default K/K_S ratio was 0.5 in keeping with observations from a variety of woody plants (Sperry et al. 2002). The default was size-invariance of K/K_S, but we also allowed it to increase with size (Martínez-Vilalta et al. 2007).

Steady-state tree water transport rate (Q, kg hr^{-1}) at midday was calculated from tree conductance using Eqn. 2.1. Default $\Delta P = 1$ MPa (Mencuccini 2002), making it size-invariant as seen for *Acer grandidentatum* and *Quercus gambelii* (von Allmen et al. 2012). Thus, the ($\Delta P - \rho gH$) driving force decreased with tree size. In an alternative "gravity compensation" scenario, the ($\Delta P - \rho gH$) term was size-invariant. These two options cover the range of gravity responses of trees (see Discussion). The Savage et al. model and earlier models (West et al. 1997, 1999; Enquist et al. 2000) assume isometry between Q and K, thus implicitly adopting gravity compensation. Linear regressions of log-transformed Q vs. D_{B0} data yielded the water use allometry equation: $Q = k_2 D_{B0}^q$.

2.4 Model results

2.4.1 Size dependent water-use allometry

We investigated size effects using the model parameterized as in Savage et al.: no pith, sapwood or bark, no leaves or roots and no radial taper (Table 2.2 shows remaining default inputs). The only difference from Savage et al. was that we allowed for gravitational effects.

Size effects had two causes: juvenile growth that was not elastically similar (Supporting information, S2.1, Fig. S2.1) and gravitational reduction in $(\Delta P - \rho g H)$ in tall trees. In combination, these created a nonlinear (in log-log space) water use allometry (Q) with trunk diameter (D_{B0}; Fig. 2.2). In small trees, a power-law fit gave an approximate scaling exponent of $Q \propto D_{B0}^{q=1.12}$ (Fig. 2.2, grey). The exponent increased to a maximum as elastic similarity was approached in medium sized trees: $Q \propto D_B 0^{q=1.72}$ (Fig. 2.2, dark grey). In large trees, the exponent decreased as gravity ($\rho g H$) subtracted an increasing portion of the pressure difference between soil and canopy ($\Delta P = 1$ MPa, Table 2.2). Thus, Q scaling became flatter in tall trees: $Q \propto D_{B0}^{q=0.91}$ (Fig. 2.2, black).

In the gravity compensation scenario, ΔP increased with H such that the $(\Delta P - \rho g H)$ term was size-invariant and Q scaling did not flatten. Instead it reached $Q \propto D_{B0}^{q=1.86}$ in large sized trees (Fig. 2.2, dash-dotted no g line) as estimated for the Savage et al. model at their optimal taper ($p = 1/3$). Increasing tree size towards infinity gave the $q = 2$ asymptote (Savage et al. 2010).

2.4.2 Influence of individual traits on water use scaling

New variables added to the Savage et al. framework altered water use scaling. We report effects on the exponent, q, and the multiplier, k_2, for medium-sized trees ($2 < D_{B0} \leq 72$ cm) where Q by D_{B0} scaling was nearly linear in log-log space (Fig. 2.2). Rather than cite k_2 values, we substitute a more intuitive proxy: the rate of water transport at a reference tree size (Q_{ref} for $D_{B0} = 72$ cm).

Although the effects were quantitatively complex (Fig. 2.3), the take-home message is simple. All variables influenced Q_{ref} because they either increased tree hydraulic conductance (e.g., more, wider functioning conduits, higher leaf or root conductances) or reduced it (fewer, narrower functioning conduits, lower leaf or root conductances). A subset also altered q because they influenced the bottleneck effect: either increasing the difference in distal-to-proximal balance of hydraulic conductance in the shoot (greater q) or decreasing it (lower q). One variable (size-dependent K/K_S) altered q independently of the bottleneck effect.

Figure 2.3(a) shows the cumulative effect of adding new variables. Incorporating pith and bark (defaults in Table 2.2) reduced Q_{ref} by reducing xylem cross-sectional area, with thicker bark having a greater effect (Fig. 2.3a); q was not materially changed. Adding radial taper to the thin-barked default model decreased Q_{ref} further (Fig. 2.3a, radial taper) because of the narrowing of vessel diameter towards the pith; again, q changed little. Adding heartwood reduced both Q_{ref} and q (Fig. 2.3a, sapwood%). Reducing basal sapwood area from 74 to 30% (reducing sapwood thickness from 18.9 to 6.1 cm) caused q to drop from 1.72 to below 1.64 and Q_{ref} to drop by 24% (Fig. 2.3a). Heartwood decreased Q_{ref} by reducing the cross-sectional area for water conduction. Most of this reduction was in the larger branches and trunk, which decreased the bottleneck effect of the distal branches and lowered q.

The 74% basal sapwood function was adopted as the default (Table 2.2) for assessing the further effect of adding leaves in Fig. 2.3b. As the K_L/K_T ratio was decreased from 1 to 0.01, Q_{ref} dropped by over 80% relative to the default no-leaf model (Fig. 2.3b) because leaves reduced network conductance. The reduction was at the distal end, which increased the bottleneck effect, and q increased from 1.72 to 1.92. The measured K_L/K_T range was relatively narrow: from 0.27 in *Quercus gambelii* to 0.38 in *Acer grandidentatum* (von Allmen et al. 2012).

The intervessel resistance factor (C, Eqn. 2.9) caused a proportional change on Q_{ref}, but no change in q because it did not influence the bottleneck. The same was true for adding below-ground resistance (Table 2.2, $K/K_S = 0.50$). However, if K/K_S was allowed to increase with D_{B0} as estimated for *Pinus sylvestris* ($K/K_S = 0.75 D_{B0}^{0.36}$ from Martínez-Vilalta et al. 2007), q rose to 2.12. This was the only input that gave $q \geq 2$. It did so not by increasing the shoot bottleneck effect, but because root conductance increased faster than shoot conductance with size.

Varying taper and packing from the universal functions assumed by Savage et al. was simulated for a default $K_L/K_T = 0.30$ (Table 2.2; grey symbol in Fig. 2.3c,d). Figure 2.3c shows the effect of taper. The default taper was $D_C = 7.9 D_{Bi}^{p=1/3}$, corresponding to D_C *twig* $= 10$ μm. D_C *twig* was held constant while varying the taper exponent, p, by adjusting the multiplier. Decreasing taper from $p = 1/3$ to $p = 0.2$ resulted in narrower conduits proximally, which reduced network conductance (51% drop in Q_{ref}) and the bottleneck effect (decrease in q from 1.76 to 1.59). Increasing taper above $p = 1/3$ had the opposite effect: Q_{ref} increased by almost 5-fold and q rose to 1.93. At $p \geq 0.6$, conduit diameter in the proximal trunk and branches had to be capped at D_C *max* $= 240$ μm (Fig.

2.3c, asterisked points). Saturation in q and Q_{ref} occurred at $p > 9$ because vessels had reached the 240 μm cap at every branch rank except the twigs. The 240 μm cap, heartwood and gravity prevented q from saturating at $q = 2$.

Figure 2.3d shows the influence of the packing function, $F = k_4 D_C^d$. The greater the value of coefficient k_4, the greater the fraction of wood area devoted to water conduction (C_F). Increasing C_F caused a proportional increase in Q_{ref} (C_F = 0.01 to 0.6) with no effect on q (Fig. 2.3d). When varying the packing exponent d, we covaried the multiplier to keep C_F constant in the terminal twigs. Increasing d (less negative), resulted in more big trunk vessels and hence increased both the relative flow rate (Q_{ref}) and the Q by D_{B0}^q scaling exponent. Decreasing the exponent had the opposite effect (Fig. 2.3d, d = 2.5 to 1.5). Effects of the exponent on Q_{ref} were small compared with the effect of conducting area fraction, C_F.

2.4.3 Functional tree types in scaling space

While Fig. 2.3 isolates the consequences of particular traits, actual scaling integrates variation across all traits at once to create a 2D cloud of species-specific Q_{ref} by q combinations. We used the model to circumscribe this "scaling space" for major tree categories: ring-porous temperate, diffuse-porous temperate, diffuse-porous tropical and conifers. For each category, we estimated the range for input variables for which multispecies data were available (Table 2.3; Supporting information, S2.2); remaining inputs, including K/K_S, were defaults (Table 2.2). A version of the model (available from the second author) scanned input combinations that defined the extremes of Q_{ref} and q for medium-sized trees ($2 < D_{B0} \leq 72$ cm).

The four tree categories occupied distinct, but substantially overlapping, scaling space (Fig. 2.4). The most efficient transporters, with the greatest Q_{ref} and scaling exponent q, were the tropical diffuse-porous trees (Fig. 2.4, green DP tropical outline). Tropical trees combined largest trunk and twig vessels with extensive sapwood area. The only parameter compromising efficiency in tropical trees was a somewhat lower C_F (Table 2.3; fewer vessels per sapwood area).

Temperate ring-porous angiosperms achieved the next highest Q_{ref} (Fig. 2.4, black RP outline). Although their vessel diameter is similar to tropical trees, their limited sapwood area (Table 2.3) compromised transport and contributed to their broad q range. Their broad Q_{ref} range corresponded to a wide range in C_F (Table 2.3). Ring-porous trees overlapped considerably with their chief cohabitants, the temperate diffuse-porous angiosperms (Fig. 2.4, red DP temperate outline). Although temperate diffuse-porous trees

have narrower vessel diameters than ring-porous trees, this was compensated by their greater sapwood area (Table 2.3).

The most surprising result was the performance of the conifers (Fig. 2.4, blue conifer outline). Although conifer tracheids have by far the narrowest conduit diameter range, they compensate by having high C_F (Table 2.3), owing to the double role of tracheids in water transport and mechanical support. The high C_F of conifers placed them almost entirely within the transport capacity of temperate diffuse-porous angiosperms. Assuming "metabolic isometry," the hydraulic scaling in Fig. 2.4 predicts growth rate scaling with tree mass ($G \propto M^{cq}$). Assuming $c = 0.369$ for medium-sized trees (Supporting information, S2.1), the range for the $G \propto M^{cq}$ exponent was mapped onto the four tree types in Fig. 2.4 (cq values on upper axis). The metabolic scaling exponents ranged from 0.26 to 0.71 and excluded three-fourth power scaling.

2.4.4 Intraspecific vs. interspecific scaling

Each Q_{ref} by q coordinate in the scaling space of Fig. 2.4 corresponds to a unique water use allometry ($Q = k_2 D_{B0}^q$; Eqn. 2.4) of a theoretical "species." Each species also has a potentially unique mass allometry ($D_{B0} = k_1 M^c$) because of interspecific variation in wood density (Supporting information, S2.3). These "species" were sampled to simulate intraspecific vs. interspecific scaling of the metabolic cq exponent. Theoretical species with $q < 1.5$ were excluded because they are unlikely to exist (Supporting information, S2.3 and Discussion). When species were chosen at random and assumed to reach the same maximum size regardless of Q_{ref} and q, the intraspecific cq averaged 0.63 ± 0.0011 (mean $\pm$ SE, $n = 1000$ trees) and the interspecific cq averaged 0.66 ± 0.0018 (Fig. 2.5, "random"). Both intraspecific and interspecific exponents fell short of $cq = 0.75$. In an alternative "height-biased" sampling, we assumed that species from the upper right corner of scaling space in Fig. 2.4 (greater Q_{ref} and q) would have less of a hydraulic limitation on their maximum height and grow taller than species towards the lower left corner. Average intraspecific scaling was no different from the random scenario ($cq = 0.63 \pm 0.0020$), but the interspecific cq could be significantly steeper depending on the sensitivity of species stature to their water use allometry and the size distribution of the interspecific sample. The particular case shown (see Supporting information, S2.3 for details) shows that interspecific cq can match three-fourth power scaling ($cq = 0.75 \pm 0.0041$; Fig. 2.5; "height-biased").

2.5 Discussion

The model answers our opening question by providing species-specific predictions of the water use multiplier (k_2) and scaling exponent (q) in the water use allometry equation: $Q = k_2 D_{B0}^q$. Greater k_2 indicates greater water transport, gas exchange and growth as predicted by metabolic scaling theory and shown empirically (e.g., Hubbard et al. 2001). A larger scaling exponent q means a greater rate of increase in these presumably competitive capacities with tree size (Hammond & Niklas 2012). In general, fertile and consistently moist habitats with low threat of cavitation should favour conducting efficiency over safety. Species adapted to such habitats should cluster towards the upper right portions of Q_{ref} by q scaling space of Fig. 2.4. Conversely, arid and freezing habitats should push species to the lower left towards greater safety but lower transport capacity.

The considerable overlap in scaling space between the functional tree types exemplifies how trait variation presumably arises from ecological and evolutionary circumstances, and how divergence in scaling space is minimized by compensation between traits (Marks & Lechowicz 2006). Despite the overlap, tropical trees were distinguished by reaching the greatest maximum capacity by having large vessels with a long functional lifetime (= large sapwood areas). These features are consistent with selection favouring efficiency over safety in their relatively permissive habitat where the threat of cavitation by freezing or water stress is low (McCulloh et al. 2010).

The temperate diffuse- and ring-porous trees had lower peak transport capacities than the tropical trees. Accordingly, their habitat is not so permissive, certainly not in the case of freezing-induced cavitation. The adaptation to winter freezing takes different forms in ring- vs. diffuse-porous types (Sperry et al. 1994). Ring-porous trees had essentially the same range of vessel diameters and taper exponents as tropical trees, but the large vessels are sacrificed annually to cavitation by freezing. Hence, their drop in predicted transport capacity (lower Q_{ref}) and flatter scaling (lower q) relative to tropical trees results from giving up sapwood area.

Diffuse-porous temperate trees arguably adapted to freezing by having vessels narrow enough to limit the extent of cavitation (and many also reverse cavitation in spring; Hacke & Sauter 1996; Sperry et al. 1994). Their drop in transport capacity relative to tropical trees results from narrower vessels and less taper rather than less sapwood area. Both ring- and temperate diffuse-porous adaptations to freezing result in fairly similar estimated transport capacities: short-functioning and hence few, large vessels in ring-porous trees roughly equated to long-functioning and hence numerous, narrow vessels in diffuse-porous

trees.

The conifers exhibit convergent scaling with temperate angiosperms despite very divergent wood structure. Their unicellular tracheids are limited in diameter for developmental and mechanical reasons compared with multicellular vessels (Pittermann et al. 2006). Hence tracheid taper functions are flatter (lower p range, Table 2.3). The greater impact of interconduit pits in conifers (lower C, Table 2.2) is because tracheids are much shorter than vessels and water encounters more interconduit walls as it flows through a given length of branch. However, these disadvantages are largely compensated for by the efficiency of the torus-margo structure of their intertracheid pitting (Pittermann et al. 2005). The narrow tracheid diameters and low taper are made up for by maximally efficient packing functions (Sperry et al. 2008). Conifer wood is a honeycomb of tracheids and consequently has a much greater conducting area (C_F up to 0.42, Table 2.3) than angiosperm xylem with its vessels dispersed in a fibre-parenchyma matrix ($C_F < 0.37$). Conifer wood partially dodges the efficiency vs. safety trade-off by increasing efficiency with conduit number rather than conduit diameter.

Conifers also had packing exponents consistently less negative than $d = 2$ (Table 2.3; McCulloh et al. 2010), leading to a high water use exponent (q) despite their low taper exponent (p) range. Less negative d in conifers means there is a greater fraction of space devoted to water conduction in trunks vs. twigs. Anatomically, this is likely owing to a lower ratio of tracheid wall thickness: tracheid lumen diameter ("thickness-to-span" ratio) in trunks vs. twigs. The thickness-to-span ratio in turn scales with the strength of tracheids against implosion by internal negative sap pressures (Hacke et al. 2001). Thus, low thickness-to-span in trunk tracheids corresponds with less negative sap pressures proximally and vice-versa in the distal twigs.

If the model predictions are realistic, actual trees should fall within the boundaries shown in Fig. 2.4, but not necessarily fill them, because not all modeled trait combinations may have evolved. Indeed, data on intraspecific q, while limited, appear to primarily fall within the upper portion of the predicted range. Values of q much below ca. 1.5 have not been observed in trees (Enquist et al. 2000; Mencuccini 2003; Meinzer et al. 2005; Sperry et al. 2008), which is why lower values were excluded for assessing interspecific scaling. Flow rates for trees of ca. 72 cm in diameter (ca. 4 to 125 kg hr^{-1}) are also consistent with the predicted Q_{ref} range (Enquist et al. 1998; Wullschleger et al. 1998; Meinzer et al. 2005). A review of whole-tree water use in 67 species indicated no systematic differences in daily tree water use vs. trunk diameter between the four functional types we

considered (Wullschleger et al. 1998), which is consistent with their extensive overlap in Q_{ref} (Fig. 2.4). The predicted similarity of temperate tree types is supported by observed parity in whole-tree hydraulic conductance between temperate conifers and temperate angiosperms (Becker et al. 1999)). Where differences have been seen between categories, they support model predictions. Tropical angiosperm trees in one extensive comparison moved more water per diameter than temperate conifers, consistent with our model results (Meinzer et al. 2005). A more direct test of the model in a diffuse- and a ring-porous species is the subject of the second paper in this series (von Allmen et al. 2012).

The functional type simulations indicate that there are multiple ways to "skin the cat" when it comes to achieving a given water transport capacity and size-scaling. The Savage et al. derivation of an optimal taper ($p = 1/3$, Eqn. 2.5) effectively captures the consequences of conduit taper while holding other variables constant (Savage et al. 2010). In our more detailed model, conduit taper emerges as one of several influences on water use scaling, underscoring the likelihood that selection on any single trait (like taper) can be relaxed by compensating changes in other variables (e.g., packing function, leaf hydraulics and sapwood area). Nevertheless, the boundaries of the Q_{ref} by q scaling space were finite and relate in context-specific ways to the same space-filling and safety vs. efficiency constraints emphasized by Savage et al.

The simulated scaling space excluded three-fourth intraspecific metabolic scaling. The greatest metabolic exponent was $cq = 0.71$ and random sampling yielded an intraspecific mean $cq \approx 0.63$. This mean is similar to the range predicted from observed water use scaling within the few tree species where it has been assessed (Mencuccini 2003; Meinzer et al. 2005). If metabolic scaling does indeed center on $cq = 0.75$, as has been proposed (Enquist et al. 1998, 2000; Niklas & Enquist 2001), the reason remains ambiguous based on our results.

Given the focus on three-fourth power scaling, we looked for situations where it could be consistent with the model and found two of them. Intraspecifically, if hydraulic conductance increases faster in roots than in shoots with size, q can reach or exceed 2 ($q \geq 2$) and $cq \leq 0.75$. This pattern has been proposed as a mechanism to compensate for a potential hydraulic limitation on tree height (Magnani et al. 2000). However, data are limited and equivocal, with some species showing an increase in K/K_S with size (Martínez-Vilalta et al. 2007) and others not (von Allmen et al. 2012). A related explanation that applies to interspecific scaling is that species with greater inherent transport capacity (larger k_2 and/or q) would have less of a hydraulic limitation to height and grow taller than species

with lower transport capacity. A bias for greater stature with steeper intraspecific scaling can theoretically give metabolic *cq* exponents of 0.75 or higher (Fig. 2.5). While both scenarios are compatible with three-fourth power scaling, neither predicts that particular exponent from *a priori* optimization in the WBE sense.

Our species-level model is purposefully more complex and realistic than the Savage et al. analytical version. By allowing many functional traits to simultaneously vary, the numerical model reveals how a species' metabolic scaling results from interaction between complex trait interactions and covariance. A finite scaling space appears more realistic than convergence on one particular rule. This conclusion is based on a limited number of hydraulic traits, but is likely to be reinforced when additional complexities are considered. For example, the range of branching structure is more diverse than the generic WBE default (Price et al. 2007; Bentley et al. 2013), carbon allocation may not always preserve isometry between metabolic sinks and vascular supply (Reich et al. 2006; Enquist et al. 2007b), and vascular supply itself would be modulated by dynamics of cavitation and refilling. Incorporating such complexity can translate an even broader diversity of plant functional traits into whole plant performance. Such a framework could have general utility in ecology from constraining ecosystem fluxes and stocks to exploring the optimization of trait interactions.

2.6 Acknowledgements

The authors were supported by National Science Foundation Advancing Theory in Biology Award 0742800. John S. Sperry, Duncan D. Smith and Erica I. von Allmen were partially funded by National Science Foundation Grant IBN-0743148. Lisa P. Bentley was also supported by NSF Postdoctoral Fellowship in Bioinformatics DBI-0905868.

2.7 References

Becker P., Tyree M.T. & Tsuda M. (1999) Hydraulic conductances of angiosperm versus conifers: similar transport sufficiency at the whole-plant level. *Tree Physiology* 19, 445–452.

Bentley L.P., Stegen J.C., Savage V.M., Smith D.D., von Allmen E.I., Sperry J.S., Reich P.B. & Enquist B.J. (2013) An empirical assessment of tree branching networks and implications for plant allometric scaling models. *Ecology Letters* 16, 1069–1078.

Bovard B.D., Curtis P.S., Vogel C., Su H.B. & Schmid H.P. (2004) Environmental controls on sap flux in a northern hardwood forest. *Tree Physiology* 25, 31–38.

Chave J., Coomes D., Jansen S., Lewis S.L., Swenson N.G. & Zanne A.E. (2009) Towards a worldwide wood economics spectrum. *Ecology Letters* 12, 351–366.

Ellmore G.S. & Ewers F.W. (1986) Fluid flow in the outermost xylem increment of a ring-porous tree, *Ulmus americana*. *American Journal of Botany* 73, 1771–1774.

Enquist B.J., Allen A.P., Brown J.H., Gillooly J.F., Kerkhoff A.J., Niklas K.J., Price C.A. & West G.B. (2007a) Biological scaling: does the exception prove the rule? *Nature* 445, E9–E10.

Enquist B.J., Brown J.H. & West G.B. (1998) Allometric scaling of plant energetics and population density. *Nature* 395, 163–165.

Enquist B.J., Kerkhoff A.J., Stark S.C., Swenson N.G., McCarthy M.C. & Price C.A. (2007b) A general integrative model for scaling plant growth, carbon flux, and functional trait spectra. *Nature* 449, 218–222.

Enquist B.J., West G.B. & Brown J.H. (2000) Quarter-power allometric scaling in vascular plants: functional basis and ecological consequences. In *Scaling in Biology* (eds. J.H. Brown & G.B. West), Oxford University Press, Oxford, 167–198.

Gebauer T., Horna V. & Leuschner C. (2008) Variability in radial sap flux density patterns and sapwood area among seven co-occurring temperate broad-leaved tree species. *Tree Physiology* 28, 1821–1830.

Hacke U. & Sauter J.J. (1996) Xylem dysfunction during winter and recovery of hydraulic conductivity in diffuse-porous and ring-porous trees. *Oecologia* 105, 435–439.

Hacke U.G., Sperry J.S., Pockman W.P., Davis S.D. & McCulloh K.A. (2001) Trends in wood density and structure are linked to prevention of xylem implosion by negative pressure. *Oecologia* 126, 457–461, in press.

Hacke U.G., Sperry J.S., Wheeler J.K. & Castro L. (2006) Scaling of angiosperm xylem structure with safety and efficiency. *Tree Physiology* 26, 689–701.

Hammond S.T. & Niklas K.J. (2012) Computer simulations support a core prediction of a contentious plant model. *American Journal of Botany* 99, 508–516.

Horn H.S. (2000) Twigs, trees and the dynamics of carbon in the landscape. In *Scaling in Biology* (eds. J.H. Brown & G.B. West), Oxford University Press, Oxford, 199–220.

Hubbard R.M., Stiller V., Ryan M.G. & Sperry J.S. (2001) Stomatal conductance and photosynthesis vary linearly with plant hydraulic conductance in ponderosa pine. *Plant Cell and Environment* 24, 113–121.

Hultine K.R., Bush S.E. & Ehleringer J.R. (2010) Ecophysiology of riparian cottonwood and willow before, during, and after two years of soil water removal. *Ecological Applications* 20, 347–361.

Macinnis-Ng C., Zeppel M., Williams M. & Eamus D. (2011) Applying a SPA model to examine the impact of climate change on GPP of open woodlands and the potential for woody thickening. *Ecohydrology* 4, 379–393.

Magnani F., Mencuccini M. & Grace J. (2000) Age-related decline in stand productivity: the role of structural acclimation under hydraulic constraints. *Plant Cell and Environment* 23, 251–264.

Marks C.O. & Lechowicz M.J. (2006) Alternative designs and the evolution of functional diversity. *American Naturalist* 167, 55–66.

Martínez-Vilalta J., Korakaki E., Vanderklein D. & Mencuccini M. (2007) Below-ground hydraulic conductance is a function of environmental conditions and tree size in Scots pine. *Functional Ecology* 21, 1072–1083.

McCulloh K.A., Sperry J.S., Lachenbruch B., Meinzer F.C., Reich P.B. & Voelker S. (2010) Moving water well: comparing hydraulic efficiency in twigs and trunks of coniferous, ring-porous, and diffuse-porous saplings from temperate and tropical forests. *New Phytologist* 186, 439–450.

McMahon T.A. (1973) Size and shape in biology. *Science* 179, 1201–1204.

Meinzer F.C., Bond B.J., Warren J.M. & Woodruff D.R. (2005) Does water transport scale universally with tree size? *Functional Ecology* 19, 558–565.

Mencuccini M. (2002) Hydraulilc constraints in the functional scaling of trees. *Tree Physiology* 22, 553–565.

Mencuccini M. (2003) The ecological significance of long-distance water transport: short-term regulation, long-term acclimation and the hydraulic costs of stature across plant life forms. *Plant Cell and Environment* 26, 163–182.

Mencuccini M., Hölttä T., Petit G. & Magnani F. (2007) Sanio's laws revisited. Size-dependent changes in the xylem architecture of trees. *Ecology Letters* 10, 1084–1093.

Niklas K.J. (1994) The allometry of safety-factors for plant height. *American Journal of Botany* 81, 345–351.

Niklas K.J. & Enquist B.J. (2001) Invariant scaling relationships for interspecific plant biomass production rates and body size. *Proceedings of the National Academy of Sciences of the United States of America* 98, 2922–2927.

Niklas K.J. & Spatz H.C. (2004) Growth and hydraulic (not mechanical) constraints govern the scaling of tree height and mass. *Proceedings of the National Academy of Sciences of the United States of America* 101, 15661–15663.

Panshin A.J. & de Zeeuw C. (1970) *Textbook of wood technology*, vol. 1. McGraw-Hill, New York.

Pittermann J., Sperry J.S., Hacke U.G., Wheeler J.K. & Sikkema E.H. (2005) Torus-margo pits help conifers compete with angiosperms. *Science* 310, 1924.

Pittermann J., Sperry J.S., Wheeler J.K., Hacke U.G. & Sikkema E.H. (2006) Mechanical reinforcement of tracheids compromises the hydraulic efficiency of conifer xylem. *Plant, Cell and Environment* 29, 1618–1628.

Price C.A., Enquist B.J. & Savage V.M. (2007) A general model for allometric covariation in botanical form and function. *Proceedings of the National Academy of Sciences of the United States of America* 104, 13204–13209.

Reich P.B., Tjoelker M.G., Machado J. & Oleksyn J. (2006) Universal scaling of respiratory metabolism, size and nitrogen in plants. *Nature* 439, 457–461.

Richter H. (1973) Frictional potential losses and total water potential in plants: a re-evaluation. *Journal of Experimental Botany* 274, 983–994.

Richter J.P. (1970) *The notebooks of Leonardo da Vinci (1452-1519), compiled and edited from the original manuscripts*, vol. I. Dover, New York.

Ryan M.G., Phillips N. & Bond B.J. (2006) The hydraulic limitation hypothesis revisited. *Plant Cell and Environment* 29, 367–381.

Savage V.M., Bentley L.P., Enquist B.J., Sperry J.S., Smith D.D., Reich P.B. & von Allmen E.I. (2010) Hydraulic trade-offs and space filling enable better predictions of vascular structure and function in plants. *Proceedings of the National Academy of Sciences of the United States of America* 107, 22722–22727.

Sperry J.S., Hacke U.G., Oren R. & Comstock J.P. (2002) Water deficits and hydraulic limits to leaf water supply. *Plant Cell and Environment* 25, 251–263.

Sperry J.S., Meinzer F.C. & McCulloh K.A. (2008) Safety and efficiency conflicts in hydraulic architecture: from tissues to trees. *Plant Cell and Environment* 31, 632–645.

Sperry J.S., Nichols K.L., Sullivan J.E.M. & Eastlack S.E. (1994) Xylem embolism in ring-porous, diffuse-porous, and coniferous trees of northern Utah and interior Alaska. *Ecology* 75, 1736–1752.

Tyree M.T. (1988) A dynamic model for water flow in a single tree: evidence that models must account for hydraulic architectures. *Tree Physiology* 4, 195–217.

van den Honert T.H. (1948) Water transport in plants as a catenary process. *Discussions of the Faraday Society* 3, 146–153.

von Allmen E.I., Sperry J.S., Smith D.D., Savage V.M., Reich P.B., Enquist B.J. & Bentley L.P. (2012) A species' specific model of the hydraulic and metabolic allometry of trees II: testing predictions of water use and growth scaling in species with contrasting hydraulic traits. *Functional Ecology* 26, 1066–1076.

West G.B., Brown J.H. & Enquist B.J. (1997) A general model for the origin of allometric scaling laws in biology. *Science* 276, 122–126.

West G.B., Brown J.H. & Enquist B.J. (1999) A general model for the structure and allometry of plant vascular systems. *Nature* 400, 664–667.

Wullschleger S.D., Meinzer F.C. & Vertessy R.A. (1998) A review of whole-plant water use studies in trees. *Tree Physiology* 18, 499–512.

Zanne A., Lopez-Gonzalez G., Coomes D., Ilic J., Jansen S., Lewis S., Miller R., Swenson N., Wiemann M. & Chave J. (2009) Data from: towards a worldwide wood economics spectrum. URL http://dx.doi.org/10.5061/dryad.234.

Zimmermann M. (1978) Hydraulic architecture of some diffuse porous trees. *Canadian Journal of Botany* 56, 2286–2295.

Zimmermann M.H. (1983) *Xylem structure and the ascent of sap*. Springer Series in Wood Science, Springer, Berlin, Heidelberg, New York.

Table 2.1. Major symbols and definitions

Symbols	Definitions
A_{Si}	Sapwood area, branch level i
A_S/A_T	Sapwood area/basal area for reference tree size with $D_{B0} = 72$ cm
C_F	Fraction of wood occupied by conduit lumens (conduit lumen fraction)
C	Xylem hydraulic conductance/Hagen-Poiseuille conductance (endwall correction)
D_{B0}	Trunk diameter (branch rank 0)
D_{Bi}	Stem diameter for branch rank i
D_C	Xylem conduit diameter
$D_C\ max$	Maximum allowable conduit diameter
$D_C\ twig$	Conduit diameter in the distal-most branch rank (twigs)
D_P	Pith diameter
F	Number of conduits per wood area
g	acceleration of gravity
G	biomass growth rate of shoot
H/H_B	tree height/Euler buckling height
K	tree hydraulic conductance
K_L/K_T	Leaf hydraulic conductance/supporting twig conductance
K/K_S	Tree conductance/shoot conductance
k_0, b	Generalized scaling multiplier and exponent (e.g., $Y = k_0 M^b$)
k_1, c	Mass scaling multiplier and exponent ($D_{B0} = k_1 M^c$)
k_2, q	Water use scaling multiplier and exponent ($Q = k_2 D_{B0}^q$)
k_3, p	Taper function multiplier and exponent ($D_C = k_3 D_{Bi}^p$)
k_4, d	Packing function multiplier and exponent ($F = k_4 D_C^d$)
k_5, a	Bark thickness function multiplier and exponent ($T_{Bi} = k_5 D_{Bi}^a$)
k_6, s	Sapwood area function multiplier and exponent ($A_{Si} = k_6 D_{Bi}^s$)
L_i	Branch segment length, level i
M	Shoot (aboveground) mass
N_C	Conduit number
n	Daughter/mother branch number ratio
Q	Steady-state tree water transport rate at midday
Q_{ref}	Q for "reference" tree size of trunk diameter $D_{B0} = 72$ cm
T_{Bi}	Bark thickness, branch level i
V	Shoot (aboveground) volume
β	Daughter/mother branch diameter ratio
ΔP	Total soil to canopy water potential difference
γ	Daughter/mother branch length ratio
η	Viscosity of water
ρ	Density of water

Table 2.2. Model inputs and outputs in order of appearance in text. Power functions were used for their simplicity and good fit to empirical trends

Input	Default
n, branch number ratio	2
γ, branch length ratio	0.794 (elastic similarity for $n = 2$ symmetric branching)
β, branch diameter ratio	0.707 (area-preserving $n = 2$ symmetric branching)
H_B/H, mature tree safety factor	4
Terminal twig diameter	2 mm
Terminal twig length	8.1 cm
$D_C = k_3 D_{Bi}^p$; taper function	$k_3 = 7.9$ μm mm^{-p}, $p = 1/3$; D_C in μm, D_{Bi} in mm
D_C *max*	240 μm
D_C *twig*	10 μm
$F = k_4 D_C^d$; packing function	$k_4 = 10^5$ μm^{-d} mm^{-2}; $d = -2$; F in mm^{-2}, D_C in μm
D_P, pith diameter	1 mm
$T_{Bi} = k_5 D_{Bi}^a$ bark function	$k_5 = 0.0225$ mm^{1-a}; $a = 1.05$; T_{Bi} and D_{Bi} in mm
$A_{Si} = k_6 D_{Bi}^s$; sapwood function	$k_6 = 0.905$ mm^{2-s}; $s = 1.93$; A_{Si} in mm^2, D_{Bi} in mm
C, endwall correction factor	0.44 (angiosperms); 0.36 (conifers)
K_L/K_T, leaf/twig conductance	0.30
K/K_S, tree/shoot conductance	0.50
ΔP, total pressure drop	1 MPa
Output	
H, D_{B0} and V, yielding estimates of c: $D_{B0} \propto M^c$	
K and D_{B0}	
Q and D_{B0}, yielding estimates of q: $Q = k_2 D_{B0}^q$	
Estimates of $G \propto Q \propto M^{cq}$	

Table 2.3. Model inputs used to define the hydraulic scaling of four tree types (Fig.2.4). Ranges adapted from the literature (Supporting information, S2.2). Additional inputs were set to defaults listed in Table 2.2. The A_S/A_T trunk is the fraction of sapwood area per basal area in a tree of $D_{B0} = 72$ cm that results from the inputted sapwood function. Note that the range of leaf-to-twig conductance ratio (K_L/K_T) was assumed to be the same for all categories, as were the sapwood parameters in all but the ring-porous category.

	Ring-porous temperate	Diffuse-porous temperate	Diffuse-porous tropical	Conifers
D_C *twig*, μm	21 (16.8 - 25.2)	12 (9.6 - 14.4)	21 (16.8 - 25.2)	7 (5.6 - 8.4)
D_C *max*, μm	145 - 240	33 - 79	158 - 240	28 - 45
Taper p	0.30 - 0.59	0.14 - 0.41	0.31 - 0.61	0.20 - 0.44
Packing d	-1.34 to -2.29	-1.65 to -3.27	-2.38 to -2.0	-1.69 to -1.8
C_F	0.09 - 0.37	0.07 - 0.20	0.06 - 0.12	0.37 - 0.42
K_L/K_T	0.20 - 0.40	0.20 - 0.40	0.20 - 0.40	0.20 - 0.40
Sapwood s	1.05 - 1.36	1.55 - 1.91	1.55 - 1.91	1.55 - 1.91
A_S/A_T trunk	0.003 - 0.017	0.34 - 0.74	0.34 - 0.74	0.34 - 0.74

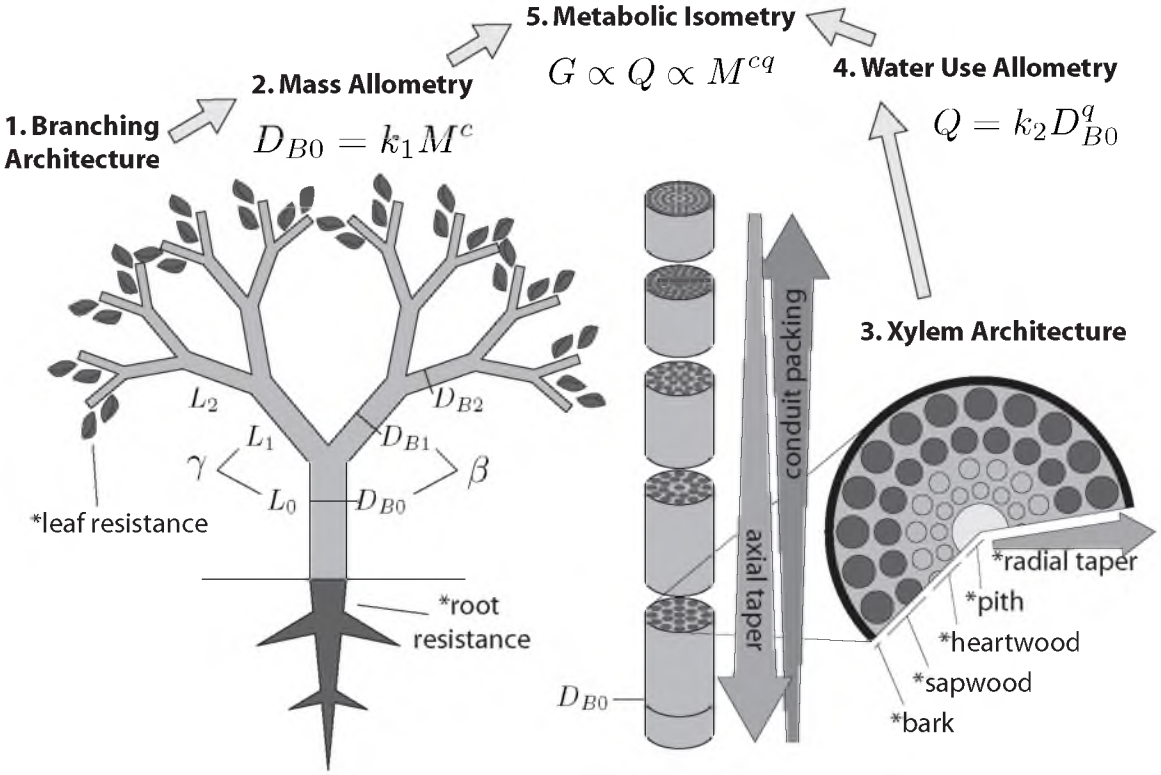

Figure 2.1. Elements of metabolic scaling theory. Self-similar and symmetric branching architecture (left) that is area-preserving (central column) yields trunk diameter (D_{B0}) by mass (M^c) scaling. Xylem conduit architecture (shown in column cross-sections) yields water use (Q, flow rate) by D_{B0}^q scaling. Combining mass and water use yields Q by M^{cq} scaling. If growth rate (G) is isometric with Q (metabolic isometry), then the theory yields growth rate (G) by M^{cq} scaling. Asterisked components represent novel parameters that were not explicit in the (Savage et al. 2010) model. See Table 2.1 for other symbols.

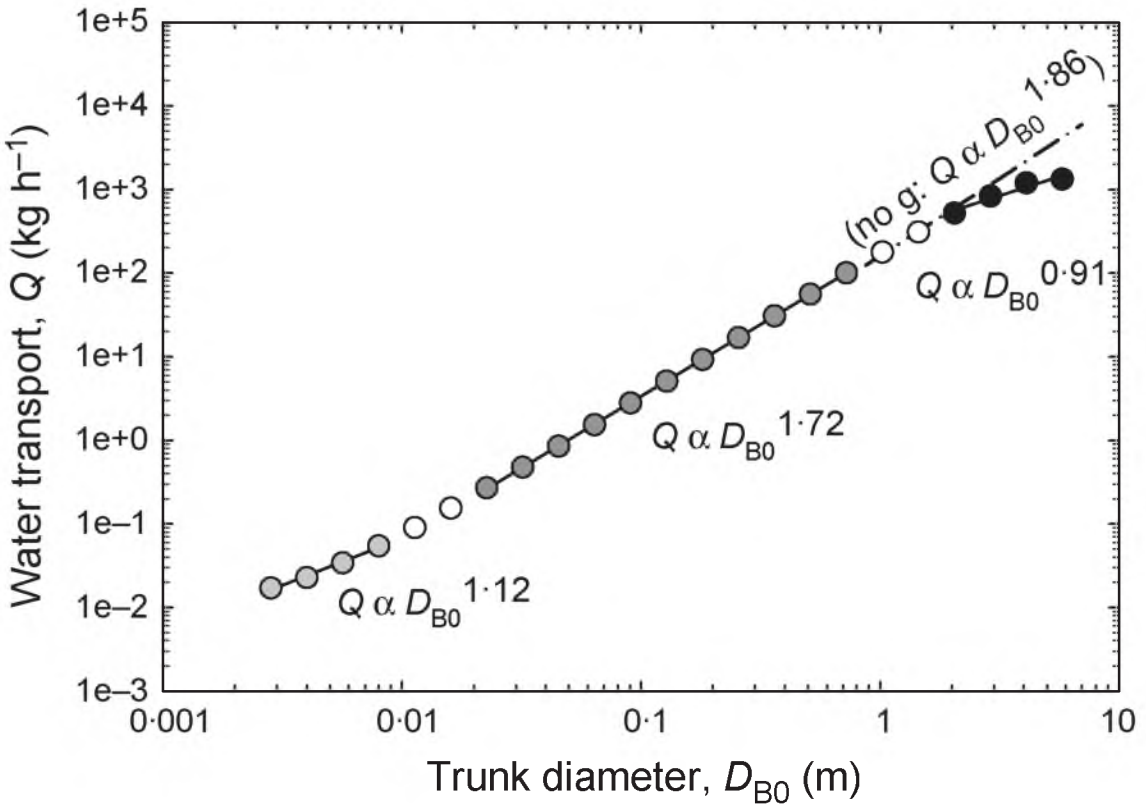

Figure 2.2. Size-dependent variation in the q exponent ($Q \propto D_{B0}^{q}$) for tree water flow rate (Q) and trunk diameter (D_{B0}) in modeled trees. Small trees exhibit flat scaling because of the nonelastically similar growth of juveniles. Medium trees are steepest because they are elastically similar and have small gravity effects. The tallest trees flatten again because of larger gravity effects, unless there is gravity compensation (dash-dotted no g line).

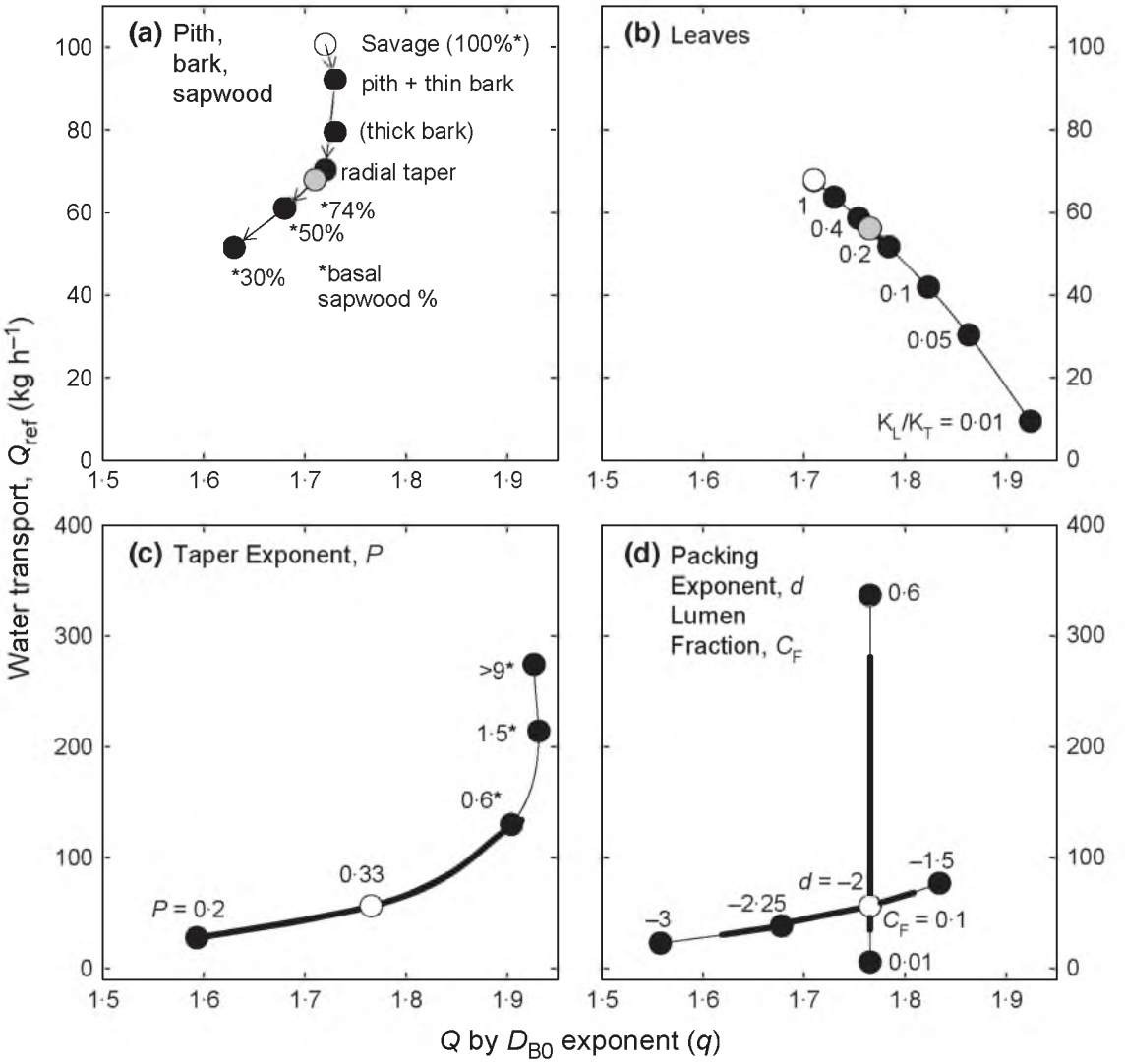

Figure 2.3. Effect of individual hydraulic traits on tree sapflow rate (Q_{ref}, at trunk diameter $D_{B0} = 72$ cm), and the Q by D_{B0}^{q} scaling exponent, q, for medium-sized trees. (a) Cumulative effects of adding pith and thin bark, radial taper and sapwood of decreasing percentage of basal area (at $D_{B0} = 72$ cm) to the Savage et al. model (open symbol). Thick bark shown separately. Grey 74% sapwood point is default for b. (b) Adding leaves of decreasing conductance (K_L) relative to twigs (K_L/K_T) decreased Q_{ref} and increased exponent q. Thick line is probable range of K_L/K_T, grey datum is default K_L/K_T (0.3) for c,d. (c) Increasing the conduit diameter taper exponent, p, makes wider conduits proximally (Eqn. 2.5) and increased Q_{ref} and q. Open symbol is default. Asterisked p exponents required proximal conduits to be capped at $D_C\ max = 240\ \mu$m. Thick line is realistic range of exponent, p. (d) Varying the packing exponent, d, (Eqn. 2.6) had a large effect on the q exponent, but little effect on Q_{ref} compared to changing the fraction of conducting wood area (C_F). Thick lines indicate realistic ranges of d and C_F.

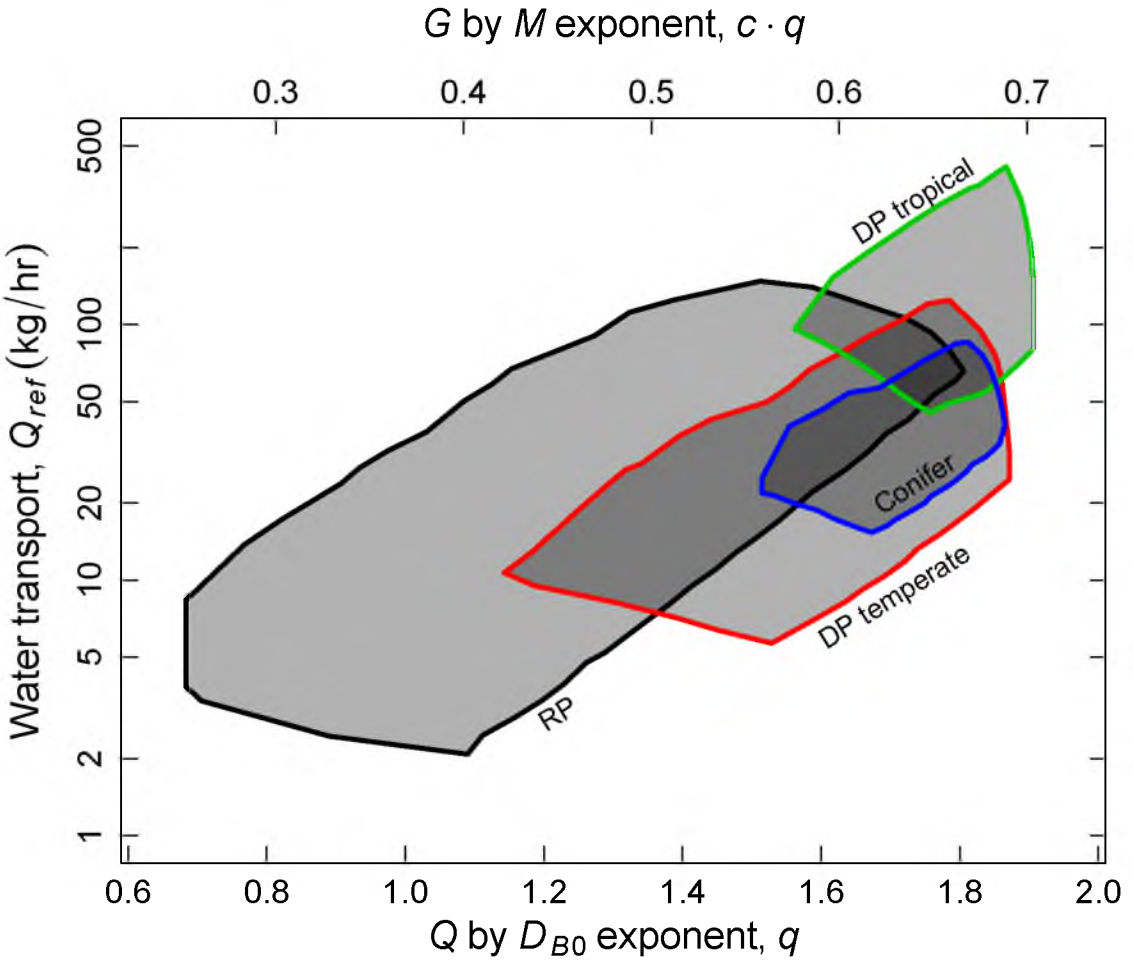

Figure 2.4. Scaling space showing tree water transport rate (Q_{ref}, at trunk $D_{B0} = 72$ cm) and the scaling exponent q ($Q \propto D_{B0}^{q}$) for four functional types. Considerable overlap existed between conifers (blue), temperate diffuse-porous (red), ring-porous (black, RP) and tropical trees (green). The corresponding growth rate by mass exponent (cq) is given on the upper axis. Parameter ranges defining these tree types are given in Table 2.3.

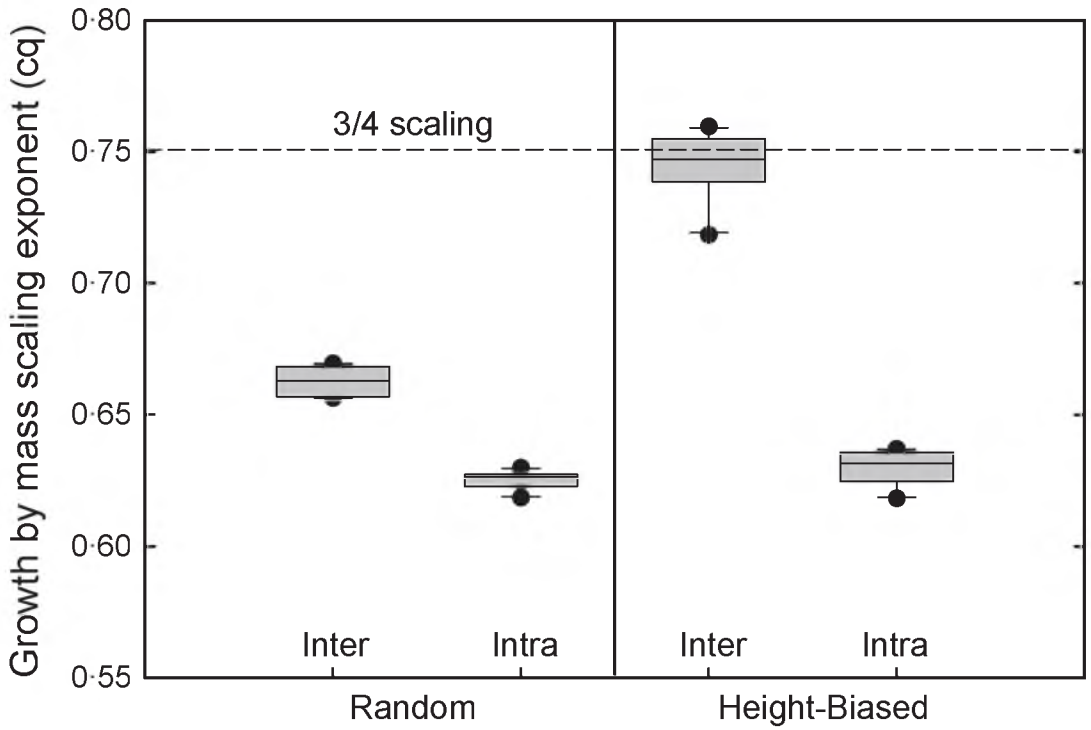

Figure 2.5. Interspecific vs. intraspecific metabolic scaling exponents (cq). Exponents obtained from $n = 10$ repetitions of the regression in Fig. S2.2 (Supporting information, S2.3). Symbols are outliers, whisker is 10th/90th percentile, box is 25th/75th percentile, line is median. Intraspecific scaling is not influenced by whether there was a random relationship between species scaling and stature, or a height-biased relationship where species with steeper and higher scaling (upper right of Fig. 2.4 scaling space) also reached greater size. The latter "height-biased" scenario greatly steepened interspecific scaling and was the only interspecific sampling scheme that could yield exponents matching three-fourth power scaling (dashed line).

S2 Supporting information

S2.1 Size-dependent water use allometry

Figure S2.1A shows the height (H) by trunk diameter (D_{B0}) allometry of modeled trees, which converges on elastic similarity ($H \propto D_{B0}^{2/3}$) with size. Figure S2.1B shows the consequences of this for tree volume (V, and by implication, tree mass, M) scaling with D_{B0}. Trees converge on the expected $c = 3/8 = 0.375$ value for elastic similarity. Trees of the medium size range (gray symbols), which show approximately linear scaling in log-log space (text Fig. 2.2) have $c = 0.369$ rather than the asymptotic $c = 0.375$, which is approached in very large trees.

S2.2 Functional tree types in scaling space

Inputs for the packing and taper functions, including the vessel lumen fraction (C_F), were taken from the survey data set of McCulloh et al. (2010) with additional data from the companion paper (von Allmen et al. 2012) and Sperry et al. (2008). The taper function yielded mean twig conduit diameters (D_C *twig*) per type for a fixed twig diameter of 2 mm (default, text Table 2.2). The D_C *twig* was allowed to vary ± 20% of the mean value per type (text Table 2.3, D_C *twig* range in parentheses). Because the packing and taper functions were determined on smaller trees, they were not necessarily reliable predictors of the maximum vessel diameter in major branches and trunk (D_C *max*). Instead, we obtained the type-specific range of D_C *max* for the same species from the "inside wood" data base (InsideWood, 2004-onwards and published on the Internet at http://insidewood.lib.ncsu.edu/search) and from Panshin & de Zeeuw's textbook 1970. For species in the McCulloh et al. data set that were missing from these sources, we substituted con-generic species. The maximum D_C *twig* and minimum D_C *max* within a functional type dictated the minimum taper exponent (p) for that tree type. The upper value of p for each functional type was set to the maximum from the literature, but the trunk D_C was never allowed to exceed the largest D_C *max* for that tree type (Table 2.3). The packing function was constrained to stay within the cited range of packing exponent d while not violating the literature values of C_F.

Sapwood functions were obtained from several sources (Bovard et al. 2004; Gebauer et al. 2008; Hultine et al. 2010; von Allmen et al. 2012). Functions for tropical and temperate diffuse-porous trees and conifers were all constrained to initiate heartwood at D_{Bi} between 2 and 6 cm and to yield basal sapwood areas within cited fractions of total basal area (A_S/A_T) for the reference trunk $D_{B0} = 72$ cm. For lack of information to the contrary, all three of these tree types were given the same range of sapwood functions. In ring-

porous trees, sapwood is limited to the single current year's growth ring (Ellmore & Ewers 1986; Zimmermann 1983). Ring-porous sapwood functions were accordingly constrained to initiate heartwood beginning in the first branch rank proximal to the twigs, and to yield the much lower range of A_S/A_T reported for these species.

In lieu of more information of the leaf-twig conductance ratio (K_L/K_T), we used the same range for this ratio for each category (Table 2.3). This range was a slight expansion of the range reported for the ring-porous *Quercus gambelii* (0.27) and diffuse-porous *Acer grandidentatum* (0.38) in the companion paper (von Allmen et al. 2012).

S2.3 Intra- vs. interspecific scaling

Each data set sampled from the assemblage of theoretical species in Fig. 2.4 of the text had 100 species. As noted in the text, species with $q < 1.5$ were excluded on the grounds they would be unlikely to exist. For each species we assumed a uniform distribution (on log scale) of 11 tree trunk diameters from $2 < DB0 < 72cm$ (e.g., the medium size class, text Fig. 2.2). An RMA regression through the log-transformed data ($n = 1100$ trees; 11 trees from 100 species) yielded the interspecific scaling exponent for q (D_{B0} by Q values, Fig. S2.2) and c (D_{B0} by M values). The 100 species sampling was repeated 10 times for the "random" and "height-biased" scenarios to obtain an average interspecific exponent (text Fig. 2.5). The intraspecific q exponent was averaged across the 100 sampled species. A random multispecies data set of Q by D_{B0} ($n = 1100$ trees) is shown in Fig. S2.2 (grey symbols). The RMA slope through such data sets gave an average interspecific $q = 1.81 \pm 0.0048$ (mean $\pm$ SE), which was about 6.6% greater than the intraspecific mean of $q = 1.69 \pm 0.0029$.

In the "height-biased" scenario, species with greater Q_{ref} and q (towards upper right in Fig. 2.4) were assumed to achieve greater stature than species with lower values (towards the lower left). Data sets of 100 species were randomly sampled from Fig. 2.4 of the text along an arbitrary diagonal running from lower left to upper right. The particular diagonal used for coefficients shown in text Fig. 2.5 was $Q_{ref} = 0.00033e^{7.2q}$. The D_{B0} range for species with progressively greater q was increased to reflect their greater maximum stature. We assumed that all species achieved a D_{B0} up to 0.128 m, but as q increased from 1.5 to the maximum of 1.91, the maximum D_{B0} for that species increased to 0.724 m. The bias towards steeper scaling in the taller species can be seen in Fig. S2.2 by comparing the black "coupled" species with the gray "random" ones. The RMA interspecific regression yielded an average $q = 2.039 \pm 0.0107$ vs. the intraspecific mean of $q = 1.71 \pm 0.0055$. Altering the diagonal coupling between q and Q_{ref} and altering the q-dependence of species stature yielded a wide range of exponents, even exponents greater than three-fourth. If, however,

there was no species size bias along the diagonal, the result was equivalent to the "random" scenario (simulations not shown).

The analogous process was used to generate interspecific estimates of the mass scaling exponent, c. Each species sampled for q had a common D_{B0} by V^c scaling, where $c = 0.369$ (Fig. S2.1, medium size trees). This universal scaling was converted to a species-specific $D_{B0} = k_1 M^c$ scaling by assuming that $M = V \cdot$ wood density. Wood density values were randomly assigned to each species in the multispecies data set from the 16468 values in the database of Zanne et al. (2009; http://datadryad.org/handle/10255/dryad.235; Chave et al. 2009). An RMA linear regression through log-transformed D_{B0} by M values in the data set yielded the interspecific c. No size bias was assumed with mass exponent c, in keeping with the observation that wood density does not covary with the critical buckling height, H_B (McMahon 1973; Niklas 1994). For the mass scaling exponent, c, there was little difference between interspecific c ($c = 0.367$) vs. intraspecific c (0.369) because wood density of most species in the randomly sampled data set fell within a limited span (613 ± 176 kg m^{-3},mean $\pm$ SD) despite a fairly wide total range (80 to 1360 kg m^{-3}; Zanne et al. 2009). Multiplying the q estimates by c for the same trees yielded the metabolic scaling exponent: $G \propto M^{cq}$. These are cited in the text (Fig. 2.5) for the random and height-biased sampling scenarios.

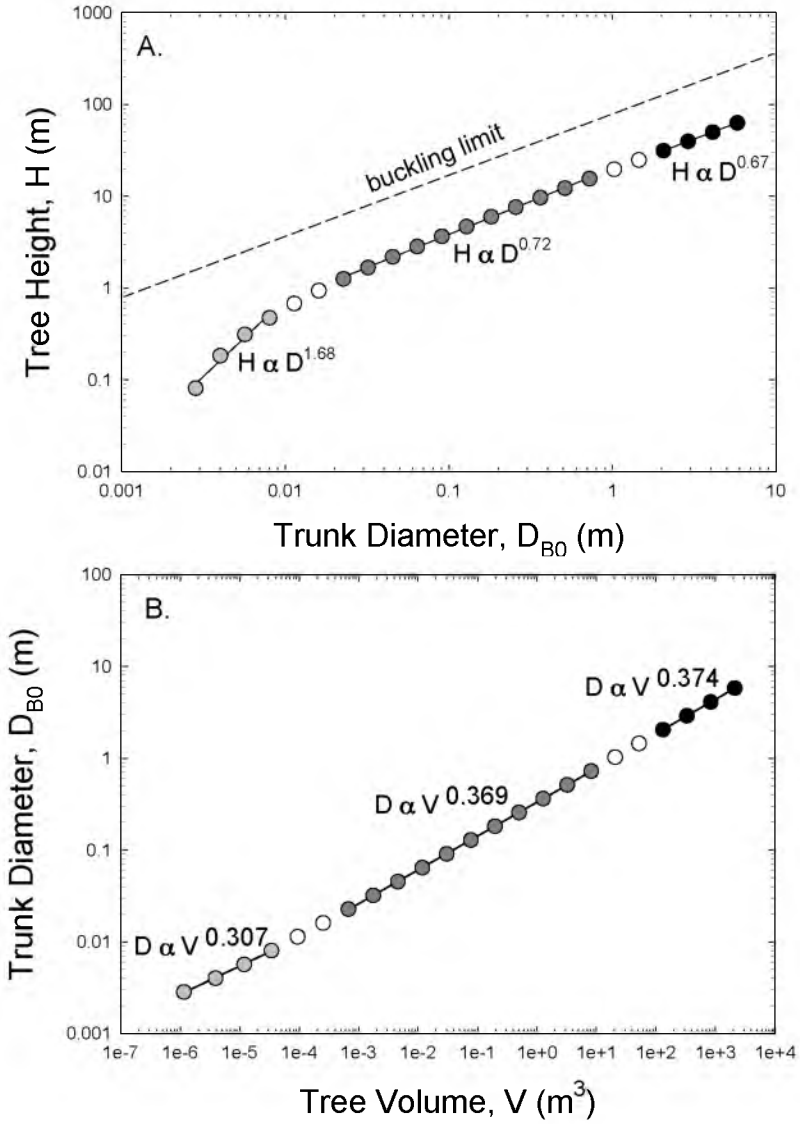

Figure S2.1. Size-dependent deviations from power-law scaling of modeled tree geometry. Trees are grouped into small (gray), medium (dark gray), and large (black) sizes to show changes in best-fit power-law scaling exponents. A. Modeled tree height (H) converges on linear scaling (in log-log space) with trunk diameter (D_{B0}) with size as required to maintain a constant safety margin from elastic buckling. B. Size-dependent variation in the c exponent ($D_{B0} \propto V^c$) for trunk diameter (D_{B0}) and tree volume (V). The same exponent applies to tree mass (M) for constant branch tissue density. Scaling converges on $c = 3/8 = 0.375$ as tree size increases.

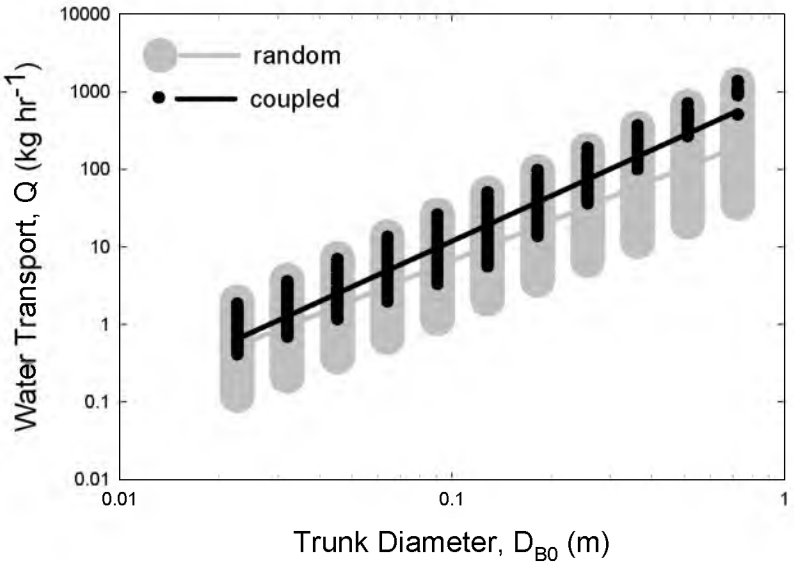

Figure S2.2. Interspecific simulations of the relationship between tree water transport rate (Q) and trunk diameter (D_{B0}). Grey represents 100 randomly chosen "species" (Q by D_{B0} allometries from text Fig. 2.4), each with 11 individuals of different trunk diameter. Although individual data points are obscured, the important point is the similarly broad Q range across all D_{B0} in the "random" scenario. A single RMA regression (q = slope of gray line) through all $n = 1100$ data points yields the interspecific exponent: $Q \propto D_{B0}^{q}$. Black represents species with coupling between Q_{ref} and q and species stature. Species that achieve larger D_{B0} also had greater Q_{ref} and q. Hence, the Q range of the tallest trees is biased upward compared to the random scenario.

CHAPTER 3

DEVIATION FROM SYMMETRICALLY SELF-SIMILAR BRANCHING IN TREES PREDICTS ALTERED HYDRAULICS, MECHANICS, LIGHT INTERCEPTION AND METABOLIC SCALING

3.1 Summary

- The West, Brown, Enquist (WBE) model derives symmetrically self-similar branching to predict metabolic scaling from hydraulic conductance, K, (a metabolism proxy) and tree mass (or volume, V). The original prediction was $K \propto V^{0.75}$. We ask whether trees differ from WBE symmetry and if it matters for plant function and scaling. We measure tree branching and model how architecture influences K, V, mechanical stability, light interception and metabolic scaling.

- We quantified branching architecture by measuring the path fraction, P_f: mean / maximum trunk-to-twig pathlength. WBE symmetry produces the maximum, $P_f = 1.0$. We explored tree morphospace using a probability-based numerical model constrained only by biomechanical principles.

- Real tree P_f ranged from 0.930 (nearly symmetric) to 0.357 (very asymmetric). At each modeled tree size, a reduction in P_f led to: increased K; decreased V; increased mechanical stability; and decreased light absorption. When P_f was ontogenetically constant, strong asymmetry only slightly steepened metabolic scaling. The P_f ontogeny of real trees, however, was "U" shaped, resulting in size-dependent metabolic scaling that exceeded 0.75 in small trees before falling below 0.65.

Reprinted with permission from John Wiley & Sons. Smith D.D., Sperry J.S., Enquist B.J., Savage V.M., McCulloh K.A. & Bentley L.P. (2014) Deviation from symmetrically self-similar branching in trees predicts altered hydraulics, mechanics, light interception and metabolic scaling. *New Phytologist* 201, 217–229.

- Architectural diversity appears to matter considerably for whole tree hydraulics, mechanics, photosynthesis, and potentially metabolic scaling. Optimal architectures likely exist that maximize carbon gain per structural investment.

3.2 Introduction

A large and growing body of research has focused on the coordination of hydraulic transport with the metabolism of photosynthesis and growth. While empirical research on this subject is quite extensive (e.g., Brodribb 2009), a prominent component is metabolic scaling theory (MST), which stems from the original development by West, Brown, & Enquist (WBE hereafter; 1997, 1999). The theory, as it applies to plants, centers on the premise that water transport is a colimiting factor for photosynthesis. Because water transport is a largely physical process dependent in part upon transport network structure, its scaling can be predicted from relatively simple allometric models, leading to scaling predictions for all dependent metabolic processes.

The WBE model is fairly simple in its design. Plant branching structure is divided into external and internal components. The external structure follows symmetrical and self-similar branching (see Fig. 3.1a, rightmost tree), which allows the structure to be easily scaled. The external structure also conforms to biomechanical principles of area preservation and safety from gravitational buckling. The internal branching structure is the network of xylem conduits within the branches. The number and dimensions of xylem conduits are linked by simple rules to the external branch network (Savage *et al.* 2010; Sperry *et al.* 2012).

Central to MST are relationships described by power functions of the form $y = ax^b$ where a is a scaling multiplier and b is a scaling exponent. Oftentimes, the focus is on the proportionality, $y \propto x^b$. The WBE model's prominent achievement is the analytical prediction in agreement with at least some empirical observations (Niklas & Enquist 2001) that metabolic rate (B) scales with mass (M) to the three-fourth power (i.e., $B \propto M^{3/4}$; symbol definitions repeated in Table 3.1). This scaling prediction may be broken into two separate components that individually relate mass and water use to the easily measured dimension of trunk diameter, D_T.

The stem mass (and volume, V) is assumed to scale with $D_T^{1/c}$. This "volume exponent," c, is predicted to converge on 3/8, which is supported by theoretical and empirical considerations (McMahon & Kronauer 1976; von Allmen *et al.* 2012). The rate of water use, Q, is assumed to scale with D_T^q. The model predicts Q from whole tree hydraulic conductance, K, which is calculated from internal vascular allometry. If the flow-induced

pressure drop from soil to leaf is size invariant, then $K \propto Q$. Because water loss and CO_2 uptake utilize the same stomatal pathway, carbon assimilation should have a direct relationship to Q. If a constant fraction of photosynthate goes towards growth (a proxy for B) the result is $B \propto Q \propto K \propto D_T^q$. The product of the "hydraulic exponent," q, and c gives the "metabolic exponent," cq: $B \propto Q \propto K \propto M^{cq}$. The WBE derivation of $cq = 0.75$ arises from the prediction that q converges on 2 for infinitely large trees. Thus, $c = 3/8$, $q = 2$, and $cq = 0.75$. Smaller values of q (0.68 to 1.91) and, hence, cq (0.25 to 0.70) are predicted for finite trees (Savage *et al.* 2010; Sperry *et al.* 2012).

Since its creation, revisions have been made to the WBE model, which have dealt with altering the branching structure within the confines of perfect symmetry (Price *et al.* 2007) and making the internal anatomy more realistic. The anatomical modifications have included more accurate scaling of xylem conduit number (Savage *et al.* 2010) and the addition of leaves, roots, and nontransporting tissues (Sperry *et al.* 2012). These revisions have led to more accurate predictions (Price *et al.* 2007; von Allmen *et al.* 2012) but trees were still assumed to follow symmetrically self-similar branching. Real trees show average branching ratios (daughter/mother branch number, diameter, and length) that can be similar to the constants predicted by WBE's symmetric self-similarity (Bentley *et al.* 2013). However, the distributions are quite broad, indicating a sizable fraction of asymmetric junctions. Even a few asymmetric junctions amongst major branches could significantly alter whole-tree symmetry.

We ask whether the branching architecture of real plants deviates substantially from the WBE structure. We then address the consequences of deviation with a model. We use the WBE model as a reference point and develop a novel numerical simulation method for building trees that represent the full range of tree morphospace from WBE symmetry to maximal asymmetry. Our numerical approach uses a minimum of deterministic branching rules and instead relies on probability distributions to build branch junctions and trees of varying symmetries. Our only major branching assumptions are that trees conform to the well established patterns of area-preserving branching (Horn 2000) and network-scale elastic similarity (McMahon & Kronauer 1976). We use the improved internal anatomy of Sperry *et al.* (2012) but hold xylem parameters constant across simulated trees so as to isolate branching effects. We use the numerical model to investigate how deviations from WBE branching affect whole tree hydraulic conductance, total stem volume, safety from gravitational buckling, and light interception. The model is also used to predict the influence of branching architecture on the scaling of tree hydraulic conductance (exponent

q) and volume (exponent c) with trunk diameter, and hence how hydraulic conductance and its dependent processes scale with mass (exponent cq).

3.3 Methods and model description

3.3.1 The path fraction index for tree form

We developed the "path fraction," P_f, to quantify how much a particular branch network deviated from the WBE ideal. The path fraction is based on the pathlengths from twig tip to trunk base. We use the symbol, $L_{\updownarrow}$, for this pathlength where the double arrow indicates that this length spans two extremes, twig tip to trunk base. In a WBE tree, all values of $L_{\updownarrow}$ are the same. In our model, deviating from WBE by removing junction symmetry adds variation to $L_{\updownarrow}$. We define the path fraction as

$$P_f = \frac{\bar{L}_{\updownarrow}}{L^*_{\updownarrow}} \tag{3.1}$$

The bar in $\bar{L}_{\updownarrow}$ refers to the mean $L_{\updownarrow}$ for the tree and the asterisk in $L^*_{\updownarrow}$ (and other symbols that follow) indicates the maximum. The $L^*_{\updownarrow}$ is an approximation of plant height so we will also use this symbol for height. The maximum possible P_f is 1, which occurs when $\bar{L}_{\updownarrow} = L^*_{\updownarrow}$ (e.g., WBE trees; see Fig. 3.1a, rightmost tree). A high P_f corresponds to a round-shaped, spreading crown while a low P_f corresponds to a narrow crown with limited spread (Fig. 3.1). The minimum P_f is made by a structure with a central axis with twigs attached alternately. This structure minimizes $\bar{L}_{\updownarrow}$ and we refer to it as the "fishbone" structure (e.g., Fig. 3.1a, leftmost tree). We use P_f as the independent branching structure variable against which we plot the functional attributes of tree hydraulic conductance, volume, mechanical stability, and light interception.

3.3.2 Empirical path fractions

As a test of how much real plants deviate from the WBE structure, 40 P_f measurements were made of real branch systems. Specimens came from 15 different species and included both whole individuals and branches of open-grown trees and shrubs (species and sources in Table 3.2 and Supporting information, S3.1). Species were chosen to represent a wide range of apparent architectures. Branches were obtained by a single cut just distal to a branch junction. Path fractions were obtained in two ways. For some (mostly the entire individuals), each segment between branching points was labeled and its length, diameter, and mother segment were recorded. Twig-to-base paths were then reconstructed from these data to get all $L_{\updownarrow}$ values. For the other specimens, $L_{\updownarrow}$ values were measured directly by

following stems from base to twig tips using a marked string with 10 cm precision. For this direct method, specimens were measured in spring so the measurements were made to tips that appeared to have been active the previous season.

Direct P_f measurements were time-consuming, limiting the size range to trees with trunk diameters, D_T, $< ca.$ 5 cm. To estimate the P_f of larger trees to trunk diameters over 1 m, we used the crown area vs trunk diameter data set of Olson *et al.* (2009; see Supporting information, Fig. S3.1) from angiosperm trees. From their published data (including all branches and trees in sheltered and salt-sprayed environments), we obtained an ordinary least squares (OLS) regression to predict vertically projected crown areas from D_T. We matched these predictions to 3D modeled trees with the same D_T and within 5% of the same crown area. The P_f from these matching model trees were used to construct a P_f ontogeny.

3.3.3 Tree building model

3.3.3.1 Branching

Our tree building model was written in the R language (R Core Team 2013) and is available from the senior author upon request. The model begins by sequentially defining junctions, starting with the trunk. At each junction, the mother branch (subscript m) splits into a number of daughters (subscript d). The number of daughters is f, the furcation number. Within each tree, we randomly chose a maximum furcation, f^*, and then at each junction we chose f from 2 to f^*. The f^* was 2, 3, or 4, which covers the range for most botanical trees. Our f selection contrasts with the WBE model, which uses a strictly constant f (n in their terminology). We assigned each branch an order or rank, R, equal to the number of twigs it ultimately supports (Katifori & Magnasco 2012). Therefore, the starting point of each tree, the trunk, has R_m = the total number of twigs on the tree. This ranking system, illustrated in Fig. 3.2, simplifies tree building because: R is a finite integer; branch ranks change at each junction; and total rank is preserved across junctions. Each combination of mother rank, R_m, and f defines possible daughter ranks, R_d. Each daughter can only take on a certain number of different ranks because the sum of R_d must equal R_m. The first selected daughter rank, $R_{d,1}$, was always the smallest and was restricted to the range, A_1 to Z_1, where $A_1 = 1$ and

$$Z_1 = \lfloor \frac{R_m}{f} \rfloor \tag{3.2}$$

where the floor brackets indicate the integer of the ratio. For subsequent daughter ranks, $R_{d,i}$, where $1 < i \leq f$, the Z_i is given by

$$Z_i = \left\lfloor \left(R_m - \sum_{j=1}^{i-1} R_{d,j} \right) / (f - i + 1) \right\rfloor \tag{3.3}$$

Equation 3.3 is just a variation on Eqn. 3.2 where the numerator accounts for the fact that there is "less rank" remaining to divide and the denominator indicates the "remaining rank" is being divided among fewer undefined daughters. The intermediate values of A_i (if present) are different from the first and final A_i. For $1 < i < f$, the $A_i = R_{d,i-1}$ as no daughter may be smaller than its predecessor. For the final daughter in the furcation, $R_{d,f}$, the $A_f = Z_f$ such that $R_{d,f}$ can only take on a single value that completes the mother rank.

The choice of R_d in each junction determines the symmetry of that junction. We controlled this choice by using a discrete probability distribution function to select each $R_{d,i}$ at random from its respective A_i to Z_i range. We defined this probability distribution with a power function because changing the exponent, u, allowed us to control the degrees of symmetry or asymmetry. When $u \leq 0$, the probability, P, of any R_d is given by

$$P_{R_d} = R_d^u / \sum_{j=A}^{Z} j^u \tag{3.4}$$

When $u > 0$, a slightly different equation is used,

$$P_{R_d} = (Z - A + R_d)^{-u} / \sum_{j=A}^{Z} (Z - A + j)^{-u} \tag{3.5}$$

For a given $u > 0$, Eqn. 3.5 takes the probabilities from Eqn. 3.4 with $-u$ and mirrors them over the same A to Z range. For example, comparing $u = 2$ to $u = -2$ in a junction, $P_{R_d=A}$ when $u = 2$ is equal to $P_{R_d=Z}$ when $u = -2$. When $u < 0$, asymmetrical junctions are favored while $u > 0$ favors symmetry. Using Eqns. 3.4 and 3.5 with a u range of -5 to 5 created trees that populated the P_f range from maximum asymmetry ("fishbone" trees) to perfect symmetry (WBE trees). For a given tree, we fixed u at a single value. When u was varied within a tree to produce both strongly symmetric and asymmetric junctions, the generated trees were unrealistic (Supporting information, Fig. S3.2).

As an illustration of the daughter selection process, consider the circled junction in Fig. 3.2 (left tree). This tree has 10 twigs total and $u = -2$ was selected at random from -5 to 5. First, $f^* = 3$ was selected from 2, 3, or 4 with equal probability. The f of the first junction (the trunk; with $R_m = 10$) was chosen between 2 and f^* with equal probability. Choosing $f = 3$, the rank of the smallest daughter, $R_{d,1}$, was selected next. Because $R_{d,1}$ is the smallest and all daughters must add to 10, $R_{d,1}$ must be between 1 (A_1) and 3 (Z_1), as given by Eqn. 3.2. With negative u, $R_{d,1} = 1$ will have the greatest probability

($P_{R_{d,1}} = 0.735$ from Eqn. 3.4) and 3 will be very unlikely ($P_{R_{d,1}} = 0.082$). Suppose $R_{d,1} = 1$ is chosen. The second daughter, $R_{d,2}$ is the next smallest so it may range from 1 to 4, as given by Eqn. 3.3. Again, the minimum, 1, is most likely to be chosen. Here, $R_{d,2} = 2$ was chosen. The final daughter has only one option, $R_{d,f} = 7$, resulting in a fairly asymmetrical junction. After creating this first junction, each daughter with $R_d > 1$ became a mother and junction selection continued, keeping $f^* = 3$ and $u = -2$. The right tree in Fig. 3.2 shows how $u = +2$ can create much more symmetrical junctions.

3.3.3.2 Branch diameters

After assigning all ranks, branch diameters and lengths were determined. Diameters were defined using constant twig diameters and area-preservation (i.e., $D_m^2 = \sum_{i=1}^{f} D_{d,i}^2$). With R defined as the total number of supported twigs, each with constant cross-sectional area, R is proportional to the cross-sectional area of the branch. As such, diameter, D, is a function of R and twig diameter, D_t:

$$D = D_t R^{0.5} \tag{3.6}$$

This property is illustrated by the trees in Fig. 3.2 where diameters increase with R.

3.3.3.3 Branch lengths

Length determination is more complicated but the guiding principle is that lengths must coordinate with diameters to achieve a constant safety factor from whole tree elastic buckling from gravity. Here, we define a new pathlength, $L_{\uparrow}^*$, where the upward arrow indicates this length is from branch base (i.e., just above its lower junction) up to twig tip. This contrasts with the double arrow in $L_{\updownarrow}$, which indicates trunk to twig path. The asterisk in $L_{\uparrow}^*$ signifies the maximum pathlength (i.e., to the most distant twig).

Empirical data indicate that once a trunk or branch reaches a modest D, its longest supported path, $L_{\uparrow}^*$, tends to scale as $L_{\uparrow}^* \approx aD^{2/3}$ (Niklas 1994; von Allmen *et al.* 2012). The exponent of 2/3 is consistent with elastic similarity (i.e., constant deflection per length; McMahon & Kronauer 1976). The critical height at elastic buckling, L_{crit}, is also predicted to follow 2/3 scaling with D: $L_{crit} = bD^{2/3}$, where b can be explicitly calculated from tree form and wood properties (Greenhill 1881). The shared 2/3 exponent means the safety factor from buckling ($L_{crit}/L_{\uparrow}^*$) becomes constant at larger D. This ultimately constant safety factor, s, is equal to the ratio of the scaling multipliers: $s = b/a$. At smaller D, however, the $L_{\uparrow}^*$ by D scaling is steeper than 2/3. McMahon & Kronauer (1976) attribute this steeper exponent to a "virtual length," l_o. If the tree is represented as an elastically

similar doubly tapered beam, then l_o is the distance from the free end of the beam (i.e., the twig tip) to the point where the beam would taper to zero at its theoretical origin. McMahon & Kronauer (1976) show that $L^*_\uparrow$ by D scaling across all D can be fit by an equation of the form:

$$L^*_\uparrow = aD^{2/3} - l_o \tag{3.7}$$

As D increases, the l_o term becomes comparatively negligible and the equation converges to $L^*_\uparrow = aD^{2/3}$ (see Supporting information, Fig. S3.3).

Branch lengths were assigned from a single version of Eqn. 3.7 (Eqn. 3.8) that was applied across all trees regardless of their branching topology. The multiplier, a, was defined as $a = b/s$, where $s = 4$ and b was calculated from a WBE tree ($b = 107.94$ m$^{1/3}$; see Mechanical stability of model trees section). The value of l_o was derived from WBE trees (see Supporting information, S3.2) and plugged into Eqn. 3.7 to produce the $L^*_\uparrow$ by D equation for all modeled trees:

$$L^*_\uparrow(D) = \frac{b}{s}D^{2/3} - 0.794\frac{b}{s}D_t^{2/3} \tag{3.8}$$

Equation 3.8 gives maximum length distal to each branch segment and from this, individual branch lengths (i.e., between junctions) were determined. At a given junction, the mother branch will have a certain $L^*_\uparrow$ and its daughters will have respective $L^*_\uparrow$ values. Because larger diameters support longer paths, it will be true that the daughter with the largest diameter, D^*_d, will be part of the mother's longest path. Therefore, the segment length of the mother, l_m, is

$$l_m = L^*_\uparrow(D_m) - L^*_\uparrow(D^*_d) \tag{3.9}$$

Twigs, which do not support daughters, have lengths equal to their $L^*_\uparrow$:

$$l_t = L^*_\uparrow(D_t). \tag{3.10}$$

The use of Eqn. 3.9 can be illustrated by the left tree in Fig. 3.2. The trunk ($R_m = 10$) supports a maximum path of $L^*_\uparrow = 0.58$ m (using model parameters in Eqn. 3.8). Of its three daughters, only the largest daughter ($R^*_d = 7$) lies along this path. This daughter supports a maximum path of $L^*_\uparrow = 0.48$ m. Therefore, the length of the trunk segment must be the difference: $l_m = 0.10$ m.

3.3.4 Hydraulic conductance of model trees

The hydraulic conductance, K, for each model tree was calculated from the internal network of xylem conduits. The internal anatomy is defined from the external anatomy

following the recent WBE revision by Sperry *et al.* (2012). Briefly (see Supporting information, S3.3 for details), hydraulic conductance of each stem segment is calculated from the diameter, number, and length of functional xylem conduits (Savage *et al.* 2010; Sperry *et al.* 2012). Additional hydraulic resistances come from leaves, roots and conduit endwalls (Sperry *et al.* 2012). Segment conductances were combined using rules of network analysis to calculate K.

Sperry *et al.* (2012) used the external branching parameters of WBE to study the effects of variable internal anatomy. Here, we did much the opposite, using the Sperry *et al.* (2012) default internal parameters while studying the consequences of branching pattern and P_f on hydraulic conductance and the hydraulic exponent, q.

3.3.5 Volume of model trees

Tree volumes were calculated to determine their sensitivity to P_f and, hence, the sensitivity of the volume exponent, c. Total stem volume, V, was the summed volume of all cylindrical branch segments. The volume of roots and leaves was not computed but assumed proportional to stem volume. If tissue density is invariant, then V becomes a proxy for stem (and plant) mass for purposes of metabolic scaling predictions.

3.3.6 Mechanical stability of model trees

The effect of branching structure on mechanical stability was assessed for all model trees by comparing estimated critical heights at elastic buckling (L_{crit}) relative to estimated L_{crit} of WBE trees ($L_{crit,WBE}$). Typically, L_{crit} is estimated by folding all branches up to make a column and assuming the tree mechanically behaves as this column (Niklas 1994). Furthermore, this column is assumed to have straight sides. To represent the full spectrum of more realistic trees, we used the alternative method of Jaouen *et al.* (2007), which identifies the "main stem" (i.e., the thickest trunk-to-twig path) as the tallest mechanical structure that must support itself and all attached branches. The Jaouen *et al.* method accounts for the important effects of branching architecture on vertical mass distribution and L_{crit}. The diameter, D, of the main stem may be described as a function of height, z, using

$$D = D_T \left(1 - \frac{z}{L_{\updownarrow}^*}\right)^n \tag{3.11}$$

Likewise, the stem mass of all branches supported above z may be defined by

$$M = M_{tot} \left(1 - \frac{z}{L_{\updownarrow}^*}\right)^m \tag{3.12}$$

where M_{tot} is the total tree stem mass. The exponents n and m approximate the distributions of support capacity (D) and support requirement (M) in the main stem. For each tree, these exponents were calculated from Eqns. 3.11 and 3.12 by standardized major axis (SMA) regression of logged data using the SMATR package for R (http://bio.mq.edu.au/ecology/SMATR/; Warton *et al.* 2006).

With some modifications to Eqn. 1 from Jaouen *et al.* (2007; see Supporting information, S3.4), we predicted L_{crit} using

$$L_{crit} = \frac{c_\nu^{2/3}(|m-4n+2|)^{2/3}}{4P_f^{1/3}} \left(\frac{E}{\rho_g}\right)^{1/3} D_T^{2/3} \tag{3.13}$$

Values for the ratio of E (Young's elastic modulus; N m^{-2}) and ρ_g (specific weight of supporting tissue; N m^{-3}) for wood are approximately constant (Niklas 1994). The c_ν (determined numerically in R) is the first positive root of the Bessel function of the first kind with parameter $\nu = (4n-1)/(m-4n+2)$ (Greenhill 1881; Jaouen *et al.* 2007). The value of b in Eqn. 3.8 corresponds to all the terms in front of $D_T^{2/3}$ in Eqn. 3.13 where m, n, c_ν, and P_f were from a WBE tree. When calculating L_{crit}, two requirements were imposed. (1) Values of n and m are only meaningful when the data are well fit by Eqns. 3.11 and 3.12. We removed trees where fits had $r^2 < 0.95$. (2) When $\nu < -1$, the c_ν becomes somewhat erratic so these trees were also removed. Less than 7% of all modeled trees were removed for poor fits to Eqns. 3.11-3.12 and only three trees in total were excluded for $\nu < -1$.

3.3.7 Light interception of model trees

The importance of light interception is implied in the WBE model through "space-filling branching" but it has not been quantified (Duursma *et al.* 2010). To estimate how P_f influenced light interception, we extended the model to three dimensions. For simplicity, we restricted 3D construction to trees where $f^* = 2$ was chosen. Determining spatial structure required specification of branching angles and rotations with respect to connecting stem segments. Each branch segment was assigned an axis that runs along its length. "Branching angle" shall refer to the angle a daughter axis makes *away* from its mother's axis. "Rotation" refers to the rotation *around* its mother's axis. We adopted a set of maximally simple rules to set these angles and applied them equally across modeled trees. Thus, we emphasize the general effects of P_f on light interception and not secondary influences of branching angle variation.

To our knowledge, the only work that comes close to a general branching angle theory for plants is Murray's (1927) volume minimization equations (see also Zhi *et al.* 2001).

However, these equations are inconsistent with area-preserving branching (two symmetric, area-preserving daughters are predicted to not diverge at all from their mother's axis). Nevertheless, Murray's (1927) Eqns. 2-3 do produce realistic branch angle trends and so, despite their theoretical short-comings, we used them.

For rotation, daughters diverge from their mother's axis in opposite directions. Therefore, the daughters lie in the same plane. Accordingly, the mother also shares a plane with its sister branch. Each daughter plane was rotated 137.5° relative to its mother plane. The actual angle of rotation will depend on phyllotaxy and exactly which buds are released to form branches. However, our model is not an ontogenetic one and 137.5°, the golden angle, is often observed and may minimize self-shading (Valladares & Brites 2004).

As part of the 3D construction, we calculated crown area by projecting each tree from above and drawing a convex boundary linking the twig tips. Crown areas were used to estimate P_f from angiosperm crown scaling data of Olson *et al.* (2009; see above). We also quantified tree shape as the aspect ratio (height/width). Height was actual height (instead of $L^*_{\updownarrow}$), which was similar for all trees with equivalent twig numbers. Crown width was obtained from the diameter of a circle with equivalent area to the crown area.

The 3D trees were subjected to a light interception model using the turbid medium analogy (Campbell & Norman 1998). Following Sinoquet *et al.* (2001), the 3D space occupied by each tree was discretized into voxels (i.e., 3D pixels) of side length l_{vox}. LAI of each voxel was calculated from the number of twig tips it contained and leaf area per twig (0.01 m^2). Interception by stems was ignored and we only modeled direct light with PPFD = 1500 μmol PAR $m^{-2}s^{-1}$. To address the effect of source angle, we specified zenith angles every 3° from horizontal to directly overhead. For each zenith angle, we averaged light interception from eight azimuth angles. For each source angle, voxels were delineated to form columns parallel to the light source. As such, the LAI of each column of voxels was calculated. Absorbed PAR (μmol s^{-1}) is

$$PAR_{abs} = l_{vox}^2 PPFD \sum_{i=1}^{N_c} [1 - \exp(-G_i\ LAI_i)] \tag{3.14}$$

where N_c is the number of voxel columns and G is the ratio of projected and one-sided leaf area (Sinoquet *et al.* 2001). Leaves were considered spherically arranged, making $G = 1/2$ for all columns and independent of source angle (derived from Monteith & Unsworth 1990).

3.3.8 Scaling predictions

Using K, V, and D_T from the model, we tested how deviation from WBE branching affected the scaling exponents in: $K \propto D_T^q$; $V \propto D_T^{1/c}$; and $K \propto V^{cq}$. We identified three

scaling scenarios (S_1, S_2, and S_3) for the relationship between P_f and tree size. Scenario S_1 was a constant P_f with increasing tree size. Size-invariant P_f is perhaps most comparable to WBE scaling, as WBE trees always have $P_f = 1$. We selected six target P_f values from 0.4 to 1.0. We then modeled 10,000 trees at each of seven twig counts from 2^6 to 2^{12} twigs and isolated trees that had a P_f within 0.005 of each target. For trees with 2^5 twigs or fewer, $P_f = 0.4$ was not possible. The maximum twig number was limited by computation time.

Scenario S_2 modeled the observed decrease in P_f with size from our P_f measurements. In this scenario, we fit a log function to our interspecific P_f vs twig number data. We used this function to choose a target P_f at each modeled size up to 2^9 twigs (near the maximum in our data) and selected individuals that matched each P_f target $\pm$ 0.005.

In scenario S_3, we used the P_f ontogeny estimated from angiosperm crown scaling data in Olson *et al.* (2009). The Olson *et al.* data covered a wider range of tree sizes. To accommodate this range, we built a limited set of 3D trees with up to 2^{18} twigs (D_T = 1024 mm). The subset of modeled trees that followed the crown scaling data showed a P_f-decreasing phase in small trees (as in our empirical measurements), followed by a P_f-increasing phase in larger trees (see Results). We defined the phase boundary at 2^{11} twigs and modeled the scaling exponents separately for each P_f phase: $2^6 - 2^{10}$ twigs (P_f decreasing) and $2^{12} - 2^{18}$ twigs (P_f increasing). For all scaling scenarios, we obtained q, c, and cq from SMA regressions of logged data.

3.4 Results

3.4.1 Measured, modeled and estimated path fractions

The P_f range is bound by WBE trees at the maximum ($P_f = 1$) and "fishbone" trees at the minimum. Among modeled trees, a high P_f corresponded to a broad crown (aspect ratio near one) while low-P_f trees had narrower crowns (larger aspect ratio; Fig. 3.1a,b). Among our 40 P_f measurements from real plants, P_f ranged from 0.357 to 0.930. No specimen met either the WBE prediction or the "fishbone" prediction. There was a significant trend for P_f to decrease with increasing size (Fig. 3.3, characters and solid regression line). While these data included both whole individuals (black) and branches (white), regressions fit to each were not significantly different. Parallel to the observed decline in empirical P_f, the model predicts that as trees add twigs, the minimum possible P_f (the "fishbone" structure) rapidly decreases from 1 before asymptoting around 0.25 (Fig. 3.3, shaded area). It makes sense that the potential to deviate from WBE becomes greater with more twigs. More

twigs equals more and larger junctions and, therefore, more and greater opportunities to be asymmetrical.

Analysis of the Olson *et al.* (2009) data indicated a two-phase P_f trajectory (Fig. 3.3, dashed line). The first phase, in smaller trees ($D_T < ca.$ 6 cm), was a decline in P_f similar to what we measured. The second phase in larger trees showed a bottoming out of P_f followed by a gradual increase for $D_T > ca.$ 12 cm.

3.4.2 P_f and whole tree hydraulic conductance

The model was run to produce 10,000 trees at each of nine different twig counts (2^4 to 2^{12}). However, to illustrate the functional consequences of P_f, we only show 1024-twig trees as a representative. Similar trends were evident at all modeled tree sizes. Deviation from WBE structure (i.e., lower P_f) tended to increase K (Fig. 3.4a) with the "fishbone" structure having the greatest conductance and the WBE structure having the lowest. A more than 2-fold increase was observed across the P_f range in the 1024 twig example with all trees having the same basal diameter and height. As P_f decreased, K increased because the average transport distance from trunk-to-twig decreased. Shorter average transport distances translated into higher average trunk-to-twig conductances. For each tree size, the K vs P_f data were fit with power functions. All fits were very good ($r^2 > 0.98$). Some of the residual K variation was due to f^* with linear regressions of residuals vs f^* producing positive correlations with $r^2 = 0.30 \pm 0.09$ (mean $\pm$ SD). Hence, larger f^* tended to increase K at a given P_f. This is expected because greater f means branches become thicker (i.e., greater hydraulic conductivity) at a faster rate.

3.4.3 P_f and total stem volume

Reducing P_f caused V to decrease in a singularly linear fashion (Fig. 3.4b). Perfect linearity exists because of area-preservation and invariant twig diameters. As such, each $L_{\updownarrow}$ represents a "tube" of tissue with constant volume per length, as in the pipe model (Shinozaki *et al.* 1964). This relationship allowed us to define the volume fraction, V_f, as a corollary to P_f. The stem volume of each tree was standardized by the volume of a cylinder with equivalent height and basal diameter,

$$V_f = \frac{V}{\frac{\pi}{4} L^*_{\updownarrow} D_T^2} \tag{3.15}$$

For modeled trees, $V_f = P_f$. The volume of a WBE tree is that of the reference column (i.e., $V_f = 1$). Other structures have lower V_f due to volumes less than the reference column (i.e., profiles more akin to a frustum).

3.4.4 P_f and mechanical stability

The L_{crit} relative to the WBE tree was lowest near $P_f = 1$ (6.46% lower) and greatest near minimum P_f (30.97% greater; Fig. 3.4c). This P_f-dependent trend was due to the effects of m, n, and total stem mass. The mass distribution exponent, m, was fairly constant across the P_f range: 2.97 ± 0.10 (mean ± SD; $m = 1$ corresponds to a straight column, $m > 1$ to a tapered column). Near $P_f = 1$, m was quite variable, which is reflected in L_{crit} variability near $P_f = 1$ in Fig. 3.4c. Meanwhile, the main stem taper exponent, n, increased as P_f dropped (range = 0.93 to 1.23; $n = 0$ corresponds to a straight column). A larger n indicates stronger taper in the main stem and therefore less support tissue up high. This alone tends to reduce L_{crit}. However, a smaller P_f indicates there is less total mass that requires support and therefore greater L_{crit}.

3.4.5 Light absorption and P_f

Regarding light absorption, PAR_{abs}, we were limited to trees modeled in 3D (i.e., those with $f^* = 2$). Trees with the same number of twigs also have the same total leaf area. Therefore, for a given number of twigs, PAR_{abs} variations are solely due to different leaf arrangements. At a given zenith angle, PAR_{abs} increased with P_f such that "fishbone" trees absorbed the fewest photons and WBE trees absorbed among the most (Fig. 3.4d). This P_f effect increased as the light angle was shifted from horizontal side-illumination to overhead.

3.4.6 Scaling and P_f

We modeled three scaling scenarios: S_1) P_f is constant through ontogeny of a particular species but can vary across species ($P_f = 0.4 - 1.0$; 2^6 to 2^{12} twigs); S_2) P_f decreases through ontogeny both within and across species, following the regression on our P_f data for small trees ($D_T <$ *ca.* 5 cm; 2^6 to 2^9 twigs; Fig. 3.3, solid line); and S_3) P_f decreases in small trees (2^6 to 2^{10} twigs) and reaches a nadir before gradually increasing in larger trees (2^{12} to 2^{18} twigs), as estimated from the Olson *et al.* (2009) data (Fig. 3.3, dashed line). In the three scenarios, the modeled data used for each scaling relationship (K by D_T^q, V by $D_T^{1/c}$ and K by V^{cq}) were well fit by power functions ($r^2 > 0.99$).

The hydraulic exponent, q, was obtained from K by D_T^q relationships. In S_1, where P_f was constant with size, $P_f = 1$ predicted $q = 1.80$, which falls short of the original WBE prediction of $q = 2$ because of finite size effects and revisions to the internal anatomy (Savage *et al.* 2010; Sperry *et al.* 2012). As P_f decreased to 0.4, q increased to 1.85 (Fig. 3.5a); still shy of $q = 2$. In S_2, P_f decreased with size, which caused K to increase at a faster rate than

for constant P_f. Therefore, q steepened to 2.04: very near the WBE requirement. Similarly, in S_3, as P_f decreased, hydraulic scaling steepened relative to constant P_f: $q = 1.96$. However, as P_f increased in larger trees, K increased more slowly and q decreased to 1.81.

Similar results existed for the volume exponent, c, in $V \propto D_T^{1/c}$. In S_1 (P_f constant through ontogeny), c was essentially unaffected by P_f: $c = 0.364 \pm 0.001$ (mean $\pm$ SD; Fig. 3.5b). All values were near but below the WBE prediction of $c = 3/8 = 0.375$. As shown by rearranging Eqn. 3.15, $V = \frac{\pi}{4} V_f L_{\updownarrow}^* D_T^2$ and because $V_f = P_f$, an ontogenetically-invariant P_f makes $V \propto L_{\updownarrow}^* D_T^2$, meaning the scaling exponents among trees or species with different but constant P_f will be identical. Over the modeled size range, $L_{\updownarrow}^*$ by D_T is not a perfect power function because it has yet to converge on $L_{\updownarrow}^* \propto D_T^{2/3}$ (Eqn. 3.8). This fact, combined with a variable number of trees at each P_f-D_T combination, made $c < 0.375$ and created some variation in c. In scenario S_2 (P_f decreases through ontogeny), V increased at a slower rate relative to constant P_f, which lowered $1/c$ and increased c up to 0.41, exceeding the WBE prediction. When P_f decreased then increased (S_3), the decrease produced a steeper c (0.389) followed by a flatter c (0.355) as P_f increased in larger trees.

The metabolic exponent, cq, in $K \propto V^{cq}$, follows the q and c results. When P_f was constant through ontogeny, as in S_1, cq showed a meager increase from 0.655 at $P_f = 1$ to 0.671 at $P_f = 0.4$ (Fig. 3.5c), well below the WBE prediction of $cq = 0.75$ due to the same finite-size effects as above. However, when P_f decreased throughout growth of smaller trees (S_2), the larger q and c together exceeded the WBE prediction of 0.75: $cq = 0.843$. When P_f decreased and then increased with greater tree size (S_3), cq initially exceeded 0.75 (0.760), before decreasing below all other values: $cq = 0.642$ (see Supporting information, Fig. S3.4).

3.5 Discussion

In answer to our opening question, the results show that deviations from symmetrical WBE branching in real trees can be substantial and size dependent and these deviations have major effects on tree function and metabolic scaling. We used the path fraction, P_f, to quantify branching architecture in both real plants and modeled trees. We found that P_f in all of our real networks fell below the WBE ideal of $P_f = 1$. Furthermore, empirical P_f showed a biphasic ontogeny: first decreasing strongly with size before bottoming out at *ca.* $D_T = 6-12$ cm and gradually increasing thereafter. Our model predicted significant effects of deviating from the symmetrical self-similarity of the WBE model. When twig number was held constant (meaning constant height, leaf area and basal diameter), deviating from

WBE led to greater whole tree hydraulic conductance (K), lower stem volume (V), greater critical buckling height (L_{crit}), and reduced total photon absorption (PAR_{abs}). When we "grew" trees to different sizes we found that if P_f was held constant, deviations from WBE branching caused only a minor increase in the metabolic exponent, cq, owing to shifts in q. All cq values were below the original WBE prediction of 0.75. This was true even for WBE-branching trees because of finite size effects (Savage *et al.* 2010) and hydraulic architecture modifications (Sperry *et al.* 2012). If we assumed that P_f declined to a minimum before increasing with size, as observed interspecifically, the cq was size dependent. For small trees with decreasing P_f, cq could increase beyond 0.75 due to large increases in both c and q. However, for larger trees with gradually increasing P_f, cq was much lower, falling below 0.65.

The "U" shaped P_f trajectory estimated for real trees makes intuitive sense. Young trees may place a premium on height growth, which would be favored by P_f-decreasing crowns that become elongated and relatively narrow (Fig. 3.1b; Charles-Dominique *et al.* 2012). High hydraulic conductance per tissue volume, and greater mechanical stability (or greater height per trunk diameter, see below) of low-P_f crowns may also maximize height growth. As the tree reaches or exceeds the height of surrounding vegetation, broader high-P_f crowns would capitalize on greater light availability and fill canopy gaps.

For a given D_T and height, decreasing P_f was a strong predictor of increasing K. This result was somewhat surprising as P_f represents an entire branching structure with just mean and maximum pathlengths. However, the hydraulic conductance of a nontapering tube is inversely related to its length so it follows that K should increase as pathlengths are shortened (Fig. 3.4a). Indeed, individual trunk-to-twig hydraulic conductances within a tree were always negatively correlated with path length (not shown). In the model, the length-dependence of K is reduced but cannot be eliminated or reversed by observed xylem conduit taper or leaf resistance (Sperry *et al.* 2012). Data on path conductance and actual path length are limited, but support the prediction of greater conductance for shorter trunk-to-leaf paths (Sperry & Pockman 1993). Whole-path conductance to branches lower in the canopy can be equivalent to (Hubbard *et al.* 2002; Yoshimura 2011) or even lower than (Kupper *et al.* 2005; Sellin & Kupper 2005) branches higher up, but the pathlengths were not measured in these studies. However, it is possible that shorter paths could develop lower conductances if shading caused senescence or growth of narrower twigs (Protz *et al.* 2000). Variation in twig properties within a canopy was not modeled, but could obscure the pathlength effect.

At the whole tree level, the xylem architecture component of the model is known to yield realistic ranges of water use and K across different functional tree types (Sperry *et al.* 2012; von Allmen *et al.* 2012). Rigorous tests of the additional effects of branching await information on the ranges of P_f across major tree types. The P_f is a novel metric and there are no data on it outside of this paper. Although it is difficult to measure on large trees, in principle the model can be used to estimate it from the allometries of crown area and height vs trunk diameter. In real trees, the effects of variable branching structure are superimposed on effects of variable xylem anatomy. A virtue of the model is the ability to separate out the hydraulic contributions of these two networks.

The model showed that total stem volume decreased as P_f decreased (Fig. 3.4b). Trees with shorter transport distances on average require less construction tissue, even for the same height and basal diameter. Furthermore, V vs P_f was a perfect linear relationship, resulting in the volume fraction, V_f, being equal to the path fraction, P_f. The V_f is potentially much easier to estimate than P_f, which would facilitate its measurement in trees.

As P_f was decreased, the model also predicted that critical heights, L_{crit}, increased for a given D_T (Fig. 3.4c). The greater mechanical stability of conical low-P_f trees is an intuitive result because they carry more of their mass closer to the ground than round-crowned high-P_f trees. In the scenario we modeled, all trees of a given D_T were the same height. Therefore, the increase in L_{crit} resulted in greater safety from buckling in low-P_f trees. Alternatively, if trees grow towards the same safety from buckling, low-P_f trees should grow taller for a given D_T than high-P_f trees.

The latter prediction appears to be supported by the available data. Among temperate trees, evergreens (mostly conifers) have been shown to grow taller with diameter than deciduous (mostly angiosperm) trees (Ducey 2012). Although phenology was stressed in that study, our model suggests an alternative explanation: a tendency for large conifers to have a lower P_f may allow them to grow taller than angiosperms for the same trunk diameter. Lower P_f for large conifers is suggested by their tendencies to be taller (Ducey 2012) and to have narrower crowns (see Supporting information, Fig. S3.1; Krajicek *et al.* 1961; Vezina 1962; Leech 1984; Farr *et al.* 1989) than similarly large-trunked angiosperms. Low P_f in large conifers would favor height growth per basal diameter by: increasing L_{crit}; decreasing volume investment; and increasing tree hydraulic conductance.

PAR_{abs} was also influenced by P_f (Fig. 3.4d). In WBE trees, symmetric branching means there is no distinct main stem and branches can spread large distances in all direc-

tions. As P_f is lowered, a distinct main stem starts to develop with branches extending from this stem (see Fig. 3.1a). This configuration limits the horizontal spread of branches, leading to more self-shading of leaves and less light absorption (Pearcy *et al.* 2004a). Changing the light angle from vertical to horizontal reduced this disadvantage of low-P_f trees, but did not eliminate it. Lowering P_f should always limit the lateral spread of leaves, so using a different light model or alternative branching angles should not impact our general prediction.

Our results suggest how the local environment may select for optimal branching architecture. For three out of the four modeled tree properties (hydraulic conductance, volume, mechanical stability and light interception), low-P_f trees are at a competitive advantage, as they can transport water more easily despite a smaller investment in tissue and have greater mechanical stability. However, these advantages come at the expense of reduced light absorption. Hypothetically, the diverse spectrum of tree forms in nature could result from optimizing this tradeoff for a diverse set of requirements, depending on life history and habitat (Horn 1971). In general, selection for a given branching architecture will depend on the relative advantages of transporting water, growing fast, growing tall, and gathering light. As already discussed, the optimal P_f of an angiosperm canopy tree may change through ontogeny, with decreasing P_f favoring early height growth followed by increasing P_f to favor canopy gap-filling (Horn 1971). Alternatively, short shade-tolerant species adapted to the high humidity and low light of the understory are expected to always have a high P_f. Such species lack a prolonged height growth phase and need to avoid self-shading (Pearcy *et al.* 2004b). The associated low hydraulic conductance would not be a liability for short stature and low evaporative demand. Conversely, high-P_f shrubs or treelets would also be expected in open habitats where competition for light is absent and height growth is less advantageous.

While it was beyond the scope of this study to fully quantify the tradeoffs of different architectures, the concept of a P_f optimum can be illustrated by normalizing PAR_{abs} by V. Figure 3.6 shows broad peaks at midrange P_f for all light angles. Moving the light source from vertical to horizontal sharpened and elevated the peak and shifted it to lower P_f. Increasing the tree size had comparatively little effect on peak shape or position (not shown). As PAR_{abs} is closely tied to photosynthesis and V to mass, the results are suggestive of peaks in carbon gain per carbon spent. Photosynthesis will also depend on water supply to the leaves and its influence on stomatal conductance. As such, the higher K associated with lower P_f (Fig. 3.4a) would tend to further benefit the midrange-P_f trees relative to high-P_f trees.

Systematic changes in branching architecture with size, either through ontogeny or across species, have potentially major effects on metabolic scaling. With size-invariant P_f, changing P_f had fairly small effects on the hydraulic and metabolic exponents (q and cq). Much larger effects have been seen by changing the internal structure such as xylem conduit taper and sapwood area scaling (Sperry *et al.* 2012). This result offers some support that the scaling of the WBE tree can be reasonably representative of non-WBE branching structures. This may explain why retaining the WBE structure resulted in generally good fits to sapflow data (von Allmen *et al.* 2012). The result also shows agreement with Bentley *et al.* (2013) that junction asymmetry is not a predictor of whole tree scaling. However, the P_f appears to change systematically with tree ontogeny, making scaling exponents size-dependent and allowing cq to reach or exceed the original WBE prediction of $cq = 3/4$ in small trees. Within the constraints of WBE architecture, the only other identified mechanism of $cq \geq 0.75$ in a finite individual is ontogenetically increasing the root-to-shoot hydraulic conductance ratio (Sperry *et al.* 2012).

The model quantifies basic trade-offs between branching structure and major aspects of tree function. Narrow, elongated crowns are predicted to maximize vascular supply and mechanical stability, and minimize tissue investment. Broad, round crowns maximize light interception. No single shape is likely to be optimal across all habitats and tree sizes, and shape appears to shift though ontogeny. The model provides a framework for ultimately predicting optimal architectures. Although differences in architecture exist across at least some functional tree types (e.g., angiosperm vs conifer), such variation needs to be expressed in terms of path fractions or the equivalent for a functional analysis. Our branching structure analysis adds another layer of complexity to the evolving theory of metabolic scaling in trees. The central, elegant predictions of the original WBE model for three-fourth scaling become fascinatingly complex when the variable structures of real plants are considered.

3.6 Acknowledgements

Mathematical interpretations were improved by discussions with Fred Adler. Peter Reich provided helpful input at various stages of the project. Jake Olsen and Erica von Allmen assisted with empirical measurements from Utah. We thank Will Driscoll for helping collect the ponderosa pine data. Duncan D. Smith and John S. Sperry were supported by NSF IBN-0743148. Funding from ATB Award 0742800 helped develop the initial ideas for this work.

3.7 References

Bentley LP, Stegen JC, Savage VM, Smith DD, von Allmen EI, Sperry JS, Reich PB, Enquist BJ. 2013. An empirical assessment of tree branching networks and implications for plant allometric scaling models. *Ecology Letters* **16**: 1069–1078.

Brodribb TJ. 2009. Xylem hydraulic physiology: the functional backbone of terrestrial plant productivity. *Plant Science* **177**: 245–251.

Campbell GS, Norman JN. 1998. *An Introduction to Environmental Biosphysics*. New York: Springer 2 edn.

Charles-Dominique T, Edelin C, Brisson J, Bouchard A. 2012. Architectural strategies of *Rhamnus cathartica* (Rhamnaceae) in relation to canopy openness. *Botany* **90**: 976–989.

Ducey MJ. 2012. Evergreenness and wood density predict height-diameter scaling in trees of the northeastern United States. *Forest Ecology and Management* **279**: 21–26.

Duursma RA, Mäkelä A, Reid DEB, Jokela EJ, Porté AJ, Roberts SD. 2010. Self-shading affects allometric scaling in trees. *Functional Ecology* **24**: 723–730.

Farr WA, DeMars DJ, Dealy JE. 1989. Height and crown width related to diameter for open-grown western hemlock and Sitka spruce. *Canadian Journal of Forest Research* **19**: 1203–1207.

Greenhill AG. 1881. Determination of the greatest height consistent with stability that a vertical pole or mast can be made, and of the greatest height to which a tree of given proportions can grow. *Proceedings of the Cambridge Philosophical Society* **4**: 65–73.

Hacke UG, Sperry JS, Wheeler JK, Castro L. 2006. Scaling of angiosperm xylem structure with safety and efficiency. *Tree Physiology* **26**: 689–701.

Horn HS. 1971. *The Adaptive Geometry of Trees*. Princeton, New Jersey: Princeton University Press.

Horn HS. 2000. Twigs, trees and the dynamics of carbon in the landscape. in JH Brown, GB West (eds.) *Scaling in Biology* 199–220 Oxford: Oxford University Press.

Hubbard RM, Bond BJ, Senock RS, Ryan MG. 2002. Effects of branch height on leaf gas exchange, branch hydraulic conductance and branch sap flux in open-grown ponderosa pine. *Tree Physiology* **22**: 575–581.

Jaouen G, Alméras T, Coutand C, Fournier M. 2007. How to determine sapling buckling risk with only a few measurements. *American Journal of Botany* **94**: 1583–1593.

Katifori E, Magnasco MO. 2012. Quantifying loopy network architectures. *PLoS One* **7**: 1–14.

Krajicek JE, Brinkman KA, Gingrich SF. 1961. Crown competition - a measure of density. *Forest Science* **7**: 35–42.

Kupper P, Sellin A, Tenhunen J, Schmidt M, Rahi M. 2005. Effects of branch position on water relations and gas exchange of European larch trees in an alpine community. *Trees* **20**: 265–272.

Leech JW. 1984. Estimating crown width from diameter at breast height for open-grown radiata pine trees in South Australia. *Australian Forest Research* **14**: 333–337.

McMahon TA, Kronauer RE. 1976. Tree structures: deducing the principle of mechanical design. *Journal of Theoretical Biology* **59**: 443–466.

Monteith JL, Unsworth MH. 1990. *Principles of Environmental Physics*. London: Edward Arnold 2 edn.

Murray CD. 1927. A relationship between circumference and weight in trees and its bearing on branching angles. *The Journal of General Physiology* **10**: 725–729.

Niklas KJ. 1994. The allometry of safety-factors for plant height. *American Journal of Botany* **81**: 345–351.

Niklas KJ, Enquist BJ. 2001. Invariant scaling relationships for interspecific plant biomass production rates and body size. *Proceedings of the National Academy of Sciences of the United States of America* **98**: 2922–2927.

Olson ME, Aguirre-Hernández R, Rosell JA. 2009. Universal foliage-stem scaling across environments and species in dicot trees: plasticity, biomechanics and Corner's Rules. *Ecology Letters* **12**: 210–219.

Pearcy RW, Muraoka H, Valladares F. 2004a. Crown architecture in sun and shade environments: assessing function and trade-offs with a three-dimensional simulation model. *New Phytologist* **166**: 791–800.

Pearcy RW, Valladares F, Wright SJ, de Paulis EL. 2004b. A functional analysis of the crown architecture of tropical forest *Psychotria* species: do species vary in light capture efficiency and consequently in carbon gain and growth? *Oecologia* **139**: 163–177.

Price CA, Enquist BJ, Savage VM. 2007. A general model for allometric covariation in botanical form and function. *Proceedings of the National Academy of Sciences of the United States of America* **104**: 13204–13209.

Protz CG, Silins U, Lieffers VJ. 2000. Reduction in branch sapwood hydraulic permeability as a factor limiting survival of lower branches of lodgepole pine. *Canadian Journal of Forest Research* **30**: 1088–1095.

R Core Team. 2013. *R: A Language and Environment for Statistical Computing*. R Foundation for Statistical Computing Vienna, Austria. URL http://www.R-project.org/.

Savage VM, Bentley LP, Enquist BJ, Sperry JS, Smith DD, Reich PB, von Allmen EI. 2010. Hydraulic trade-offs and space filling enable better predictions of vascular structure and function in plants. *Proceedings of the National Academy of Sciences of the United States of America* **107**: 22722–22727.

Sellin A, Kupper P. 2005. Variation in leaf conductance of silver birch: effects of irradiance, vapour pressure deficit, leaf water status and position within a crown. *Forest Ecology and Management* **206**: 153–166.

Shinozaki K, Yoda K, Hozumi K, Kira T. 1964. A quantitative analysis of plant form–the Pipe Model Theory: I. Basic analysis. *Japanese Journal of Ecology* **14**: 97–105.

Sinoquet H, Le Roux X, Adam B, Ameglio T, Daudet FA. 2001. RATP: a model for simulating the spatial distribution of radiation absorption, transpiration and photosynthesis within canopies: application to an isolated crown. *Plant, Cell and Environment* **24**: 395–406.

Sperry JS, Pockman WT. 1993. Limitation of transpiration by hydraulic conductance and xylem cavitation in *Betula occidentalis*. *Plant Cell and Environment* **16**: 279–287.

Sperry JS, Smith DD, Savage VM, Enquist BJ, McCulloh KA, Reich PB, Bentley LP, von Allmen EI. 2012. A species-level model for metabolic scaling in trees I. boundaries to scaling space within and across species. *Functional Ecology* **26**: 1054–1065.

Valladares F, Brites D. 2004. Leaf phyllotaxis: Does it really affect light capture? *Plant Ecology* **174**: 11–17.

Vezina PE. 1962. Crown width-DBH relationships for open-grown balsam fir and white spruce in Quebec. *Forestry Chronicle* **38**: 463–473.

von Allmen EI, Sperry JS, Smith DD, Savage VM, Reich PB, Enquist BJ, Bentley LP. 2012. A species' specific model of the hydraulic and metabolic allometry of trees II: testing predictions of water use and growth scaling in species with contrasting hydraulic traits. *Functional Ecology* **26**: 1066–1076.

Warton DI, Wright IJ, Falster DS, Westoby M. 2006. Bivariate line-fitting methods for allometry. *Biological Reviews* **81**: 259–291.

West GB, Brown JH, Enquist BJ. 1997. A general model for the origin of allometric scaling laws in biology. *Science* **276**: 122–126.

West GB, Brown JH, Enquist BJ. 1999. A general model for the structure and allometry of plant vascular systems. *Nature* **400**: 664–667.

Yoshimura K. 2011. Hydraulic function contributes to the variation in shoot morphology within the crown in *Quercus crispula*. *Tree Physiology* **31**: 774–781.

Zhi W, Ming Z, Qi-Xing Y. 2001. Modeling of branching structures in plants. *Journal of Theoretical Biology* **209**: 383–394.

Table 3.1. Symbol definitions and modifiers from the main text in order of appearance

Basic Symbols and Definitions		**Input**
B	metabolic rate	
M	mass	
D	stem diameter	
V	total stem volume	
c	"volume exponent" in $M \propto V \propto D_T^{1/c}$	
Q	whole tree sapflow rate	
K	whole tree hydraulic conductance	
q	"hydraulic exponent" in $B \propto K \propto D_T^q$	
cq	"metabolic exponent" in $B \propto K \propto V^{cq}$	
P_f	path fraction = mean $L_\updownarrow$ / maximum $L_\updownarrow$	
$L_\updownarrow$	pathlength from trunk base to twig tip	
f	branching junction furcation number	2 to 4
R	rank = number of supported twigs	
A	minimum possible R for a given daughter in a given junction	
Z	maximum possible R for a given daughter in a given junction	
P_{R_d}	probability of choosing a given daughter rank	
u	exponent used to shift P_{R_d} towards choosing A or Z	-5 to 5
$L_\uparrow^*$	maximum pathlength from branch base to twig tip	
a	$L_\uparrow^*$ scaling multiplier ($m^{1/3}$)	26.99
L_{crit}	theoretical $L_\uparrow$ at which tree of given D_T should buckle	
b	L_{crit} scaling multiplier ($m^{1/3}$)	107.94
s	eventual safety factor from buckling	4
l_o	virtual length: distance beyond twig tip to theoretical origin (m)	0.34
l	stem segment length between junctions	
n	scaling exponent for how diameter of main stem varies with height	
m	scaling exponent for how supported mass varies with height	
c_ν	first positive root of Bessel function with input, ν	
PAR_{abs}	total absorbed photosynthetically active radiation (μmol s^{-1})	
V_f	volume fraction = actual stem volume / volume of a column of equivalent height and basal diameter	
Subscript Modifiers		
T	trunk	
m	mother	
d	daughter	
t	twig	
Superscript Modifier		
$*$	maximum	

Table 3.2. Empirical P_f measurements from trees and shrubs

Species	Species Code	Twigs/P_f[1]	Source[2]
Acer glabrum	Ag	82/0.56	RBC
Acer grandidentatum	Ag	93/0.71, **189/0.64**, **315/0.42***	RBC
Acer negundo	An	86/0.50, 130/0.53	RBC
Cornus sericea	Cs	**75/0.79**, 497/0.69	RBC
Elaeagnus angustifolia	Ea	26/0.67	RBC
Fraxinus nigra	Fn	**5/0.92**, **6/0.93**, **10/0.92** **13/0.84**	CC
Pinus ponderosa	Pp	**10/0.86***, **29/0.67***, **31/0.85***, **33/0.80***, **68/0.72***	CNF
Populus tremuloides	Pt	81/0.81, **113/0.65**, **118/0.72**	RBC
Quercus ellipsoidalis	Qe	**13/0.83**, **17/0.86**, **34/0.69**, **35/0.78**	CC
Quercus gambelii	Qg	**56/0.62***, 71/0.57, 86/0.43, **147/0.63**	RBC
Rhus glabra	Rg	26/0.84	RBC
Rhus trilobata	Rt	174/0.55	RBC
Robinia pseudoacacia	Rp	**25/0.56**, **59/0.64**	CC
Salix exigua	Se	**11/0.88**, **46/0.76**, **48/0.80**	RBC
Ulmus pumila	Up	122/0.56, 227/0.36, 253/0.56, 338/0.55	RBC

[1] Bold values indicate whole individuals. Branches otherwise.
[*] Networks also analyzed by Bentley *et al.* (2013)
[2] RBC = Red Butte Canyon; CNF = Coronado National Forest; CC = Cedar Creek

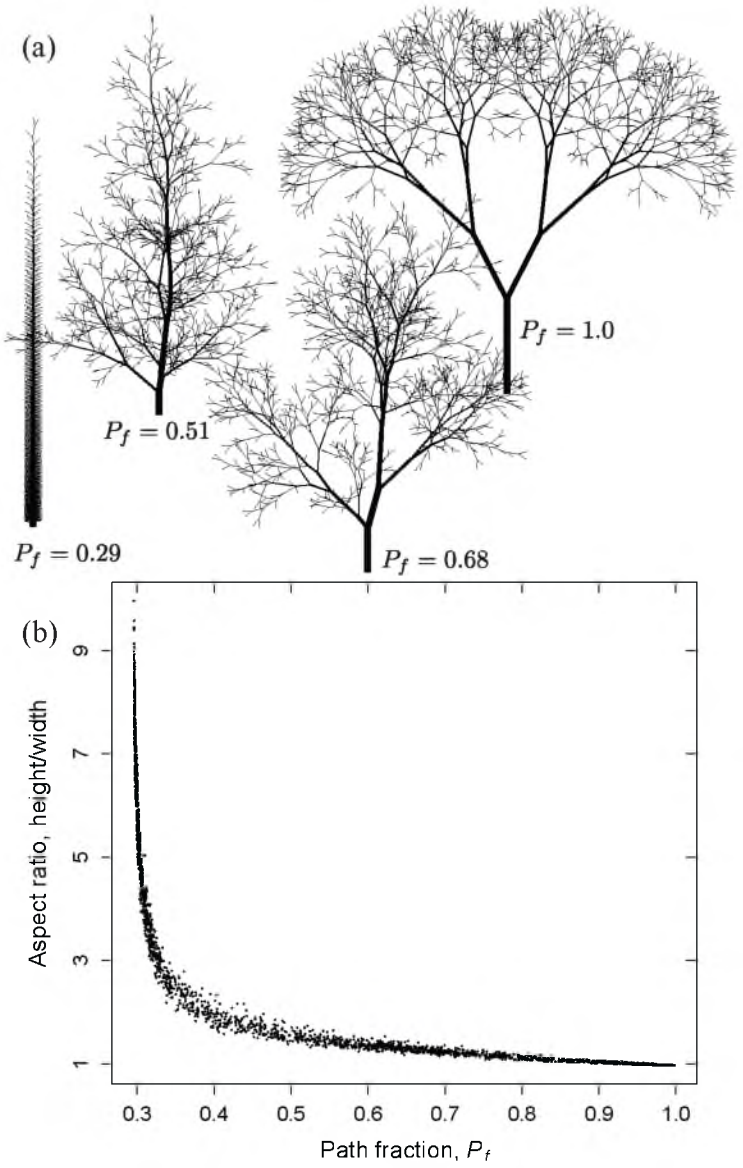

Figure 3.1. Tree shape in relation to tree path fraction. Simulations are for trees of the same basal diameter, height, and twig number (1024). Furcation was set to $f^* = 2$ as required when specifying branch angles. **a**) The rightmost tree ($P_f = 1$) is the WBE structure with perfect symmetry at each junction. The leftmost tree is the "fishbone" structure that represents the minimum P_f. The two intermediate trees were generated by the model. **b**) The aspect ratio quantifies whole tree shape where an aspect ratio of one may be thought of as a sphere (or hemisphere) while larger values indicate a narrower crown.

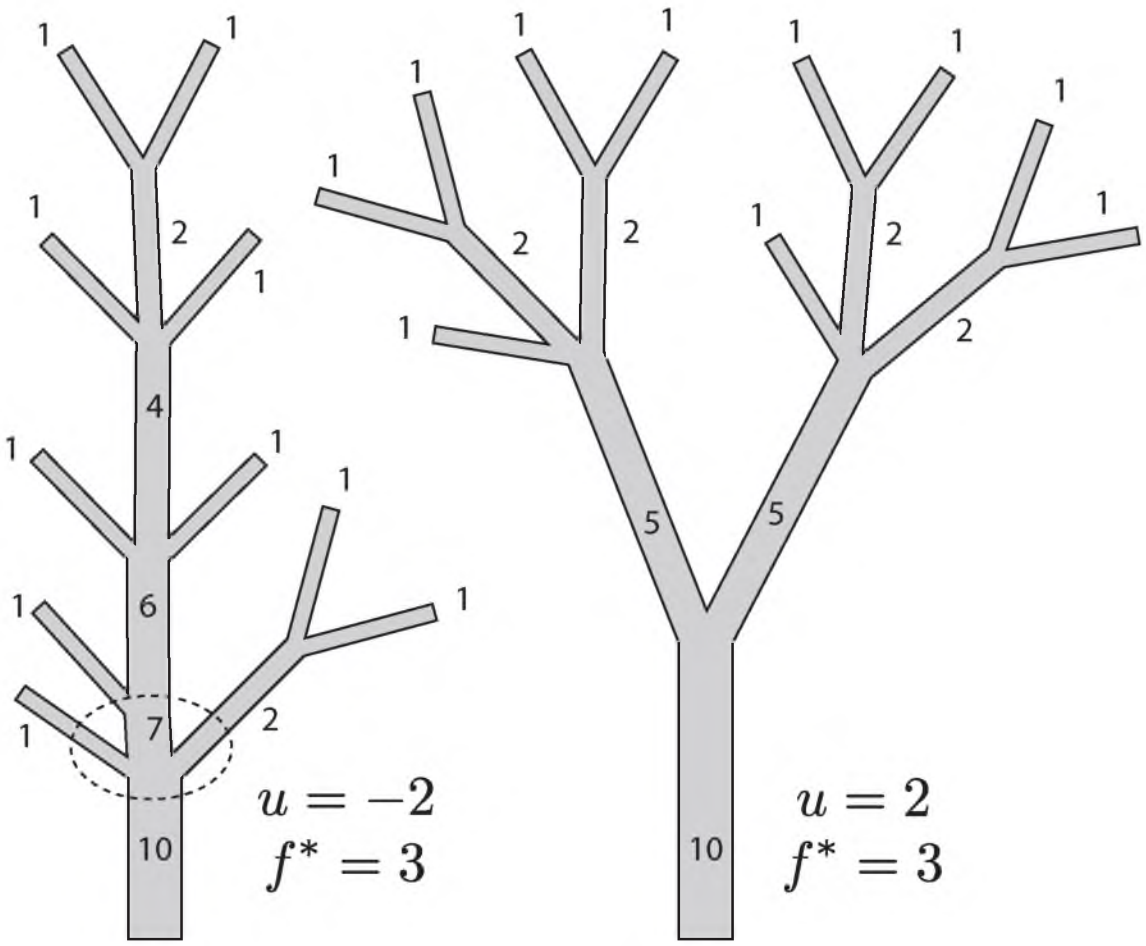

Figure 3.2. Two trees with 10 twigs each illustrate several model properties. Numbers at each branch segment indicate the rank, R, where R must balance across each junction. Each rank is chosen at random but the symmetry of each junction and the overall structure is influenced by parameter u. The furcation, f, of each junction is also selected randomly although both trees have the same maximum furcation, f^*. The selection process for the circled junction is detailed in the main text. The trees also show branch diameters (exaggerated) that result from area- and rank-preservation and invariant twigs ($R = 1$). Branch lengths are drawn to scale and reflect the length selection process detailed in the main text.

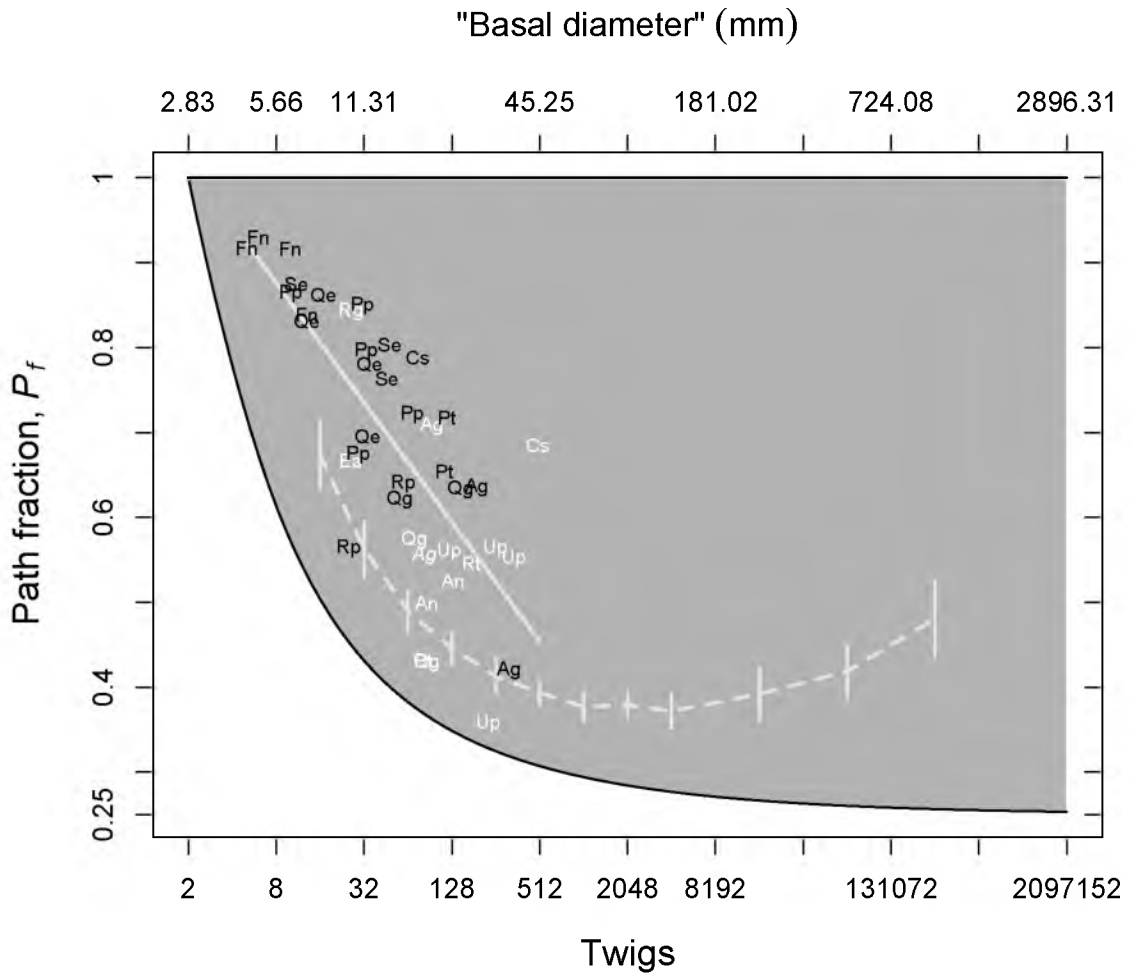

Figure 3.3. Modeled range of possible P_f values (shaded) across a large range of twig numbers and basal diameters. Basal diameters assume a twig diameter of 2 mm and are only shown to give a sense of scale. Maximum P_f is 1.0 by definition and includes WBE trees. Minimum P_f uses a "fishbone" structure with twigs attached alternately (i.e., $f = 2$) to a central axis (e.g., Fig. 3.1a, leftmost tree). Characters indicate empirical P_f values in 15 species (abbreviations and values in Table 3.2). Whole individuals are in black and branches are in white. The solid regression line through all empirical values ($P_f = -0.102 \log(\text{twigs}) + 1.088$) was used as the basis for scaling scenario S_2. The dashed line (mean ± SD) is based on crown area scaling from Olson *et al.* (2009) and was used for scenario S_3.

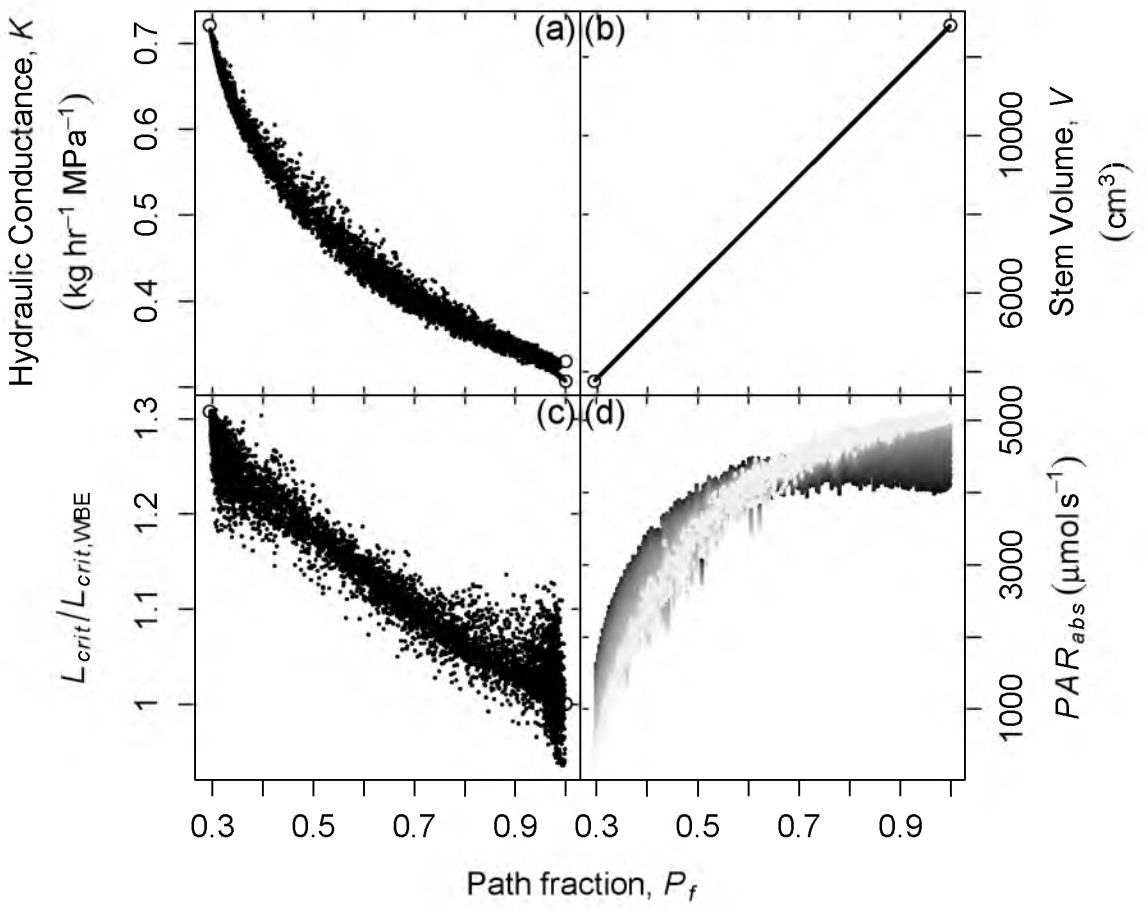

Figure 3.4. Predicted tree function vs path fraction. Simulations are shown for trees with the same basal diameter, height and twig number (1024), but the same trends applied regardless of tree size. In **a-c**, open circles represent the P_f extremes. **a**) Tree hydraulic conductance decreased with P_f. The open circles at $P_f = 1$ correspond to $f^* = 4$ (upper) and $f^* = 2$ (lower). **b**) Total stem volume increased in perfect linear proportion to P_f. **c**) The critical height at elastic buckling, L_{crit}, relative to a WBE tree decreased with P_f. **d**) Tree light absorption increased with P_f at all light source angles, but more strongly so as source angle shifted from horizontal (black) to vertical (shading to white).

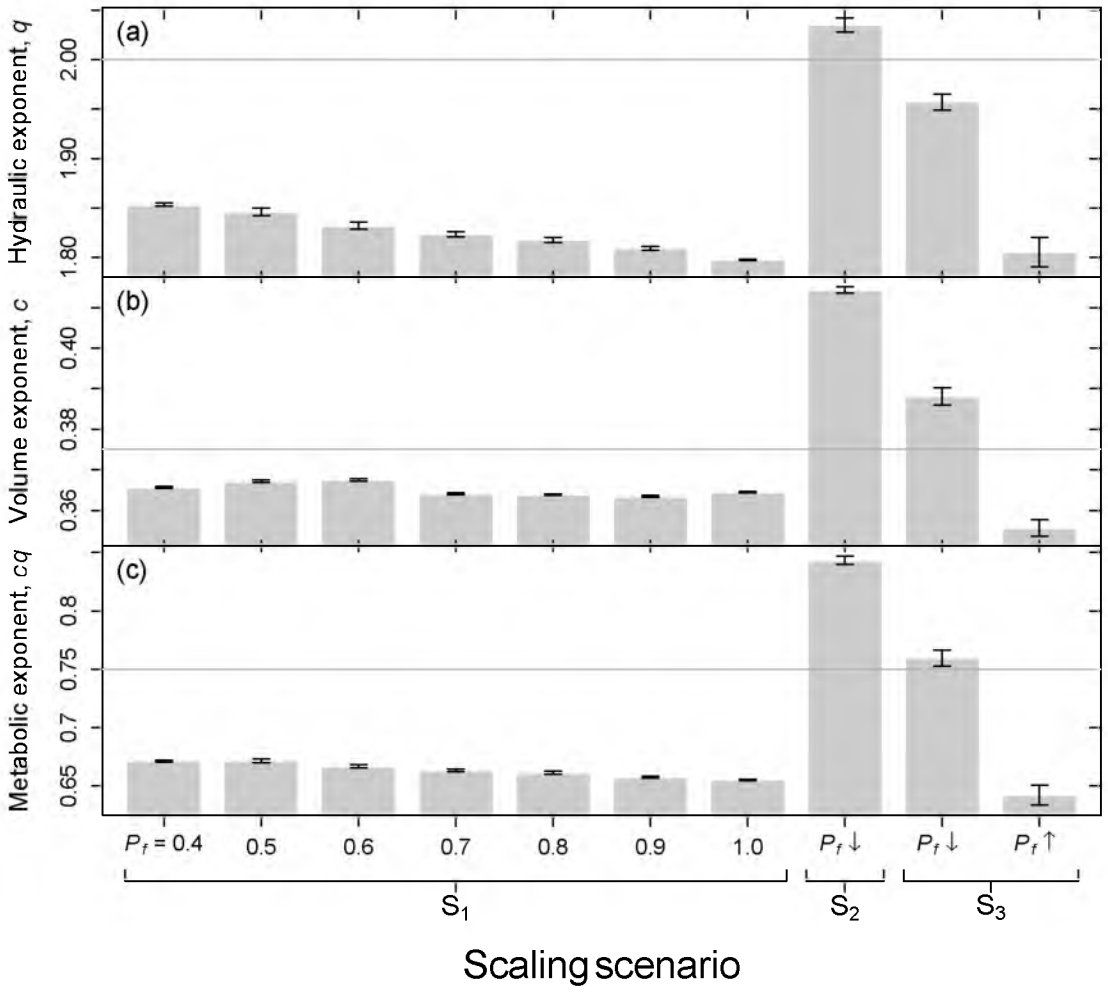

Figure 3.5. Summary of SMA scaling exponents with 95% confidence intervals for the three P_f ontogenies we considered. In scenario S_1, path fractions were constant during growth. $P_f = 1.0$ includes WBE trees (constant f), as well as other trees that maintain perfect or nearly perfect junction symmetry but variable f. In S_2 and S_3, P_f was size dependent, either decreasing ($P_f\downarrow$) along the solid line in Fig. 3.3 (S_2; based on our data), or decreasing and then increasing ($P_f\uparrow$) according the dashed line in Fig. 3.3 (S_3; based on Olson *et al.* crown scaling). Horizontal lines indicate the original WBE predictions.

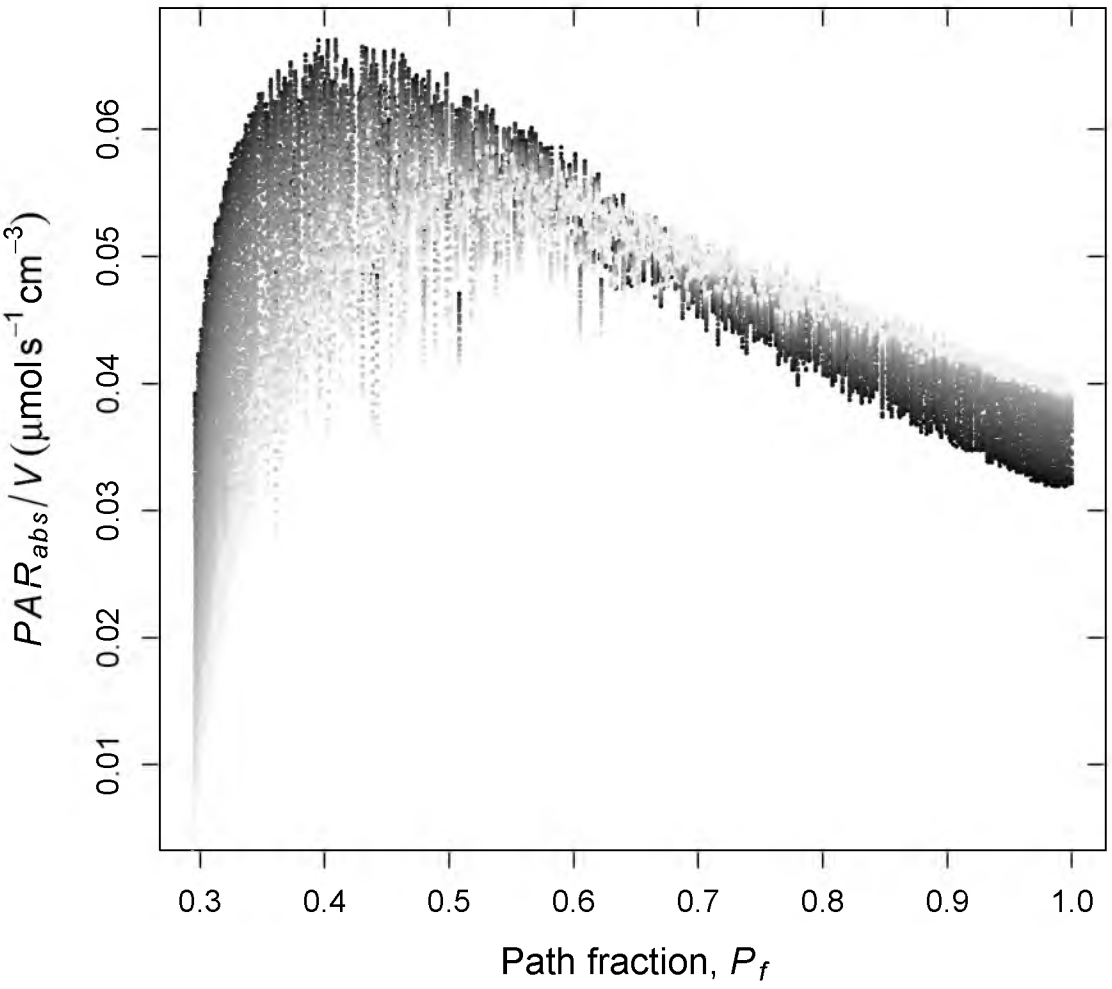

Figure 3.6. Volume normalized light interception for the same trees shown in Fig. 3.4d. Shading corresponds to mean absorption at each zenith angle from horizontal (black) to directly overhead (white). The peaks observed at each zenith angle are suggestive of optimal architectures that maximize carbon gain per carbon spent.

S3 Supporting information

S3.1 Materials used in P_f measurements

Trees and shrubs used for empirical P_f measurements came from three locations within the United States. All networks came from healthy looking plants with minimal dieback. All species were either native or naturalized and harvested from natural settings.

Red Butte Canyon (RBC; 40.8° N, 111.8° W) is located adjacent to the University of Utah in Salt Lake City, UT. One *Quercus gambelii* and one *Acer grandidentatum* were collected in the spring of 2008 while others from the area were collected during the late winter and spring of 2010. Only *Cornus sericea*, *Rhus glabrum*, and *Salix exigua* were located near permanent surface water. Self-supporting networks were preferred although shrubby *Rhus trilobata* was more prostrate and clonal *Salix exigua* likely leaned against neighbors. Plants overshadowed by neighbors were avoided but many had similar sized neighbors nearby.

Cedar Creek (CC; 45.4° N, 93.2° W) is part of the eastern deciduous forest located *ca.* 45 km north of Minneapolis, MN. Plants were collected in 2008 from sites without permanent surface water and soils ranging from very wet to sandy and drier. All plants were self-supporting and received direct sun for at least half of the daytime.

The *Pinus ponderosa* trees came from the Coronado National Forest (CNF) near Tucson, AZ during February 2007. The trees chosen were relatively isolated from neighbors.

S3.2 WBE compatibility with $L^*_\uparrow(D)$ function (Eqn. 3.8)

The WBE model achieves an eventual 2/3-power $L^*_\uparrow$ by D relationship by scaling individual lengths with $D^{2/3}$ and summing those lengths. The form of this relationship conforms to

$$L^*_\uparrow = aD^{2/3} - l_o \tag{S3.1}$$

which is given by McMahon & Kronauer (1976) to apply to all trees regardless of their branching architecture. We use Eqn. S3.1 as a starting point and show how it is entirely consistent with the special case of WBE architecture when the correct l_o is used. We derive this WBE-compatible l_o and use it in Eqn. S3.1 for application to all modeled trees (see Eqn. 3.8 in main text). We do this in order to be able to compare the properties of WBE and non-WBE trees.

In the special case of WBE structure, segment lengths, l, scale with their diameters to the 2/3 power:

$$l = cD^{2/3} \tag{S3.2}$$

Twig length, l_t, may be calculated independently both by Eqn. S3.2 and as $L^*_\uparrow(D_t)$ (Eqn. 3.10 in the main text). Therefore,

$$l_t = L^*_\uparrow(D_t) = aD_t^{2/3} - l_o = cD_t^{2/3} \tag{S3.3}$$

making,

$$l_o = D_t^{2/3}(c - a) \tag{S3.4}$$

As a is already defined by safety from buckling, finding l_o requires a value of c that satisfies WBE.

In the WBE architecture, symmetric self-similarity produces levels of identical branch segments. Using WBE terminology, k is the level index where the trunk is level $k = 0$ and the twigs comprise level $k = N$. The diameter and length ratios between segments in adjacent levels are β and γ.

$$\beta \equiv \frac{D_{k+1}}{D_k} = f^{-1/2} \tag{S3.5}$$

$$\gamma \equiv \frac{l_{k+1}}{l_k} = f^{-1/3} \tag{S3.6}$$

The second equalities only apply to WBE structures. Using the twig level as a reference in Eqn. S3.6, it follows that $l_N/l_{N-1} = f^{-1/3}$. Then, applying Eqn. S3.4 to Eqn. S3.1 and using Eqns. 3.9-3.10 to get segment lengths gives

$$\frac{l_N}{l_{N-1}} = \frac{aD_t^{2/3} - l_o}{(aD_{N-1}^{2/3} - l_o) - (aD_t^{2/3} - l_o)} = \frac{aD_t^{2/3} - (c-a)D_t^{2/3}}{aD_{N-1}^{2/3} - aD_t^{2/3}} \tag{S3.7}$$

Based on Eqn. S3.5, the D of any level k may be defined using D_N $(= D_t)$ as

$$D_k = D_N f^{(N-k)/2} \tag{S3.8}$$

With $k = N - 1$, plugging Eqn. S3.8 into Eqn. S3.7 produces

$$\frac{l_N}{l_{N-1}} = \frac{aD_N^{2/3} - (c-a)D_N^{2/3}}{aD_N^{2/3} f^{1/3} - aD_N^{2/3}} = \frac{2a - c}{af^{1/3} - a} \tag{S3.9}$$

Recalling the requirement that $l_N/l_{N-1} = f^{-1/3}$, we get

$$c = a(1 - f^{1/3}) \tag{S3.10}$$

and plugging Eqn. S3.10 into Eqn. S3.4 finally gives

$$l_o = af^{-1/3} D_t^{2/3} \tag{S3.11}$$

Equation S3.11 provides an l_o that satisfies $\gamma = f^{-1/3}$ at the twig level in WBE trees when plugged into Eqn. S3.1. The resulting equation (Eqn. 3.8 in the main text) was then used for all trees, regardless of structure.

However, the preceding equations only explicitly show that the length ratio between twigs and their mothers complies to WBE. We must additionally check the length ratio between all other adjacent levels by applying Eqn. S3.4 to Eqn. S3.1 and using Eqn. 3.9 to get segment lengths:

$$\frac{l_{k+1}}{l_k} = \frac{(aD_{k+1}^{2/3} - l_o) - (aD_{k+2}^{2/3} - l_o)}{(aD_k^{2/3} - l_o) - (aD_{k+1}^{2/3} - l_o)} = \frac{aD_{k+1}^{2/3} - aD_{k+2}^{2/3}}{aD_k^{2/3} - aD_{k+1}^{2/3}} \tag{S3.12}$$

Substituting diameters from Eqn. S3.8 into Eqn. S3.12 produces

$$\frac{l_{k+1}}{l_k} = \frac{aD_N^{2/3} f^{(N-k-1)/3} - aD_N^{2/3} f^{(N-k-2)/3}}{aD_N^{2/3} f^{(N-k)/3} - aD_N^{2/3} f^{(N-k-1)/3}} = f^{-1/3}, \tag{S3.13}$$

which meets the WBE requirement. Note that all l_o values canceled out in Eqn. S3.12. Therefore, in a WBE tree, across all levels except the twig level, any value of l_o in Eqn. S3.1 satisfies the WBE length ratio requirement. However, a specific l_o (Eqn. S3.11) is needed to make the twig level comply. In the strict rules of WBE architecture, l_o is a function of f, which is a constant. We used $f = 2$ to obtain the generic l_o for use in all trees. In non-WBE trees, branching only needs to follow Eqn. S3.1 where l_o can be set to any value. Because l_o only influences twig length (Eqn. S3.12), the only real consequence of using $f = 2$ for all trees is that symmetrically branching trees with $f > 2$ have twigs that are slightly shorter than WBE would predict.

S3.3 Branch segment hydraulic conductance

As stated in the main text, we follow the Sperry *et al.* (2012) model of xylem architecture to determine hydraulic conductance of each branch segment. To summarize, their model takes branch diameter as an input and a number of equations are used to define the dimensions and numbers of functional conduits in that branch. Incorporating conduit length (= branch segment length) allows hydraulic conductance to be calculated with the Hagen-Poiseuille equation. In general, we utilize the default coefficients given by Sperry *et al.* The equations used are as follows.

Conduit diameters, D_c (μm), increase with stem diameter, D (mm). This taper occurs both within stems and across stems and is given by

$$D_c = a_{tap} D^{b_{tap}} \tag{S3.14}$$

The exponent, $b_{tap} = 1/3$, provides the optimal tapering defined by Savage *et al.* (2010) while the multiplier, $a_{tap} = 7.9$, corresponds with a maximum D_c of 10 μm in the default twig diameter, $D_t = 2$ mm.

The number of conduits per xylem area, N_c/A_x (mm^{-2}), tends to decrease as conduits become wider

$$N_c/A_x = a_{pak} D_c^{b_{pak}} \tag{S3.15}$$

The exponent, $b_{pak} = -2$, also comes from Savage *et al.* (2010) and it corresponds to a constant fraction of xylem area being occupied by conduits, regardless of their diameter. The multiplier, $a_{pak} = 10^5$ indicates that 10% of xylem area is occupied.

Part of the stem area is devoted to a pith in the center, which is given a constant diameter of 1 mm. On the outside of the stem is phloem, periderm, and possibly cortex. These are collectively the "bark" and bark thickness, T_{brk} (mm), increases with D as

$$T_{brk} = a_{brk} D^{b_{brk}} \tag{S3.16}$$

Parameters $b_{brk} = 1.05$ and $a_{brk} = 0.0225$ come from thin-barked *Acer grandidentatum*. The area between pith and bark is the total xylem area, ΣA_x. However, the oldest xylem near the pith eventually loses function and becomes heartwood with functional sapwood on the outside. Sapwood area, A_{sap} (mm^2), increases with D but cannot exceed ΣA_x. Therefore,

$$A_{sap} = \begin{cases} a_{sap} D^{b_{sap}} & \text{if } a_{sap} D^{b_{sap}} < \Sigma A_x, \\ \Sigma A_x & \text{otherwise} \end{cases} \tag{S3.17}$$

The parameters, $b_{sap} = 1.93$ and $a_{sap} = 0.905$, are also based on *A. grandidentatum*, which is diffuse-porous with multiple years of functional xylem.

Equations S4.6–S4.8 collectively define the numbers and diameters of all functional conduits within a stem of any diameter. Using the Hagen-Poiseuille equation, one can then predict stem hydraulic conductivity. The Hagen-Poiseuille equation makes predictions for laminar flow through open, cylindrical tubes. We account for resistive endwalls in xylem with an angiosperm correction factor, $a_{ew} = 0.44$, meaning actual conductivity is 44% of that predicted by Hagen-Poiseuille (Hacke *et al.* 2006). For our model, we combined all of the above into a single integral that predicts branch segment hydraulic conductivity, κ ($\mathrm{mm}^4\ \mathrm{MPa}^{-1}\ \mathrm{s}^{-1}$):

$$\kappa = c_2 \left[\frac{x^{c_1}}{c_1} - \left(\frac{2 a_{brk} (b_{brk} + 1) x^{c_1 + b_{brk} - 1}}{c_1 + b_{brk} - 1} \right) + \left(\frac{4 a_{brk}^2 b_{brk} x^{c_1 + 2b_{brk} - 2}}{c_1 + 2b_{brk} - 2} \right) \right] \Bigg|_{x = D_v}^{D} \tag{S3.18}$$

where

$$c_1 = 4 b_{tap} + b_{tap} b_{pak} + 2$$

$$c_2 = a_{ew}\left(\pi^2 a_{pak} a_{tap}^{b_{pak}+4}\right) / \left(256\mu 10^{12}\right)$$

and μ (MPa s) is the dynamic viscosity of water. The D_v is a "virtual" diameter. By way of explanation, note that Eqn. S4.6 predicts D_c at the bark-xylem interface (not at the stem surface). When integrating over the sapwood area, we recognize that the current heartwood-sapwood interface is where the bark-xylem interface was at one time. Therefore, in order to predict D_c at this location, we need to know what the overall stem diameter was at that time. That diameter is D_v, which must be found numerically. Branch segment hydraulic conductance (mm^3 MPa^{-1} s^{-1}) is just κ/l.

S3.4 Partial derivation of $L_{crit}(D_T)$ function (Eqn. 3.13)

Based on Greenhill (1881), Jaouen *et al.* (2007) define L_{crit} as

$$L_{crit} = \frac{\pi^{1/2} E^{1/2} r_T^2 c(|m - 4n + 2|)}{4(M_{tot} g)^{1/2}} \tag{S3.19}$$

The r_T is trunk radius, g is gravity and E is Young's elastic modulus (N m^{-2}). Equation S3.19 is somewhat problematic as both M_{tot} and r_T are inputs; this means L_{crit} is predicted for a constrained mass and trunk radius. We prefer that M_{tot} be a function of r_T and tree form. We express M_{tot} as a function of r_T by using tissue density, ρ, and volume, V, predicted using Eqn. 3.15 and $V_f = P_f$.

$$M_{tot} g = V \rho g = \pi r_T^2 L_{crit} P_f \rho_g \tag{S3.20}$$

We also combine ρ and g into ρ_g, which is the specific weight of supporting tissue (N m^{-3}). The ratio of E/ρ_g is approximately constant across woody plants (125^3 m; Niklas 1994). Substituting Eqn. S3.20 into Eqn. S3.19, rearranging, and converting r_T to D_T leads to Eqn. 3.13 in the main text. To predict b in Eqn. 3.8, we used a WBE tree with 1024 twigs and $f^* = 2$. This tree resulted in $m = 2.91$ and $n = 0.96$. Among other WBE trees ($2^4 - 2^{12}$ twigs), larger size tended to increase both m (2.28 to 3.06) and n (0.64 to 1.03). However, the resulting b changed very little as size increased (range = 107.55 to 108.25). By comparison, a "fishbone" tree with 1024 twigs would have $b = 141.19$.

It should be noted that using parameters that correspond to a straight column ($P_f = 1$, $m = 1$ and $n = 0$) in Eqn. 3.13 produces

$$L_{crit}(D) = 0.788 \left(\frac{E}{\rho_g}\right)^{1/3} D^{2/3} \tag{S3.21}$$

which is essentially[1] the common equation used for critical heights (e.g., Niklas 1994).

[1]A constant of 0.792 instead of 0.788 is often cited but this apparently stems from Greenhill's (1881) imprecise estimation of the first positive root of the Bessel function. However, this 0.5% overestimation is likely of little consequence

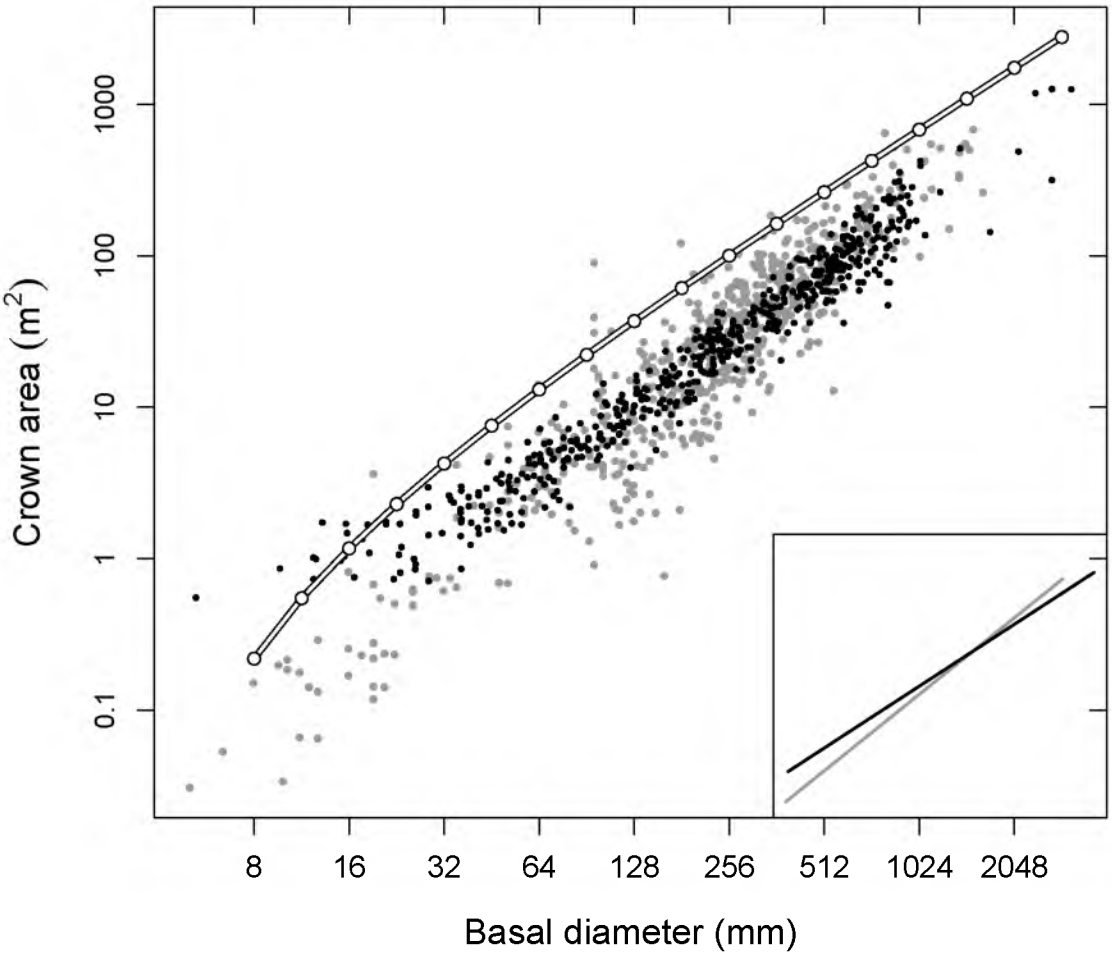

Figure S3.1. Measured and modeled crown area scaling. Closed circles indicate data from angiosperms (grey) and conifers (black). OLS regressions for these data (inset) had similar but significantly different slopes ($p < 0.01$). Random model trees (not shown) whose crown areas matched the angiosperm regression $\pm$ 5% were used to predict a P_f ontogeny (see Fig. 3.3). Open circles indicate WBE trees from the model. The model was built agnostic to the empirical crown area data. Therefore, it is somewhat surprising that not only did model trees fall among the data, but the WBE trees (which should have among the largest crowns for their trunk diameter) more or less followed the upper bound of the empirical data.

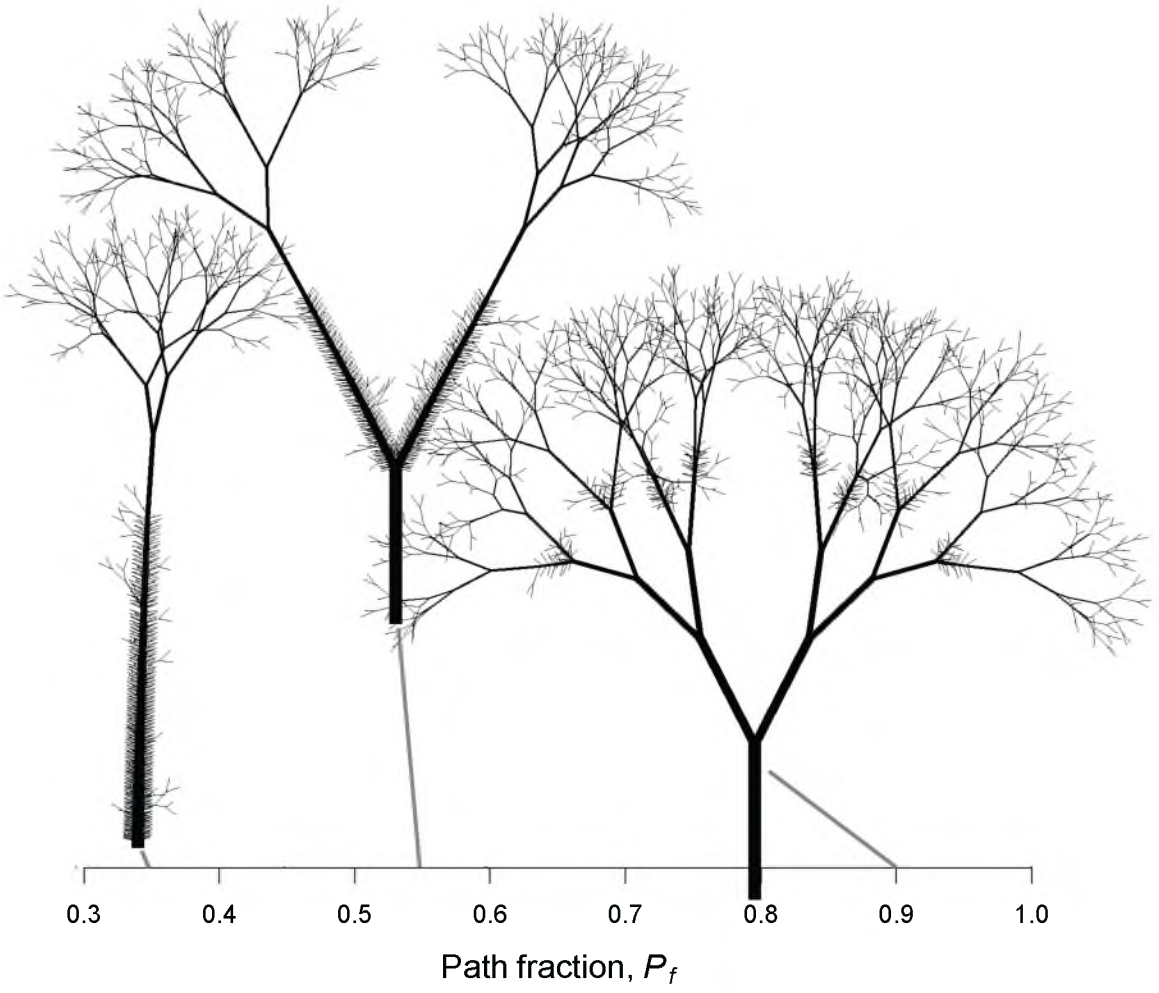

Figure S3.2. Three sample 1024-twig trees formed when more than one asymmetry parameter, u, is used in each tree. Such trees were excluded from the model due to their unrealistic nature.

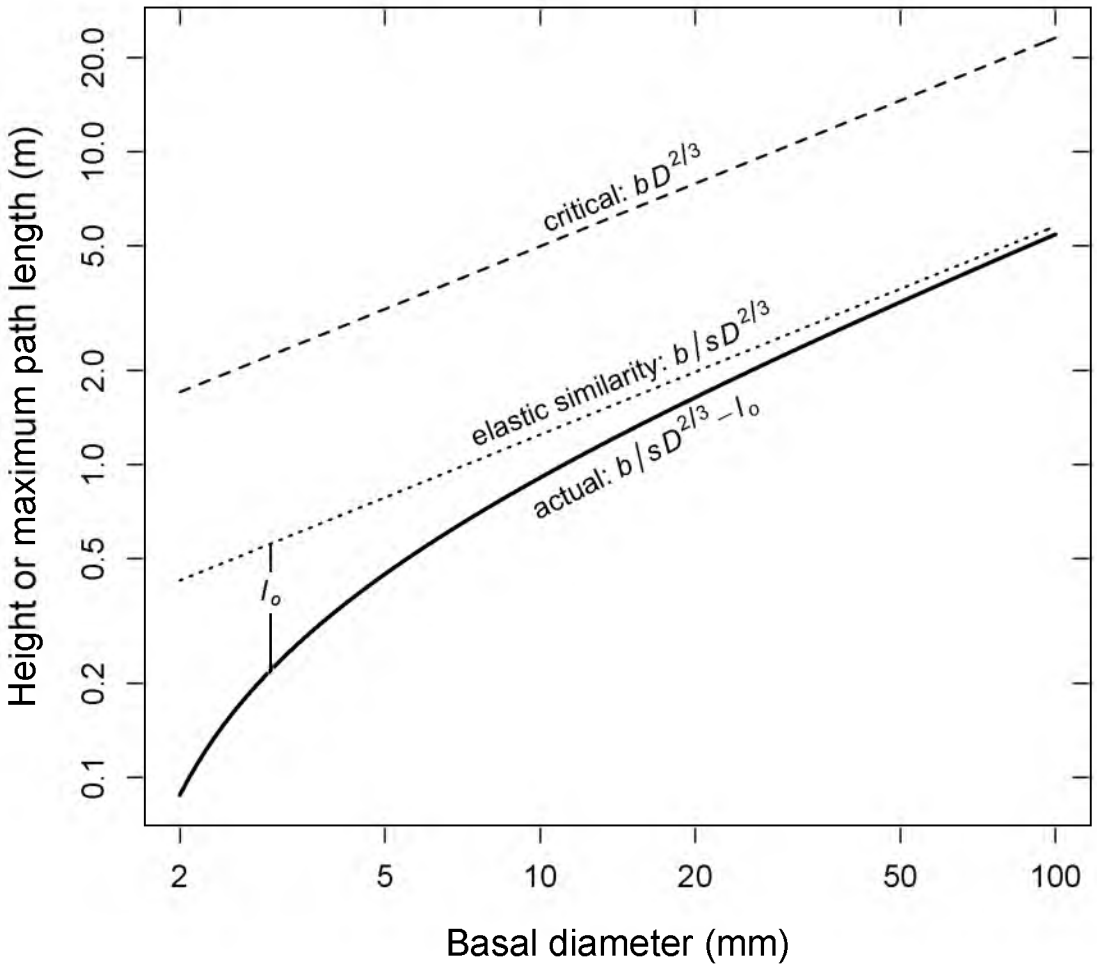

Figure S3.3. Illustration of the equations used to determine tree heights and path lengths. Plots use model inputs with an eventual safety factor of 4 and $D_t = 2$ mm. From top to bottom, the "critical" path (dashed; Eqn. 3.13) predicts the heights of WBE trees at elastic buckling. The "elastic similarity" path (dotted) parallels the critical line and thereby provides a constant safety factor from buckling. The "actual" path (solid; Eqn. 3.8) only approaches elastic similarity because of the constant virtual length, l_o, that exists because twigs do not taper to zero. Note that l_o is constant but does not appear so due to the log-log plotting axis.

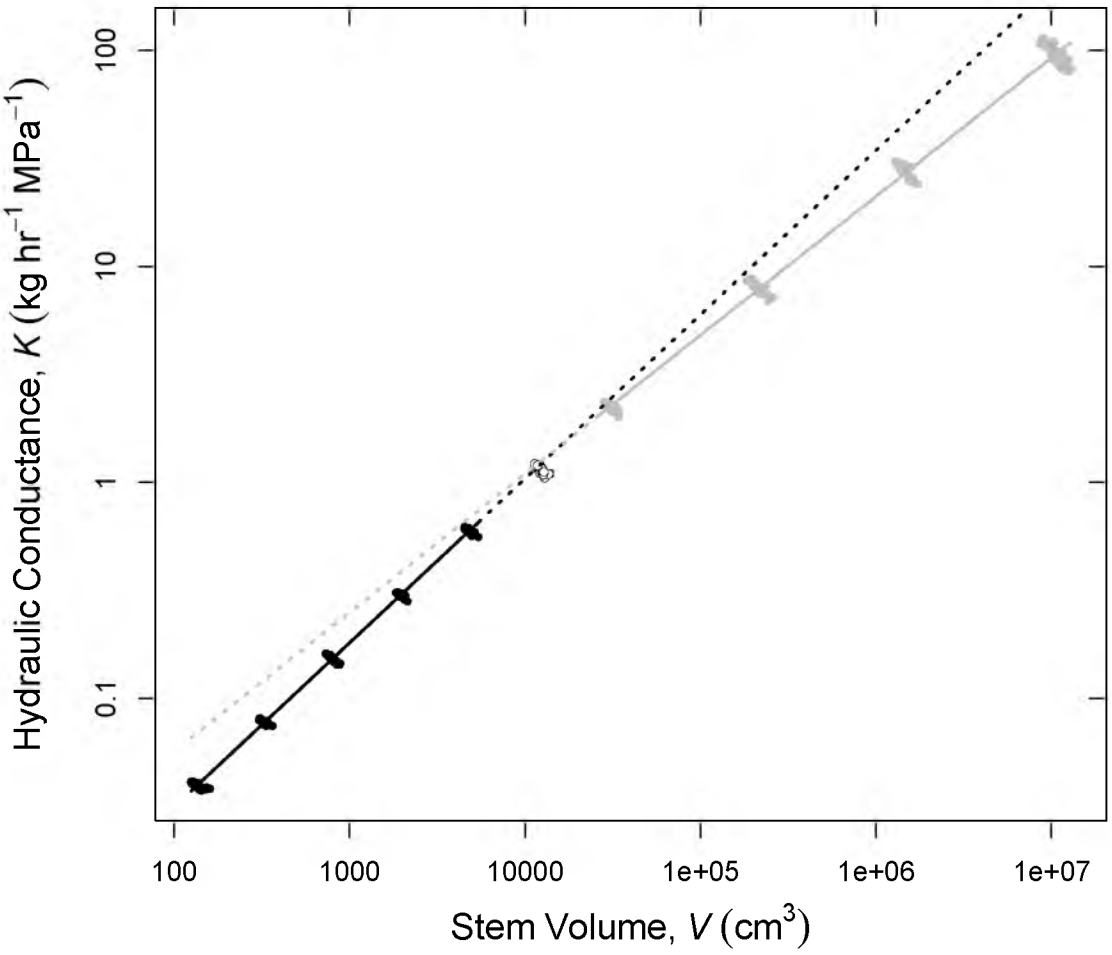

Figure S3.4. Metabolic scaling (i.e., $K \propto V^{cq}$) for trees that follow the crown area scaling measured by Olson *et al.* (2009; i.e., scenario three, S_3). The three colors correspond to P_f decreasing (black; $2^6 - 2^{10}$ twigs), P_f increasing (grey; $2^{12} - 2^{18}$ twigs) and trees in between (open; 2^{11} twigs; see Fig. 3.3, dashed line and Fig. 3.5, "S_3"). Solid SMA regression lines are extended by dotted lines to highlight the nonlog-linearity caused by decreasing and then increasing P_f.

CHAPTER 4

COORDINATION BETWEEN WATER TRANSPORT CAPACITY, BIOMASS GROWTH, METABOLIC SCALING AND SPECIES STATURE IN CO-OCCURRING SHRUB AND TREE SPECIES

4.1 Abstract

The significance of xylem function and metabolic scaling theory begins from the idea that water transport is strongly coupled to growth rate. At the same time, coordination of water transport and growth seemingly should differ between plant functional types. We evaluated relationships between water transport, growth, and species stature in six species of co-occurring trees and shrubs. Within species, a strong proportionality between plant hydraulic conductance (K), sapflow (Q), and shoot biomass growth (G) was generally supported. Across species, however, trees grew more for a given K or Q than shrubs, indicating greater growth-based water use efficiency (WUE) in trees. Trees also showed slower decline in relative growth rate (RGR) than shrubs, equivalent to a steeper G by mass (M) scaling exponent in trees (0.77 - 0.98). The K and Q by M scaling exponents were common across all species (0.80, 0.82), suggesting the steeper G scaling in trees reflects a size-dependent increase in their growth-based WUE. The common K and Q by M exponents were statistically consistent with the 0.75 of ideal scaling theory. A model based on xylem anatomy and branching architecture consistently predicted the observed K by M scaling exponents but only when deviations from ideal symmetric branching were incorporated.

Reprinted with permission from John Wiley & Sons. Smith D.D. & Sperry J.S. (2014) Coordination between water transport capacity, biomass growth, metabolic scaling and species stature in co-occurring shrub and tree species. *Plant, Cell and Environment* 37, 2679–2690.

4.2 Introduction

Studies of plant water transport often assume that greater transport or efficiency of transport leads to greater carbon gain and growth. How valid is this assumption? Theoretically, this idea is based on the shared stomatal pathway for water loss and carbon gain. Water vapor lost by evaporation induces sapflow, Q, to replace this loss and keep cells hydrated. By Darcy's law, Q is the product of hydraulic conductance, K, and the transport driving force, ΔP: $Q = K\Delta P$. For a given ΔP, increasing K by making the xylem network more efficient will support more leaves and/or allow the stomata to open wider, which will increase Q and the potential for CO_2 assimilation. This theory is generally consistent with observed rates of assimilation and growth. Assimilation decreases when hydraulic conductance is reduced by cutting roots or embolizing the xylem (Wan et al. 1993; Hubbard et al. 2001). Growth, measured as basal area increment, increases with K and Q (Pataki et al. 1998; von Allmen et al. 2012). Rootstocks that produce larger fruit trees also have higher K and wider xylem vessels (Solari et al. 2006; Tombesi et al. 2010). Less direct evidence is shown by exponential increases in K and mass over time (Tyree et al. 1998) and studies in which growth and water use generally respond in the same direction to experimental treatments (Grewal 2010; Wolken et al. 2011). In this paper, our basic goal is to evaluate the relationship between biomass growth rate, G, and both K and Q. The K represents a plant's structural investment in water transport while Q can be more meaningful for explaining growth when ΔP changes within or across species.

The coordination between growth and hydraulic conductance is a key component of metabolic scaling theory (MST; West et al. 1999), wherein the nature of this relationship affects numerous downstream predictions about plant and community scaling. G vs K may be described by the power function,

$$G = a_1 K^{b_1} \tag{4.1}$$

with scaling multiplier a_1 and exponent b_1. MST predicts isometry (i.e., $b_1 = 1$) across species. The link from K to G and the prediction of isometry involves assumptions about how K and G scale with Q. Specifically, isometry is required in

$$Q = a_2 K^{b_2} \tag{4.2}$$

and

$$G = a_3 Q^{b_3} \tag{4.3}$$

As per Darcy's law, a_2 and b_2 in Eqn. 4.2 describe how ΔP varies with K. A constant ΔP makes $b_2 = 1$ and $a_2 = \Delta P$, which requires that as plants grow in height, they compensate

for the increasing effects of gravity. In Eqn. 4.3, coefficients a_3 and b_3 integrate instantaneous WUE and carbon allocation and how they vary with Q. If instantaneous WUE is constant and a constant portion of fixed carbon is allocated to growth, then $b_3 = 1$ and a_3 will equal G/Q: a proxy for growth-based WUE.

Assuming, as a null hypothesis, that $b_1 = b_2 = b_3 = 1$ across species, how G, Q, and K scale individually with mass, M, may differ interspecifically. These relationships can be written as

$$K = a_4 M^{b_4} \tag{4.4}$$

$$Q = a_5 M^{b_5} \tag{4.5}$$

and

$$G = a_6 M^{b_6} \tag{4.6}$$

If isometry exists in Eqns 4.1-4.3, then $b_4 = b_5 = b_6$ within species. In MST, the classic prediction is that these "metabolic" exponents equal 0.75 (West et al. 1999). Three-quarter power scaling has since been revised as an upper limit for symmetrically branching trees, based on the effects of finite size and the observed taper and packing of xylem conduits (Savage et al. 2010; Sperry et al. 2012). Recently, however, it has been demonstrated that ontogenetic deviation from symmetric to asymmetric branching and corresponding elongation of crown shape — as observed in young trees — can drive the exponent back up to 0.75 and beyond; this trend is reversed as trees mature and crowns become more spherical (Smith et al. 2014).

Metabolic scaling may also be coordinated with species stature (Sperry et al. 2012). The role of water transport in limiting the maximum size of trees has received much attention (Ryan et al. 2006), but coordination of hydraulic scaling and species-specific stature and growth has not been explored in depth. Taller species may put more of a premium on maximizing the increase in water transport with size, and in converting carbon into height growth than smaller statured species. Hence, it has been speculated that taller statured species may have steeper metabolic and hydraulic scaling than shorter statured species (Sperry et al. 2012).

In this paper, we determine the empirical scaling relationships in Eqns. 4.1 - 4.6 for six co-occurring woody species ranging in stature from shrubs to trees. We chose a riparian community to minimize effects of soil moisture, and focussed on deciduous diffuse-porous angiosperms to minimize differences in growing season length and xylem anatomy. We evaluate the null hypothesis of isometric scaling between plant hydraulic conductance (K), midday sapflow (Q), and annual shoot biomass growth rate (G). These data allow us to

estimate the ranking of growth-based water use efficiency (WUE) among the species. We test the null hypothesis that hydraulic (K and Q) and metabolic (G) scaling with mass is common across species and not different from 0.75 as proposed by classic metabolic scaling theory. We compare our empirical K by M exponent (b_4) with model predictions based on the xylem anatomy of each species, and estimate the importance of deviation from symmetric branching (Smith et al. 2014). Finally, we investigate the coordination between scaling relationships, WUE ranking, and species stature.

4.3 Materials and methods

4.3.1 Location and species

The study took place in Red Butte Canyon Research Natural Area (40.8° N, 111.8° W), located adjacent to the University of Utah in Salt Lake City, UT, USA. Measurements were made at elevations between 1642 and 1913 m.a.s.l. We chose six species from those in and near the riparian zone, including three shrubs (*Amelanchier alnifolia* Nutt., *Cornus sericea* L., and *Symphoricarpos oreophilus* A. Gray) and three trees (*Acer grandidentatum* Nutt., *Betula occidentalis* Hook. and *Populus fremontii* S. Watson). The shrub vs tree distinction is somewhat subjective so we generally compare species in order of increasing maximum size observed in the study area. All species are angiosperms with simple, deciduous leaves. Their xylem is diffuse-porous, with the exception of *Symphoricarpos*, which we found in the course of the study to be functionally ring-porous (i.e., only the current year's growth ring was conductive).

4.3.2 Whole-plant hydraulic conductance

We measured whole-plant hydraulic conductance, K, in 13 - 22 plants per species ($n = 98$ in total). K was obtained from sapflow, Q, and xylem pressure, P, measurements made between 11 July and 3 September 2011. Q was measured using the heat balance method (Baker & Van Bavel 1987), in which a sensor containing a heater and various thermocouples is wrapped around each plant stem. Power from the heater, W_H, may be dissipated radially through the sensor, W_{rad}, or axially by either thermal conductance of the stem, W_{ax}, or convection by sapflow, W_Q. Power may also be stored by the stem, W_s, which is measured by adding another thermocouple to the sensor (Grime et al. 1995). W_Q and, hence, Q may be calculated from the power balance:

$$W_Q = W_H - W_{rad} - W_{ax} - W_s \tag{4.7}$$

We calculated each component of the power balance using standard procedures. Of note, however, W_{rad} requires the thermal conductance of the sensor sheath, k_{sh}, which varies between installations so it is calculated using Eqn 4.7 when W_Q is zero. We assumed W_Q was zero between midnight and 0600 and calculated k_{sh} when the radial temperature difference was greatest, after removing spurious peaks.

We used seven different Dynagage sapflow sensors (Dynamax, Houston, TX) that accommodated trunk diameters between 8 and 203 mm. Sensors were read every 10 s and averages stored every 10 min using a CR7 datalogger (Campbell Scientific, Logan, UT). Heater voltages were maintained at the manufacturer's recommendation with adjustable regulators (Dimension Engineering, Akron, OH). Concurrent with sapflow measurements, we recorded air temperature and vapor pressure deficit (VPD).

Sapflow sensors were generally installed over a three day period, giving one full day and two partial days of measurement. Installations were timed such that the full day occurred when the weather was warm and sunny, so as to maximize Q. These short installation times allowed for many measurements from several sites during one summer. On "full" days, the xylem pressure, P, of each individual was measured at predawn (PD) and midday (MD) using a Scholander-type pressure bomb (PMS Instrument Co., Albany, OR). The $P_{PD}-P_{MD}$ is the pressure difference required to induce flow and resist gravity. The gravity component, $\rho g H$, was calculated using the density of water, gravity and plant height, respectively. We recorded the times at which P was measured and calculated mean Q over these times $\pm$ 1 hour to get Q_{PD} and Q_{MD}. On one occasion, the sensor readings at PD and MD were lost. Because this occurred over a four day installation, we assumed P measurements from one day were similar to the following day, which had similar weather. On another occasion, two trunk thermocouples were not working during PD, which prevented us from calculating Q during this time. Therefore, we used Q_{PD} from the following day and assumed P_{PD} had not changed. The ratio of sapflow and xylem pressure differences yields K:

$$K = \frac{Q_{MD} - Q_{PD}}{P_{PD} - P_{MD} - \rho g H} \tag{4.8}$$

The numerator shall henceforth be referred to as Q. The denominator is the driving force for sapflow, ΔP. We assessed whether ΔP varies within each species, which is relevant for determining if K scaling is representative of Q scaling.

After measuring K, we used a potometer to test the accuracy of our sapflow sensors on a subset of plants. In total, 23 plants with basal diameters $<$ *ca.* 4 cm were cut underwater using a split funnel and immediately placed in a container with a premeasured volume of 20 mM KCl solution filtered to 0.2 μm. Plastic wrap was placed across the container opening

to reduce evaporation. After transpiring for at least 2 hours, the shoot was removed and the remaining solution volume measured. The average flow rates measured by the sensor and the potometer were compared.

4.3.3 Estimating aboveground growth

We estimated G in nearly all plants used to measure K ($n = 87$: 13 - 17 per species). We estimated aboveground vegetative growth only. Because our species were deciduous, we defined G (g yr^{-1}) as the annual stem mass increment plus the standing leaf mass. Using trunk diameter (D_T), growth ring thicknesses and species-specific allometric relationships, we estimated G as follows.

Firstly, from each measured D_T, we predicted the cambium diameter, D_c, using regressions on D_c vs D_T data. These data came from trunks for which we measured sapwood area (see Modeling hydraulic scaling from structure). We subtracted growth ring thickness from each D_c to get the cambium diameter in the previous year. Ring thicknesses were measured from dissecting scope and microscope photos of trunk cross-sections and cores. Cross-sections were obtained immediately after K measurements while cores were taken later in the season. In both cases, we assumed that most radial growth was already complete for the season. We then predicted D_T in the previous year from its D_c and the D_c vs D_T regressions. This method accounts for changes in D_T due to both xylem and bark.

Secondly, plant heights, H, in the current and previous years were predicted from H vs D allometry. We constructed H by D curves for each species using: whole plants ($n = 185$, including many used for K); branches ($n = 216$, from K-plants); and twigs ($n = 203$, from non K-plants). H measurements were made directly or using trigonometry for taller plants. This data set was meant to include the full range of plant sizes for each species. As such, we used the maximum D_T from this data set to define each species stature. The data were fit with the equation,

$$H = a_7 D^{b_7} - l_o \tag{4.9}$$

The l_o term is used because H by D relationships generally start out steep on a log scale and gradually asymptote towards a constant, shallower slope, b_7 (McMahon & Kronauer 1976; Smith et al. 2014).

Thirdly, dry stem mass, M_{st}, in the current and previous years was predicted from how M_{st} scaled with a shoot volume proxy, HD_T^2. We obtained M_{st} by HD_T^2 scaling from branches ($n = 209$) and a few K-plants cut down ($n = 5$), which were oven dried at 60 °C for at least a week.

Finally, we predicted total dry leaf mass, M_{lv}, in the current year from M_{lv} vs M_{st} scaling relationships. These relationships came from the same data set used in step 3 ($n = 211$ branches; $n = 5$ whole shoots). We calculated growth as the annual M_{st} increment plus the current M_{lv}.

4.3.4 Modeling hydraulic scaling from structure

Whole-plant hydraulic conductance is largely dependent on xylem conduit properties and branching structure (Sperry et al. 2012; Smith et al. 2014). To help interpret our K data in terms of contributions from the xylem and branch networks, we modeled aboveground xylem networks using measured diameters and numbers of active xylem conduits in all species. We used these data to predict aboveground K and used a root:shoot resistance ratio to predict belowground and whole-plant K. Xylem anatomy data were obtained using our own measurements and published data for *Acer grandidentatum* collected from the same area (von Allmen et al. 2012). We collected xylem samples from a wide range of stem diameters, D. From these samples, thin transverse sections were prepared with a sliding microtome, stained with 1:1 phloroglucinol (1% in EtOH): HCl (12 M), and photographed for analysis. Using at least three photos from each stem, a section of the youngest growth ring was isolated. The area of this xylem section (A_x) and all individual vessel diameters, $\dot{d}$, were measured using STEM GUI software (Charles A. Price, personal communication). From these measurements, we calculated the hydraulically-weighted mean vessel diameter ($d = \left[\frac{1}{n}\sum_{i=1}^{n} \dot{d}_i^4\right]^{1/4}$) and the vessel frequency (n/A_x) of each stem (Savage et al. 2010). Combined with stem diameter measurements, these data give vessel taper (d vs D) and packing (n/A_x vs d). Packing data were fit with power functions. A rise-to-max function was more appropriate for the taper data:

$$d = \frac{D d_{max}}{D + m} \tag{4.10}$$

The d_{max} and m are fitting parameters. Taper and packing equations together can predict the diameter and number of vessels as a function of stem diameter.

To determine which vessels are functional in water transport, we introduced dye to transpiring stems. Again, we chose a wide range of stem diameters from each species. For small stem diameters ($<$ *ca.* 4 cm), stems were cut underwater using a split funnel and the cut end immediately placed in 0.05% safranin O solution and allowed to transpire for 2 hours. Stems were later cut and photographed *ca.* 10 cm from the end and the dyed area measured. For larger stems, a hole was drilled at least half way into the trunk. To minimize air introduction to the xylem while drilling (but see Wheeler et al. 2013), a modified PVC

fitting was secured against the trunk at the drill site and filled with water. Plastic tubing was inserted into the hole and kept filled with safranin O solution as the plant transpired. After at least an hour, a core was taken ca. 10 cm above the dye point using a 5 mm increment borer. Sapwood depth was measured from the cores and converted to sapwood area. All sapwood measurements from small stems and many from larger stems came from plants used for hydraulic conductance measurements.

To obtain root:shoot resistance ratios, we measured midday root crown xylem pressures (P_{RC}) in addition to predawn and midday leaf P. Root crown P was determined by covering a basal shoot with aluminum foil and a plastic bag and measuring its xylem pressure after allowing at least an hour to equilibrate with the root crown. These measurements were obtained from some of the plants used for K as well as others measured in August and September 2013. The proportion of total resistance due to the roots, Pr_{root}, is,

$$Pr_{root} = \frac{P_{PD} - P_{RC}}{P_{PD} - P_{MD}} \tag{4.11}$$

If Pr_{root} is size-dependent, then whole-plant hydraulic scaling can differ from aboveground scaling (Martínez-Vilalta et al. 2007; Sperry et al. 2012).

We used taper, packing, sapwood and Pr_{root} in a version of the West, Brown & Enquist (WBE; 1999) model modified by Smith et al. (2014). Briefly, this model follows biomechanical rules to create trees that are "plumbed" with xylem conduits to calculate hydraulic conductance of the stem network. Conduits in leaves and roots are not explicitly modeled. Rather, proportionality constants link their hydraulic conductances to those of the twigs and shoot, respectively. The hydraulic conductances of leaves, stems and roots are added serially to predict K. Aside from adding our species-specific xylem parameters, we only changed the model to accommodate the rise-to-max taper function (Eqn. 4.10).

The model creates plants with either symmetrical WBE architecture or random branching across the spectrum of possible architectures (see Smith et al. 2014). Architecture is quantified using the "path fraction," P_f, which is the ratio of the mean and maximum trunk-to-twig pathlengths. The maximum P_f is 1, which corresponds to symmetrical branching and a round crown shape. Smaller P_f values are due to asymmetric branching and result in elongated crown shapes. We modeled hydraulic conductance under two scenarios: constant symmetric WBE architecture ($K_{m,WBE}$) and ontogenetically changing architecture ($K_{m,\Delta}$). In both scenarios, we modeled plants across the measured D_T range of each species. The D_T increments were chosen based on the discrete diameters possible for WBE structures. The M was predicted from D_T using species specific allometry as above. For $K_{m,WBE}$, we modeled WBE structures and plumbed them for each species to calculate

hydraulic conductances. The modeled points were fit with a spline to predict $K_{m,WBE}$ at each measured D_T. These predictions were used to test for species differences due to xylem anatomy alone. For $K_{m,\Delta}$, Smith et al. (2014) estimated that P_f would start high in small plants, decline rapidly and then increase gradually (see dashed curve in their Fig. 3). In order to model structures that follow this P_f trajectory, we generated 5000 random branching structures at each D_T, using the default branching inputs of the model. We then selected structures that matched each target $P_f \pm 0.01$. Five thousand was deemed sufficient to populate the range of possible architectures and resulted in 49 to 125 structures being chosen at each P_f. Each branching structure was then plumbed for each species according to its anatomy. These predictions were used to test if size-linked variation in branching architecture could be a component of observed K by M scaling results.

4.3.5 Statistics

All analyses were performed within the R modelling and data analysis environment (R Core Team 2014). Unless otherwise noted, all claims of significance were evaluated using $p = 0.05$ as the threshold. For linear regressions, we followed the advice of Warton et al. (2006) on when to use OLS or SMA (standardized major axis). In short, when the goal was to predict y data from x data, OLS was used. When the slope of a relationship was of interest, SMA was used. SMA regressions were made and compared using the SMATR package for R (Warton et al. 2012). We generally evaluated regressions by testing for common exponents and common multipliers. In the context of this study, the common exponent test considers whether regression lines fit to each species are statistically parallel to each other (on a log-log scale) regardless of their multipliers (see Fig. S4.1). For the common multiplier test, multipliers are obtained by forcing each regression to follow the common exponent. These "forced multipliers" are then tested for significant differences. Because comparing multipliers requires use of a common exponent, this test is only relevant when a common exponent is supported (Warton et al. 2006). When exponents are different, scaling relationships cross, and multipliers are not indicative of the relative heights of the relationships.

Where appropriate, we compared the exponents and multipliers of individual species using post hoc pairwise comparisons. When comparing means between species, we used ANOVA to detect differences and used Tukey Honest Significant Differences for post hoc pairwise comparisons. The p-values from all pairwise comparisons were adjusted to avoid Type I errors.

In this study, we compared a number of plant properties that are autocorrelated. For

example, we tested Q vs K scaling when K is calculated from $Q/\Delta P$. However, it should be noted that autocorrelation does not detract from the goals of our analyses. The point of Q vs K analyses was to show the effects of ΔP variation within and between species. Similarly, we analyze G vs M although M was used as part of G estimation. The G vs M analyses were meant to illustrate the net effect of different growth ring thicknesses and different allometric relationships used to predict mass.

4.4 Results

4.4.1 Sapflow sensor accuracy

We compared average flow rates measured simultaneously by sapflow sensors (Q_{sens}) and a potometer (Q_{pot}). One of the 23 measurements was removed because the potometer ran dry. The Q measurements were well correlated ($r^2 = 0.93$; Fig. S4.2). An SMA regression of Q_{pot} vs Q_{sens} indicated a slightly but significantly greater slope than one (1.17; $p = 0.01$) but the intercept (-2.47e-3) did not differ from zero. These results indicate that the sensors are reasonably accurate but tend to underestimate actual Q by a constant factor.

4.4.2 M, H, and D allometries for predicting growth

We predicted aboveground annual growth, G, using growth ring measurements and four allometric relationships for each species. Cambium vs trunk diameter scaling was very similar across species and data were well correlated within species ($r^2 > 0.98$; not shown). Using these relationships, bark growth was estimated as 1 to 12% of D_T growth. The H vs D data were fairly convergent across species and each was well fit by Eqn. 4.9 ($r^2 > 0.92$; Table 4.1; Fig. S4.3), which we used to predict H from D_T in the current and previous years. We used HD_T^2 to predict total dry stem masses, M_{st}, using M_{st} vs HD^2 data. These data were well fit by power functions ($r^2 > 0.94$; Table 4.1; Fig. S4.4) and as expected, M_{st} vs HD^2 relationships were more log-linear than M_{st} vs D^2 or H alone (not shown). Finally, we predicted dry leaf mass, M_{lv}, in the current year using regressions from M_{lv} vs M_{st} data ($r^2 > 0.65$; Fig. S4.5; Table 4.1). The good fits observed for each of these allometries gave us confidence in using them to estimate M and G.

4.4.3 Growth by conductance scaling (Eqn. 4.1)

Growth and hydraulic conductance were generally convergent across species. Scaling exponents, b_1, were significant in all but *Symphoricarpos* (Fig. 4.1a; Table 4.2). Significant exponents ranged from 0.84 to 1.19 and r^2 from 0.56 to 0.91. Our null hypothesis of isometry was supported by all species although *Populus* was weakly steeper ($b_1 = 1.19$; $p = 0.052$).

Significant species supported a common exponent ($b_1 = 1.06$) that also agreed with isometry. Regressions were forced to the common exponent to compare multipliers. These "forced multipliers" were not common across species. Additionally, there was a tendency for forced multipliers to increase with increasing species stature, meaning that larger species tended to have greater growth per K than smaller species. The multiplier of the largest statured species, *Populus*, significantly exceeded *Betula* and *Cornus* (see Fig. 4.1a). Consistent with stature-linked increases in the multiplier, the interspecific scaling exponent across all species ($b_1 = 1.18$) was significantly steeper than isometry (Table 4.2).

4.4.4 Water use by conductance scaling (Eqn. 4.2)

The Q by K scaling exponents, b_2, were significant in all species, ranging from 0.85 to 1.12 (Fig. 4.1b, Table 4.2). None differed from our null hypothesis of isometry, although *Populus* was weakly steeper ($b_2 = 1.12$; $p = 0.051$). Species supported a common exponent ($b_2 = 1.01$) that also agreed with isometry. Isometry corresponds to a constant ΔP within species, which was confirmed by nonsignificant ΔP vs K scaling exponents (not shown), although, the exponent for *Symphoricarpos* (-0.52) was almost significant ($p = 0.06$). When forced to the common Q by K exponent, species did not share a common multiplier. The forced multipliers of the shrubs were all greater than those of trees (see Fig. 4.1b), meaning that smaller species transported more water per K than larger ones. Statistically, all species exceeded *Populus* while *Amelanchier* and *Cornus* also exceeded *Betula*. Additionally, *Amelanchier* exceeded *Cornus*. The trend in multipliers suggests that larger statured species tended to have lower ΔP. Indeed, the ΔP of *Populus* (0.54 ± 0.05 MPa; mean ± SE) was significantly less than all other species. *Amelanchier* (1.46 ± 0.08 MPa) exceeded all species but *Symphoricarpos* (1.20 ± 0.11 MPa). The interspecific exponent ($b_2 = 0.93$) was significantly shallower than isometry — consistent with the decrease in multipliers with stature.

4.4.5 Environmental variation

Environmental conditions were fairly consistent across across measurement days and generally had a minimal influence on Q by K scaling. Midday VPD ranged from 1.2 to 2.7 kPa with no significant trend over time. Residuals of Q vs K increased significantly with midday VPD for *Amelanchier* ($r^2 = 0.32$). Although, *Amelanchier*'s Q vs K relationship had $r^2 = 0.94$, suggesting the magnitude of the VPD effect was small. Midday air temperature ranged from 21 to 29 °C. A significant downward trend over time was observed but this was attributed to two cooler late-season days, whose removal nullified the significance

($p = 0.96$). Residuals of Q vs K increased significantly with midday air temperature in *Amelanchier* ($r^2 = 0.45$) and *Symphoricarpos* ($r^2 = 0.53$). These species had respective Q vs K r^2 values of 0.94 and 0.73, again suggesting minor influence of environmental variation on the Q by K scaling. Soil moisture, as assessed by predawn xylem pressure (P_{PD}), ranged from -1 to -0.05 MPa with 95% of values between -0.67 and -0.11 MPa. Pressures measured midseason tended to be the least negative and a quadratic polynomial fit with day of year was significant. The Q by K residuals for *Symphoricarpos* increased significantly as P_{PD} became more negative ($r^2 = 0.39$), but again the Q by K r^2 was high (0.73), suggesting a primary influence of K over environmental factors.

4.4.6 Growth by sapflow scaling (Eqn. 4.3) and WUE

Growth vs sapflow exponents, b_3, were significant in all species except *Symphoricarpos* (Fig. 4.2a; Table 4.2). Significant exponents ranged from 0.87 to 1.12 and all agreed with the hypothesized isometry. These species shared a common exponent ($b_3 = 1.03$) which also supported isometry. A common multiplier was not supported. Forced multipliers tended to be greater in trees than in shrubs, meaning that trees put on more growth per water use than shrubs. Statistically, *Populus* had a larger multiplier than all other species. *Acer* and *Betula* exceeded *Cornus* as well. Isometry suggests that growth-based WUE (as G/Q) is approximately constant within species while the trend observed among multipliers suggest that G/Q increased with species stature. The mean G/Q was lower in shrubs than in trees though the only significant difference was between *Populus* and all other species (Fig. 4.2b). In accordance with stature-correlated multipliers, interspecific scaling ($b_3 = 1.28$) was steeper than any intraspecific exponent and significantly greater than isometry.

4.4.7 Conductance by mass scaling (Eqn. 4.4)

Hydraulic conductance and mass were significantly correlated in all species except *Symphoricarpos* (Fig. 4.3, black circles). Significant exponents ranged from $b_4 = 0.74$ to 0.90 (Table 4.2). These exponents, except that of *Acer* (0.90), supported the classic MST prediction of $b_4 = 0.75$. The significant species also supported a common exponent ($b_4 = 0.80$) that agreed with 0.75. When forced to the common exponent, a common multiplier was not supported. Forced multipliers showed no noticeable trend with stature or other traits. *Cornus* significantly exceeded *Acer*, *Amelanchier* and *Betula*. Consistent with the lack of any trend in multipliers, the interspecific exponent ($b_4 = 0.79$) did not differ from 0.75.

4.4.8 Sapflow by mass scaling (Eqn. 4.5)

Sapflow and mass were significantly correlated in all species except *Symphoricarpos*. Significant exponents ranged from $b_5 = 0.75$ to 0.92 (Fig. 4.4a; Table 4.2). These exponents, except that of *Populus*, supported the MST prediction of $b_5 = 0.75$. The significant species also supported a common exponent ($b_5 = 0.82$) that agreed with 0.75. A common multiplier was not supported when forced to the common exponent. The forced multipliers of the shrubs tended to be greater than the trees such that shrubs had greater Q at a given mass. Statistically, *Cornus* exceeded all other significant species while *Amelanchier* and *Betula* also exceeded *Populus*. The interspecific exponent ($b_5 = 0.74$) did not differ from 0.75.

4.4.9 Growth by mass scaling (Eqn. 4.6)

Growth and mass were significantly correlated in all species with exponents ranging from $b_6 = 0.70$ to 0.98 (Fig. 4.4b; Table 4.2). The MST exponent, $b_6 = 0.75$, was supported by all species except *Betula* and *Populus*. A common exponent was not supported. Shrubs tended to have shallower scaling ($b_6 = 0.70$ to 0.73) than trees ($b_6 = 0.77$ to 0.98) but the only significant difference was between trees *Populus* and *Acer*. Interspecific scaling ($b_6 = 0.95$) was significantly steeper than 0.75.

The difference between species is especially apparent when growth is expressed as relative growth rate, G/M (Fig. 4.5; Table 4.2). Because b_6 was consistently < 1, G/M declined in all species, though not significantly in *Populus*. Among the significant species, a common exponent was not supported. Shrubs tended to have more negative exponents than trees, meaning relative growth rates declined more rapidly. Statistically, *Symphoricarpos* was steeper than *Acer* and *Betula*.

4.4.10 Modeling hydraulic conductance by mass scaling

In each species we measured xylem anatomy (taper, packing, sapwood) and the proportion of hydraulic resistance in roots, Pr_{root}. From these data we modeled whole plant hydraulic conductance using WBE architecture ($K_{m,WBE}$) or changing architecture ($K_{m,\Delta}$) for comparison with K measurements. Xylem conduit packing and sapwood measurements were generally well fit by power functions while a Michaelis-Menten function (Eqn. 4.10) was more appropriate for conduit taper (see Figs. S4.6 - S4.8, Table 4.3). Xylem properties were fairly similar between species but with some notable differences. Taper functions indicated that the maximum vessel diameter, d_{max}, ranged from 26.2 μm (*Symphoricarpos*) to 79.1 μm (*Populus*; Fig. S4.6). Most packing functions had exponents near -2, indicating a constant xylem fraction devoted to conduits, while the exponent of *Symphoricarpos* was

much shallower (-1.02; higher vessel frequency in trunks than twigs) and its conduits tended to occupy a larger fraction of the xylem than other species (see Fig. S4.7). Sapwood area scaling was similar between species although *Amelanchier* and *Symphoricarpos* had notably less sapwood at a given diameter (Fig. S4.8). In *Symphoricarpos*, only the outermost growth ring tended to conduct water, which was counter to our assumption that all species were functionally diffuse porous.

The mean proportion of hydraulic resistance in roots, Pr_{root}, ranged from 0.24 (*Populus*) to 0.50 (*Acer*) but individual measurements varied substantially within each species (overall range: 0.10 to 0.97; data not shown). The variation was significantly explained by plant size (D_T) in only *Acer* and *Betula*. The Pr_{root} of *Acer* tended to decrease according to a power function ($r^2 = 0.36$) while in *Betula* it tended to increase linearly ($r^2 = 0.29$). For *Acer* and *Betula*, we used these equations to predict Pr_{root} in each plant. For the other four species we used their respective mean Pr_{root} in determining K_m.

First, we predicted $K_{m,WBE}$ based on symmetric WBE architecture. The predictions tended to exceeded K measurements (Fig. 4.3, open circles). The ratio, $K_{m,WBE}/K$, ranged from 0.5 to 14.4 (mean 3.9) with better fit at higher K. The $K_{m,WBE}$ vs M exponents ranged from 0.52 to 0.73 with $r^2 > 0.99$ (Table 4.2). All exponents were shallower than their measured K vs M counterparts. We treated the modeled exponents as parametric values to test if K vs M exponents differed significantly. Modeled exponents were significantly shallower than measured ones except for *Cornus* ($p = 0.27$) and *Populus* ($p = 0.20$). Thus, using WBE architecture, the model poorly predicted the pattern of scaling variation observed among species.

Next, we predicted $K_{m,\Delta}$ based on ontogenetically changing architecture (defined as P_f) following estimations of Smith et al. (2014). Accordingly, small plants began with P_f near 1 (WBE-type architecture) and dropped to *ca.* $P_f = 0.4$ before rising gradually again in larger plants. Shrubs occupied the initial P_f-decreasing phase, whereas the study trees extended beyond this phase to where P_f bottomed out and began its gradual rise. The $K_{m,\Delta}$ vs M exponents ranged from 0.68 to 0.82 with $r^2 > 0.99$ (Table 4.2; Fig. 4.3, dashed lines). These exponents were steeper than their $K_{m,WBE}$ vs M counterparts but still slightly shallower than measured K vs M exponents. However, all K vs M exponents agreed statistically with $K_{m,\Delta}$ vs M exponents. Furthermore, the modeled and measured exponents were well correlated ($p = 0.005$), suggesting that the model accurately predicted the observed pattern of scaling variation across species when dynamic branching architecture was incorporated.

4.5 Discussion

Our main goal was to evaluate the relationship between hydraulic conductance (K) and growth rate (G) in co-occurring woody plants. The data mainly supported the null hypothesis of intraspecific isometry between K and G. Thus, there appears to be an approximately linear connection between water conducting capacity and shoot growth within a species. The data also supported the hypothetical mechanism linking K and G. A size-invariant pressure drop, ΔP, resulted in the sapflow rate, Q, being proportional to K within a species. Also, Q was generally proportional to G, implying an approximately size-invariant fraction of assimilated carbon allocated to shoot growth. This proportionality between Q and G, and hence a constant growth-based water use efficiency (WUE proportional to G/Q), is a basic assumption of vascular-based metabolic scaling theory. Even if G and Q did not scale proportionally with K, the theory in its simplest form would still predict isometry between Q and G. This was indeed the case in *Populus*: G and Q scaled weakly steeper than isometrically with K, yet G and Q remained proportional to each other (Table 4.2). An exceptional species altogether was *Symphoricarpos*, where many scaling relationships were not significant. However, *Symphoricarpos* was also the smallest species which inherently limited the ability to assess size scaling.

Looking across species rather than within, our results showed a very different trend. Trees tended to grow more for a given K, as shown by their larger forced multipliers (a_1, Eqn. 4.1). The greater growth in trees, however, was not associated with greater sapflow rates. In fact, the opposite trend was observed: trees had lower Q than shrubs at a given K because of a trend to smaller ΔP in trees. The larger species simply grew more for a given Q, which implies greater growth-based WUE. We did not measure WUE because G was measured on an annual basis, whereas Q was a midday average representing maximum seasonal steady-state flow rates. However, the ratio G/Q provides a reasonable WUE proxy if it is assumed that Q is roughly proportional to cumulative seasonal sapflow. This is likely the case since all plants were co-occurring in a riparian setting, and had similar leaf phenologies and hence growing season length.

Greater growth-based WUE in trees could result from higher instantaneous WUE (assimilation rate per transpiration rate), and greater allocation of carbon to shoot growth vs other sinks. Greater instantaneous WUE in trees could reflect a greater average exposure of tree canopies to light (Avola et al. 2008), although we tried to minimize differences in the light environment of the study plants. From an allocation standpoint, it is likely that trees, particularly in their early years (such as those we sampled), would maximize

their shoot growth to reach the canopy, whereas shrubs remain low-growing. Due to the sapflow sensor design, our study trees tended to be small and hence were also rarely fertile. Among the material used for mass allometry, only 1 of 85 tree branches was reproductive compared to 35 of 126 among shrubs. Reduced allocation to reproduction could favor allocation to shoot growth in trees vs shrubs. Additionally, shrubs may be adapted to more frequent crown disturbances and dieback, and may allocate more carbon to underground storage to facilitate frequent resprouting rather than investing heavily in shoot growth (Pate et al. 1990; Bowen & Pate 1993; Bond & Midgley 2001). Finally, modelling shows that preferential investment in stems and roots over leaves comes at a metabolic cost which reduces productivity (Magnani et al. 2000). Accordingly, Mencuccini (2003) found that relative to shrubs, trees tended to support more leaves at a given K, which echoes our observations of greater G/Q in trees.

Somewhat surprisingly, given the numerous influences governing metabolic scaling with plant mass (M), our mass scaling exponents (b_4, b_5, b_6) were generally consistent with the classic MST prediction of 0.75. Both K and Q scaled with M to a common exponent that was not statistically different from 0.75 (Table 4.2). Four of the six species showed a G by M exponent not different from 0.75 (Table 4.2). According to MST and the observed approximate proportionality between K, Q, and G, we expected $b_4 \approx b_5 \approx b_4$. Indeed, the common exponents for K and Q scaling were quite similar ($b_4 = 0.80$ vs $b_5 = 0.82$; Table 4.2). However, there was more variation in the G by M relationships, which did not support a common b_6 exponent. Interestingly, this G by M exponent increased with species stature (Fig. 4.4b), such that relative growth rate (RGR) declined much more steeply with plant size in shrubs vs trees (Fig. 4.5).

In hindsight, it seems obvious that shrubs must have a lower G by M exponent, and hence faster decline in RGR than trees. After all, if they did not, they would grow to be trees unless they had accelerated annual dieback. This intuitive trend is not, however, demonstrably a consequence of lower Q and K by M exponents in shrubs vs trees as might be expected from MST. Instead, the G by M scaling in a species appears to have changed independently of Q and K. Seemingly the only way for this to happen is through ontogenetic variation in the WUE proxy, G/Q. Although statistically speaking we found G by Q scaling to be consistent with isometry, the mass scaling observations suggest a statistically nondetected allometry of G/Q. Algebraically, the G/Q by M exponent equals $b_6 - b_5$. In general, this difference is negative in shrubs and positive in trees (*Acer* being an exception). The implication is that growth-based WUE is not only lower in absolute terms in shrubs vs trees as discussed

above, but it also tends to decline with size in shrubs vs increase with size in trees (at least over the size range we measured). These G/Q trends remain hypothetical, however, since they were not statistically evident. Nevertheless, the ultimate outcome of a faster decline in RGR in shrubs vs trees was robust. We are not aware of any studies in which RGR of mature plants was compared between different woody functional types; most observations concern seedlings and emphasize differences between woody and herbaceous growth forms (e.g., Grime & Hunt 1975). Comparisons at the seedling stage for shrubs and trees indicate no difference (Castro-Díez et al. 2003), so the divergence we observed may develop later in ontogeny.

Our results provide some insight into the underlying complexity of how woody plant ontogeny results in a particular mass scaling exponent, which according to ideal MST theory is similar between b_4, b_5 and b_6. Previous modeling quantifies how the exponents vary with: a) size-dependent trends in WUE and carbon allocation (Enquist et al. 2007); b) the range of sizes being scaled (Savage et al. 2010); c) vascular architecture (Sperry et al. 2012); and d) ontogenetic shifts in branching symmetry (Smith et al. 2014). According to our results, any role of a) should be subtle in our data set, because as discussed above, G/Q was statistically constant within species. When our model simulations incorporated b) and c) for symmetric crowns (i.e., $K_{m,WBE}$), the modeled metabolic scaling exponent often significantly underpredicted b_4. Moreover, these modeled exponents fell below 0.75, consistent with previous predictions for realistically plumbed trees of finite size and symmetric branching architecture (Savage et al. 2010; Sperry et al. 2012). However, when we additionally incorporated d) into the model (i.e., $K_{m,\Delta}$), the scaling exponents steepened, statistically matching b_4. Though the model used the same architectural trajectory for all species, the effect on the modeled exponents varied across species due to differences in xylem anatomy and plant size. Therefore, the combined variation in xylem anatomy and branching architecture appears important for accurately predicting the K by M exponent.

Ontogenetic trends in crown architecture may also explain why our measured K by M exponents were steeper than those measured by von Allmen et al. (2012), who found $b_4 = 0.65$ and 0.62, respectively, in *Quercus gambelii* and the same *Acer grandidentatum* we measured (and in the same study site). The von Allmen et al. study measured a larger range in tree size than we did, up to the biggest trees available. As trees pass out of the juvenile stage and reach the canopy, their crown shape stabilizes and even tends to reverse to a more rounded form (Smith et al. 2014). As Smith et al. show, this drives down metabolic scaling exponents. Thus, it is possible that the scaling exponents in the present study differed from

those measured by von Allmen et al. (2012) because trees were measured over two different architectural phases.

Our observations of approximate isometry between K, Q, and G across diverse species strongly support the important idea that the hydraulic network of plants has a strong and simple coordination with carbon assimilation and growth. This validates the long-assumed adaptive significance for the evolution of greater water conducting capacity, and it supports a founding assumption of network-based derivations of metabolic scaling theory. At the same time, our results highlight that growth may be altered independently of water transport. Shrubs in our data set appeared to grow less for a given water transport capacity than the trees we studied; and the shrubs tended towards flatter growth by mass scaling than young trees. Divergence in instantaneous WUE and allocation presumably create these differences between species. Differences between species and functional types resulted in interspecific scaling being generally different from intraspecific scaling, as will usually be the case (Heusner 1982). Intraspecific scaling is complex, but as our results indicate, it can be predicted from multiple ontogenetic processes and constraints. In contrast, interspecific scaling quickly becomes ambiguous because it depends not only on the scaling for each species involved, and species sampling, but also on the size range over which each species was measured. Part of the appeal of a species-specific metabolic scaling approach is that K and how it scales may be predicted using a small (but growing) number of structural parameters that can be measured fairly easily for individual species. The Q can then be predicted from standard ΔP measurements or assumptions. Any modeling of G from Q, however, will require capturing the dominant controls on instantaneous WUE and carbon allocation.

4.6 Acknowledgments

We thank Henry Grover and David Love for their field assistance and numerous anatomical measurements. Allison Thompson also contributed to growth ring and sapwood measurements. Helpful input was provided by Lisa Bentley, Brian Enquist, Peter Reich and Van Savage in the early stages of this work. The authors were supported by NSF IBN-0743148. We declare no conflicts of interest.

4.7 References

Avola G., Cavallaro V., Patanè C. & Riggi E. (2008) Gas exchange and photosynthetic water use efficiency in response to light, CO_2 concentration and temperature in *Vicia faba*. *Journal of Plant Physiology* 165, 796–804.

Baker J.M. & Van Bavel C.H.M. (1987) Measurement of mass flow of water in the stems of herbaceous plants. *Plant Cell and Environment* 10, 777–782.

Bond W.J. & Midgley J.J. (2001) Ecology of sprouting in woody plants: the persistence niche. *Trends in Ecology and Evolution* 16, 45–51.

Bowen B.J. & Pate J.S. (1993) The significance of root starch in post-fire shoot recovery of the resprouter *Stirlingia latifolia* R. Br. (Proteaceae). *Annals of Botany* 72, 7–16.

Castro-Díez P., Montserrat-Martí G. & Cornelissen J.H.C. (2003) Trade-offs between phenology, relative growth rate, life form and seed mass among 22 Mediterranean woody species. *Plant Ecology* 166, 117–129.

Enquist B.J., Kerkhoff A.J., Stark S.C., Swenson N.G., McCarthy M.C. & Price C.A. (2007) A general integrative model for scaling plant growth, carbon flux, and functional trait spectra. *Nature* 449, 218–222.

Grewal H.S. (2010) Water uptake, water use efficiency, plant growth and ionic balance of wheat, barley, canola and chickpea plants on a sodic vertosol with variable subsoil NaCl salinity. *Agricultural Water Management* 97, 148–156.

Grime J. & Hunt R. (1975) Relative growth-rate: its range and adaptive significance in a loca flora. *Journal of Ecology* 63, 393–422.

Grime V.L., Morison J.I.L. & Simmonds L.P. (1995) Including the heat storage term in sap flow measurements with the stem heat balance method. *Agricultural and Forest Meteorology* 74, 1–25.

Heusner A.A. (1982) Energy and metabolism I. Is the 0.75 mass exponent of Kleiber's equation a statistical artifact? *Respiration Physiology* 48, 1–12.

Hubbard R.M., Stiller V., Ryan M.G. & Sperry J.S. (2001) Stomatal conductance and photosynthesis vary linearly with plant hydraulic conductance in ponderosa pine. *Plant Cell and Environment* 24, 113–121.

Magnani F., Mencuccini M. & Grace J. (2000) Age-related decline in stand productivity: the role of structural acclimation under hydraulic constraints. *Plant Cell and Environment* 23, 251–264.

Martínez-Vilalta J., Korakaki E., Vanderklein D. & Mencuccini M. (2007) Below-ground hydraulic conductance is a function of environmental conditions and tree size in Scots pine. *Functional Ecology* 21, 1072–1083.

McMahon T.A. & Kronauer R.E. (1976) Tree structures: deducing the principle of mechanical design. *Journal of Theoretical Biology* 59, 443–466.

Mencuccini M. (2003) The ecological significance of long-distance water transport: short-term regulation, long-term acclimation and the hydraulic costs of stature across plant life forms. *Plant Cell and Environment* 26, 163–182.

Pataki D.E., Oren R. & Phillips N. (1998) Responses of sap flux and stomatal conductance of *Pinus taeda* L. trees to stepwise reductions in leaf area. *Journal of Experimental Botany* 49, 871–878.

Pate J.S., Froend R.H., Bowen B.J., Hansen A. & Kuo J. (1990) Seedling growth and storage characteristics of seeder and resprouter species of Mediterranean-type ecosystems of S.W. Australia. *Annals of Botany* 65, 585–601.

R Core Team (2014) *R: A Language and Environment for Statistical Computing*. R Foundation for Statistical Computing, Vienna, Austria, URL http://www.R-project.org/.

Ryan M.G., Phillips N. & Bond B.J. (2006) The hydraulic limitation hypothesis revisited. *Plant Cell and Environment* 29, 367–381.

Savage V.M., Bentley L.P., Enquist B.J., Sperry J.S., Smith D.D., Reich P.B. & von Allmen E.I. (2010) Hydraulic trade-offs and space filling enable better predictions of vascular structure and function in plants. *Proceedings of the National Academy of Sciences of the United States of America* 107, 22722–22727.

Smith D.D., Sperry J.S., Enquist B.J., Savage V.M., McCulloh K.A. & Bentley L.P. (2014) Deviation from symmetrically self-similar branching in trees predicts altered hydraulics, mechanics, light interception and metabolic scaling. *New Phytologist* 201, 217–229.

Solari L.I., Pernice F. & DeJong T.M. (2006) The relationship of hydraulic conductance to root system characteristics of peach (*Prunus persica*) rootstocks. *Physiologia Plantarum* 128, 324–333.

Sperry J.S., Smith D.D., Savage V.M., Enquist B.J., McCulloh K.A., Reich P.B., Bentley L.P. & von Allmen E.I. (2012) A species-level model for metabolic scaling in trees I. boundaries to scaling space within and across species. *Functional Ecology* 26, 1054–1065.

Tombesi S., Johnson S.R., Day K.R. & DeJong T.M. (2010) Relationships between xylem vessel characteristics, calculated axial hydraulic conductance and size-controlling capacity of peach rootstocks. *Annals of Botany* 105, 327–331.

Tyree M., Velez V. & Dalling J.W. (1998) Growth dynamics of root and shoot hydraulic conductance in seedlings of five neotropical tree species: scaling to show possible adaptation to differing light regimes. *Oecologia* 114, 293–298.

von Allmen E.I., Sperry J.S., Smith D.D., Savage V.M., Reich P.B., Enquist B.J. & Bentley L.P. (2012) A species' specific model of the hydraulic and metabolic allometry of trees II: testing predictions of water use and growth scaling in species with contrasting hydraulic traits. *Functional Ecology* 26, 1066–1076.

Wan C., Sosebee R.E. & L. M.B. (1993) Growth, photosynthesis, and stomatal conductance in *Gutierrezia sarothrae* associated with hydraulic conductance and soil water extraction by deep roots. *International Journal of Plant Science* 154, 144–151.

Warton D.I., Duursma R.A., Falster D.S. & Taskinen S. (2012) smatr 3 — an R package for estimation and inference about allometric lines. *Methods in Ecology and Evolution* 3, 257–259.

Warton D.I., Wright I.J., Falster D.S. & Westoby M. (2006) Bivariate line-fitting methods for allometry. *Biological Reviews* 81, 259–291.

West G.B., Brown J.H. & Enquist B.J. (1999) A general model for the structure and allometry of plant vascular systems. *Nature* 400, 664–667.

Wheeler J.K., Huggett B.A., Tofte A.N., Rockwell F.E. & Holbrook N.M. (2013) Cutting xylem under tension or supersaturated with gas can generate PLC and the appearance of rapid recovery from embolism. *Plant, Cell and Environment* 36, 1938–1949.

Wolken J.M., Landhäusser S.M., Lieffers V.J. & Silins U. (2011) Seedling growth and water use of boreal conifers across different temperatures and near-flooded soil conditions. *Canadian Journal of Forest Research* 41, 2292–2300.

Table 4.1. Species properties and OLS regressions used for mass prediction. Equations correspond to D and H in cm and M in g. Data shown in Figs. S4.3 - S4.5. Species listed in order of decreasing stature.

	growth	local max	H vs D			M_{st} vs HD^2			M_{lv} vs M_{st}		
Species	form	D_T	a_7	b_7	l_o	r^2	mult	exp	r^2	mult	exp	r^2
Populus fremontii	tree	76.1	178	0.643	76.0	0.97	0.356	0.99	0.95	1.07	0.88	0.67
Acer grandidentatum	tree	21.1	191	0.597	75.1	0.98	0.358	1.02	0.99	1.47	0.67	0.79
Betula occidentalis	tree	21.0	266	0.549	99.4	0.98	0.315	1.01	0.99	0.98	0.73	0.79
Amelanchier alnifolia	shrub	5.9	160	0.795	37.2	0.96	0.411	0.97	0.98	0.81	0.67	0.75
Cornus sericea	shrub	3.1	135	0.979	13.1	0.92	0.308	1.01	0.95	1.70	0.56	0.66
Symphoricarpos oreophilus	shrub	2.5	122	0.776	18.0	0.92	0.531	0.97	0.95	0.67	0.59	0.68

$p < 0.001$ for all relationships

Table 4.2. Whole-tree (Q and K) and total aboveground (G and M) SMA scaling relationships. Equations correspond to G in g y^{-1}, K in g MPa^{-1} s^{-1}, Q in g s^{-1}, and M in g. Data shown in Figs. 4.1 - 4.5. Species listed in order of decreasing stature.

	G vs K		Q vs K		G vs Q		K vs M		Q vs M		G vs M	
Group	a_1	b_1	a_2	b_2	a_3	b_3	a_4	b_4	a_5	b_5	a_6	b_6
Populus fremontii	1.93e4	1.19†	0.57	1.12†	3.50e4	1.06	1.31e-4	0.82	2.53e-5	0.92‡	0.46	0.98‡
Acer grandidentatum	4.76e3	0.84	1.00	0.96	4.70e3	0.87	4.21e-5	0.90‡	6.02e-5	0.87	0.90	0.78
Betula occidentalis	8.01e3	1.12	0.93	1.00	8.68e3	1.12	2.34e-4	0.75	2.20e-4	0.75	0.69	0.84‡
Amelanchier alnifolia	3.16e3	0.86	1.84	1.07	2.41e3	0.87	1.75e-4	0.74	1.83e-4	0.79	1.56	0.69
Cornus sericea	2.07e3	0.94	1.14	1.00	1.83e3	0.93	3.95e-4	0.78	4.35e-4	0.78	1.35	0.73
Symphoricarpos oreophilus	n.s.		0.54	0.85	n.s.		n.s.		n.s.		0.65	0.72
common	-	1.06	-	1.01	-	1.03	-	0.80	-	0.82	-	-
interspecific	1.00e4	1.18‡	0.80	0.93‡	1.40e4	1.28‡	1.58e-4	0.79	2.41e-4	0.74	0.33	0.95‡
MST prediction		1		1		1		0.75		0.75		0.75

	G/M vs M		$K_{m,WBE}$ vs M		$K_{m,\Delta}$ vs M	
continued...	mult	exp	mult	exp	mult	exp
	n.s.		7.32e-4	0.73	8.65e-4	0.75
	1.38	-0.27	4.50e-4	0.69§	2.08e-4	0.82
	1.24	-0.23	2.64e-3	0.65§	2.56e-3	0.71
	4.26	-0.49‡	1.98e-3	0.56§	1.74e-3	0.68
	2.77	-0.40‡	2.76e-3	0.62	2.56e-3	0.69
	3.75	-0.65‡	1.85e-3	0.52§	1.39-3	0.68
	-	-	-	-	-	-
	1.19	-0.23	1.09e-3	0.68	1.11e-3	0.74
		-0.25		0.75		0.75

n.s. = exponent not significantly different from zero ($p > 0.05$). "-" = common exponent or multiplier not supported ($p < 0.05$). Significant differences from MST predictions denoted as: $\dagger = p < 0.1$; $\ddagger = p < 0.05$ (modeled results were not tested). $\S$ = K vs M exponent different from modeled ($p < 0.05$).

Table 4.3. OLS parameters for model input equations. Taper is conduit diameter (μm) vs stem diameter (mm). Packing is conduit frequency (mm^{-2}) vs conduit diameter (μm). Sapwood is dyed xylem area (mm^2) vs stem diameter (mm). Taper was fit with a rise-to-max function (Eqn. 4.10). Power functions used otherwise. Data shown in Figs. S4.6 - S4.8. Species listed in order of decreasing stature.

	taper		packing		sapwood	
Species	d_{max}	m	mult	exp	mult	exp
Populus fremontii	79.1	8.83	1.03e5	-1.66	0.21	2.15
Acer grandidentatum	28.2	2.29	5.77e4	-1.65	1.00	1.84
Betula occidentalis	55.0	4.50	3.54e5	-2.09	0.61	1.99
Amelanchier alnifolia	27.4	1.83	2.97e5	-1.98	0.41	1.89
Cornus sericea	45.5	3.34	1.38e5	-1.78	0.68	1.89
Symphoricarpos oreophilus	26.2	1.41	2.35e4	-1.02	0.38	1.50

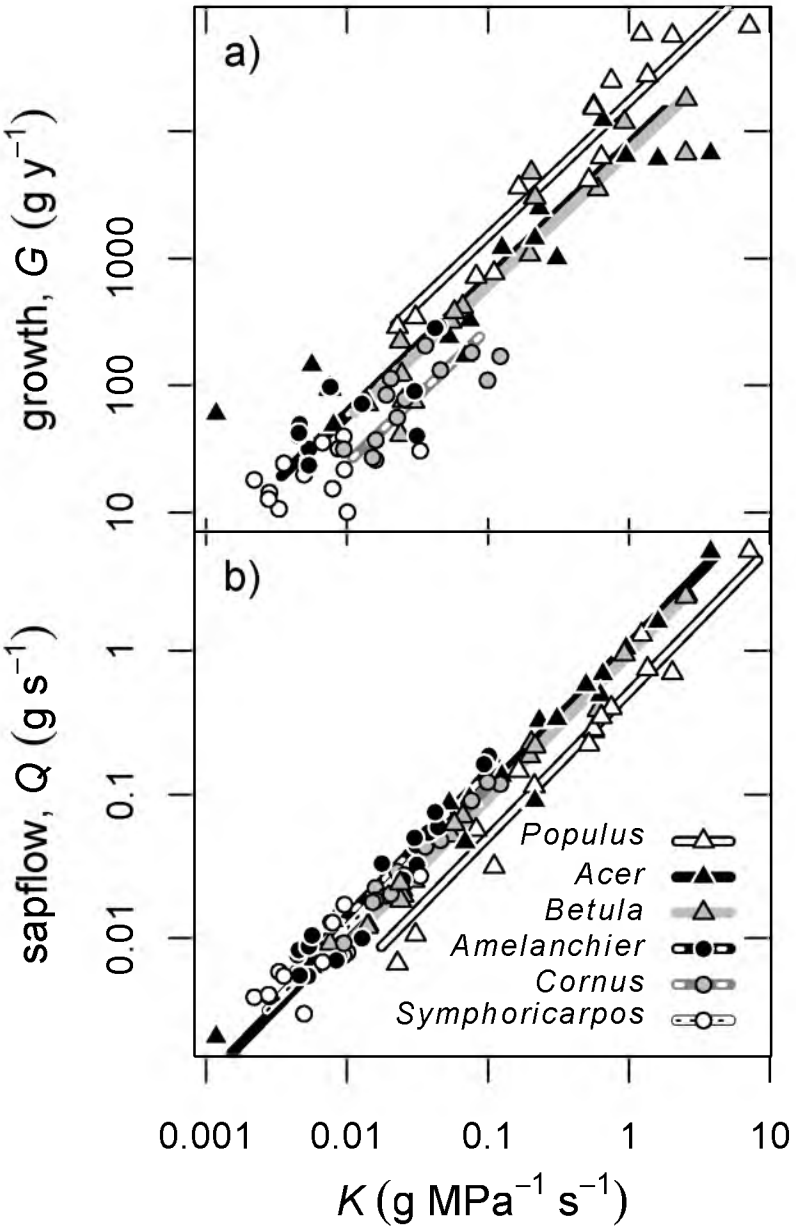

Figure 4.1. Scaling of aboveground growth and midday sapflow with whole plant hydraulic conductance. Symbols represent each plant from shrub (circles) and tree (triangles) species. The legend lists species in order of decreasing species stature. **a)** All species except *Symphoricarpos* had significant G vs K scaling. The remaining species shared a common SMA exponent (0.98). When regressions were forced to the common exponent (shown), trees tended to have greater multipliers than shrubs. **b)** All species had significant Q vs K scaling and shared a common SMA exponent (1.01). When forced to this common exponent (shown), multipliers tended to decrease with increasing species stature. Nonforced regression coefficients shown in Table 4.2.

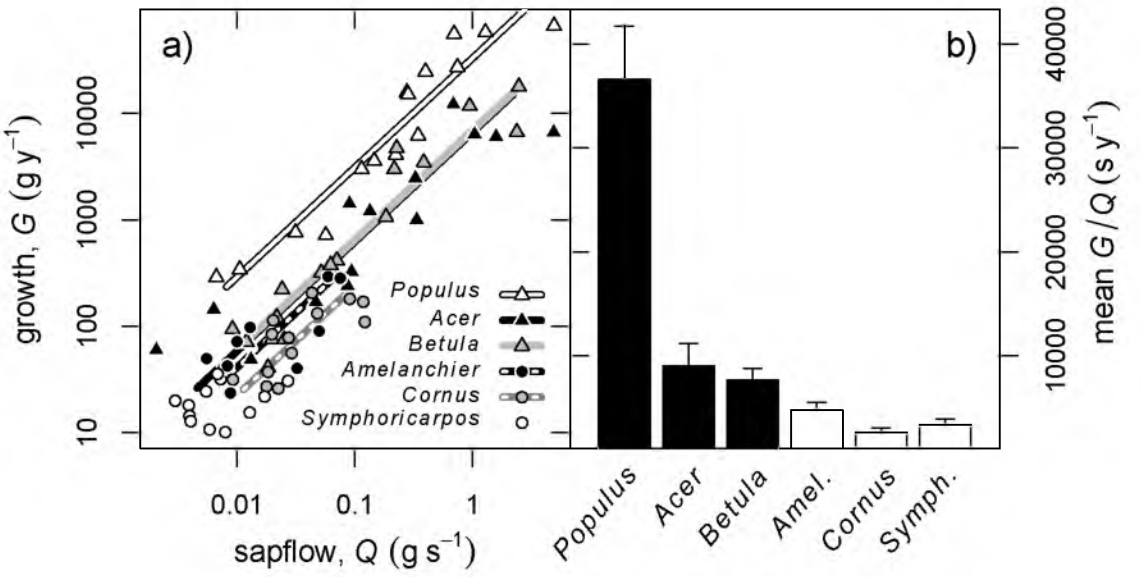

Figure 4.2. Relationships between aboveground growth and midday sapflow. Species listed in order of decreasing stature. **a)** G vs Q scaling was significant in all species but *Symphoricarpos*. Symbols represent each plant from shrub (circles) and tree (triangles) species. Species shared a common SMA exponent (0.95). When regressions were forced to the common exponent (shown), multipliers tended to be greater in larger species. **b)** Likewise, the water use efficiency proxy, G/Q, was larger in larger statured species. Shown are the mean $G/Q \pm$ SE with bar color differentiating trees and shrubs. Nonforced regression coefficients shown in Table 4.2.

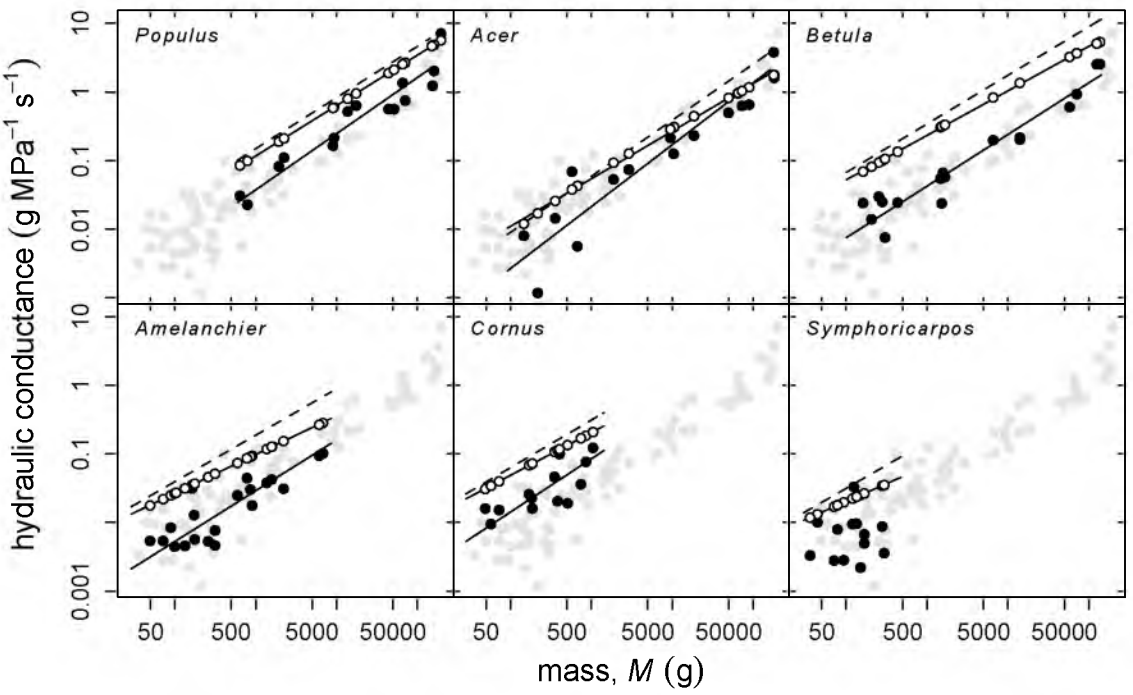

Figure 4.3. Hydraulic conductance vs aboveground dry mass relationships. Shown are measured K (black circles with solid regression) and K modeled in two ways: either constant WBE branching architecture (open circles with solid regression, $K_{m,WBE}$) or size-dependent branching architecture (dashed regression, data not shown, $K_{m,\Delta}$). In all cases, M was predicted from empirical allometric relationships. For reference, measured data points of all species are shown in grey in the background of each subplot. *Symphoricarpos* had nonsignificant scaling for measured K vs M. Species displayed in order of decreasing stature. Regression coefficients shown in Table 4.2.

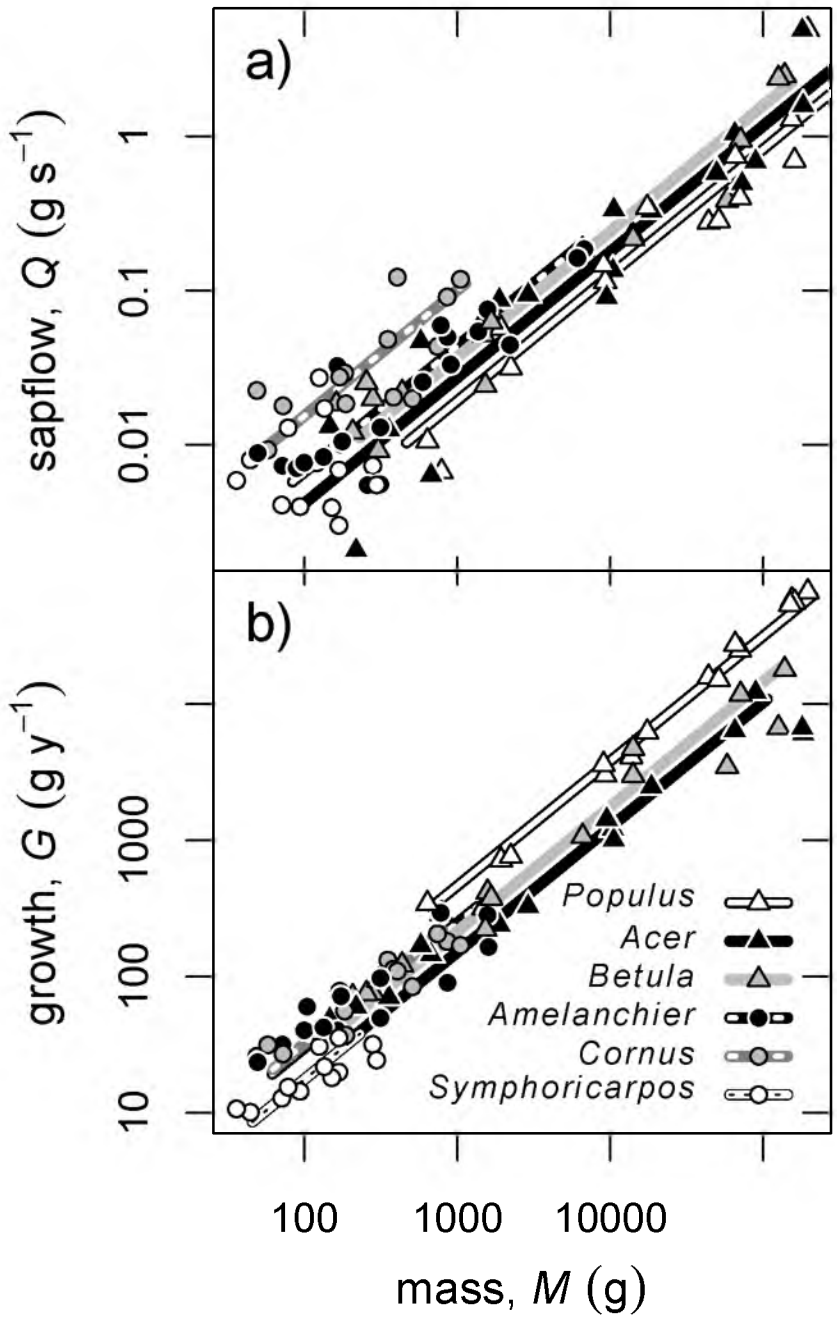

Figure 4.4. Scaling of midday sapflow and aboveground growth vs aboveground mass. Symbols represent each plant from shrub (circles) and tree (triangles) species. The legend lists species in order of increasing species stature. **a)** Q vs M was not significant for *Symphoricarpos*. A common SMA exponent (0.82) was supported. When forced to this exponent (shown), trees tended to have smaller multipliers. **b)** G vs M scaling was significant in all species. A common SMA exponent was not supported. Trees tended to have steeper exponents than shrubs. Nonforced regression coefficients shown in Table 4.2.

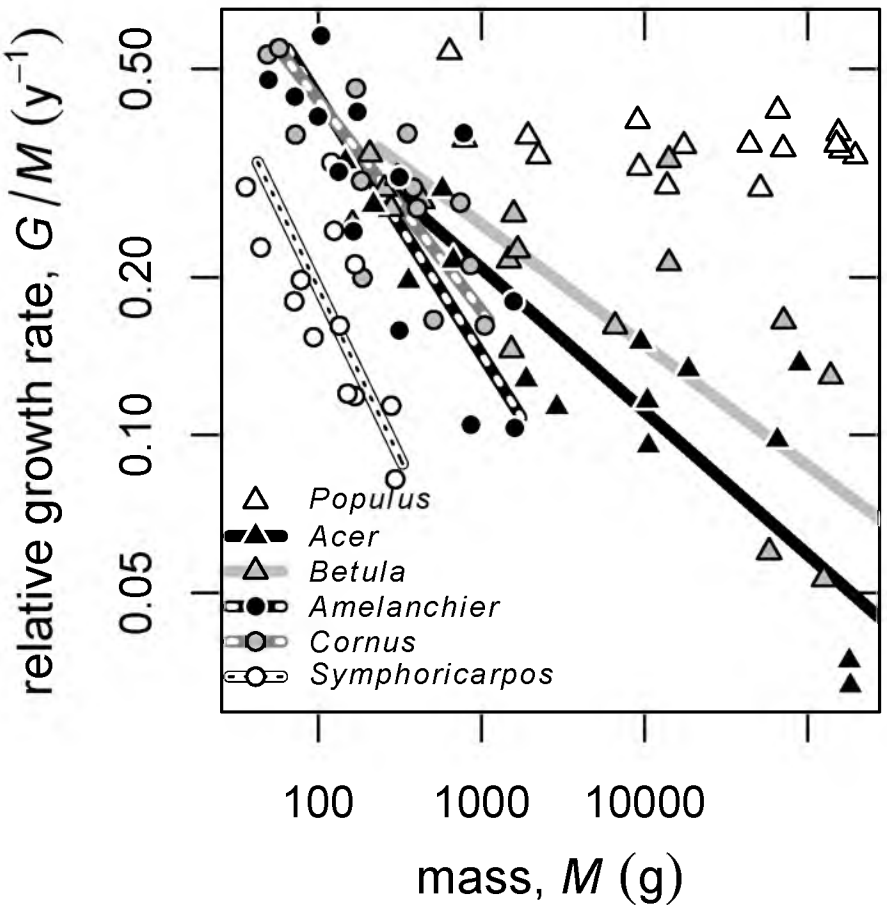

Figure 4.5. Relative growth rate of aboveground tissue vs current aboveground dry mass. Symbols represent each plant from shrub (circles) and tree (triangles) species. The legend lists species in order of decreasing species stature. Lines indicate SMA regressions. The scaling exponents significantly increased with species stature. Also, at a given M larger species tended to have higher G/M. See Table 4.2 for scaling coefficients.

S4 Supporting Information

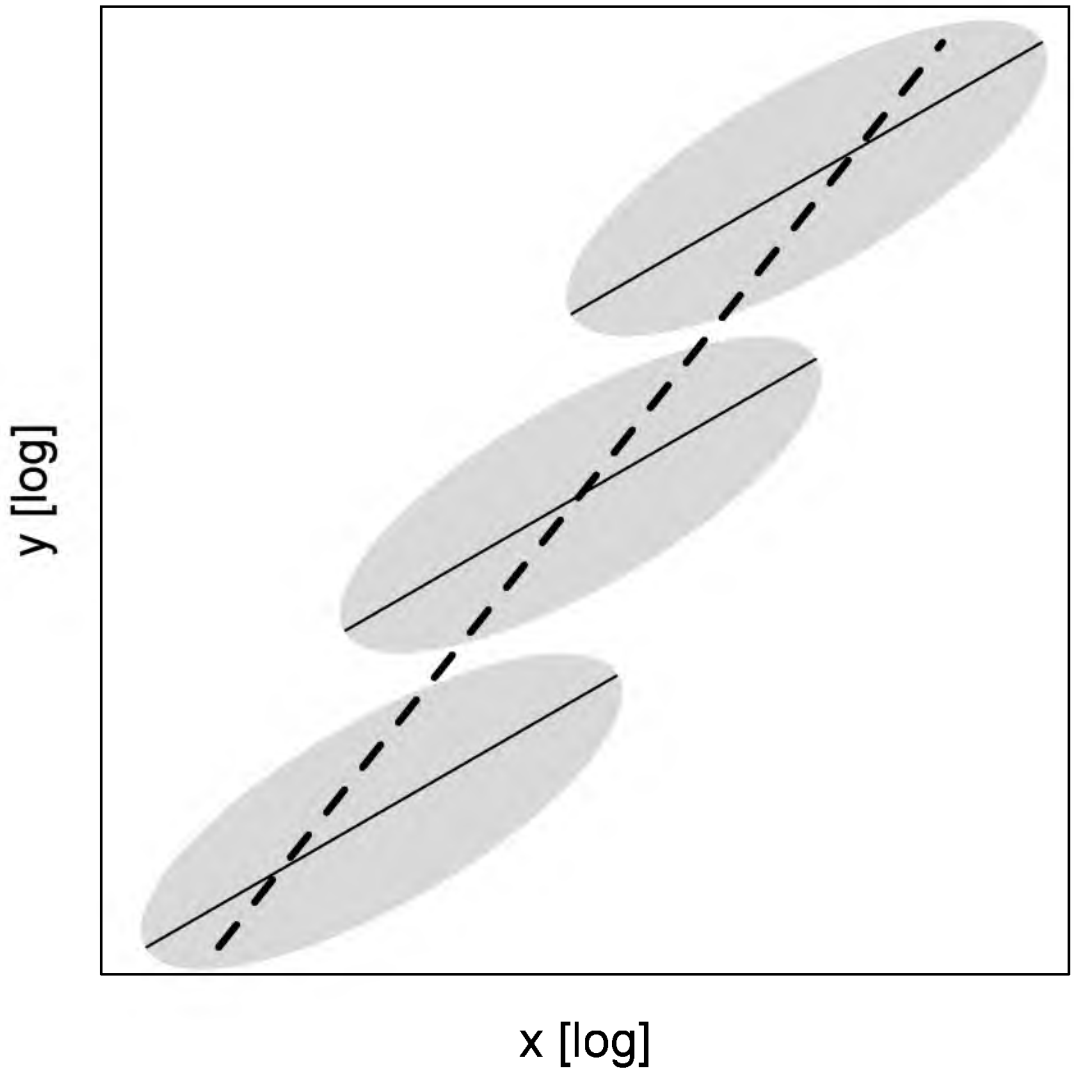

Figure S4.1. Distinction between common and interspecific scaling. Shown are hypothetical data for three species (grey ellipses) with their scaling regressions (solid lines) and the interspecific regression across all data (dashed line). In this example, species share a common exponent as seen by their parallel regression lines. Their multipliers, however, differ markedly. Species that reach a greater x also have larger multipliers, which makes the interspecific exponent considerably steeper than the common exponent.

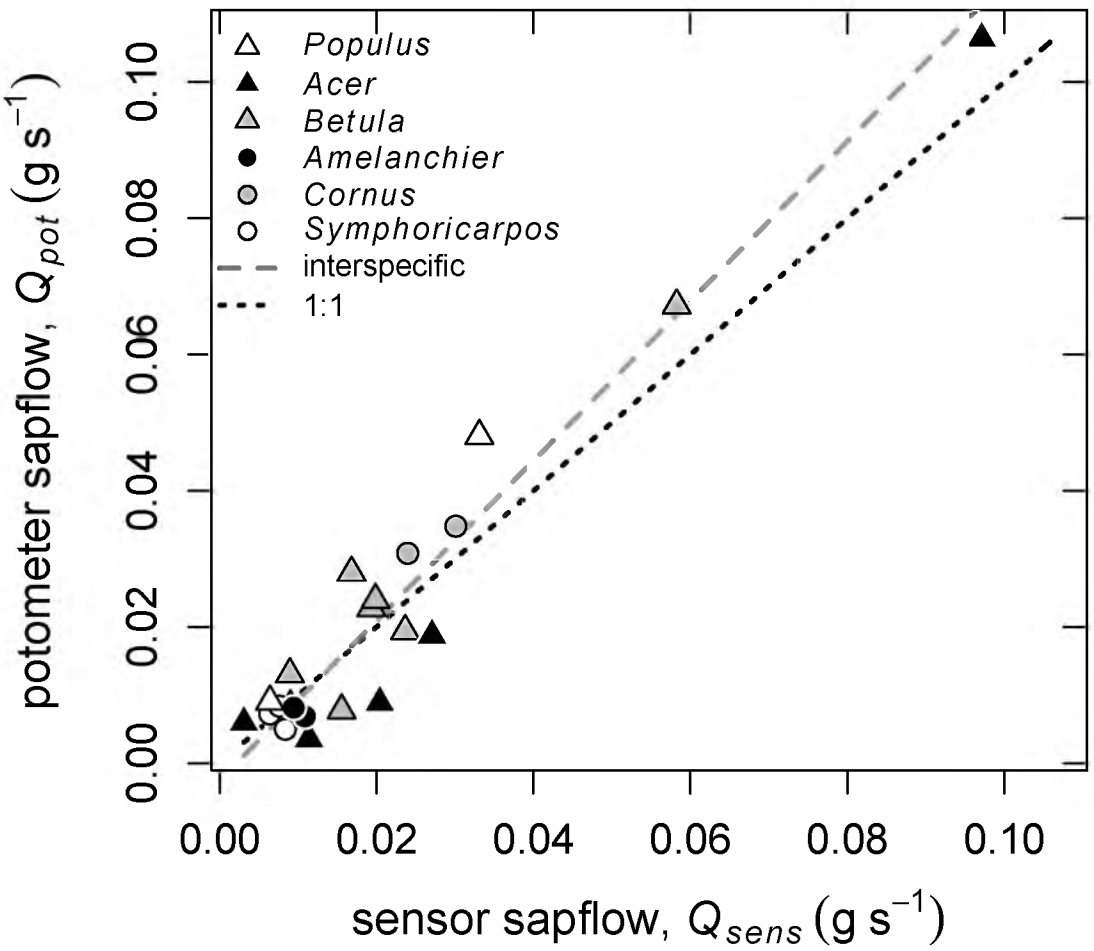

Figure S4.2. Average sapflows measured simultaneously by potometer and sapflow sensor. The SMA regression (dashed grey; linear scale) was slightly, but significantly, steeper than the dotted 1:1 line.

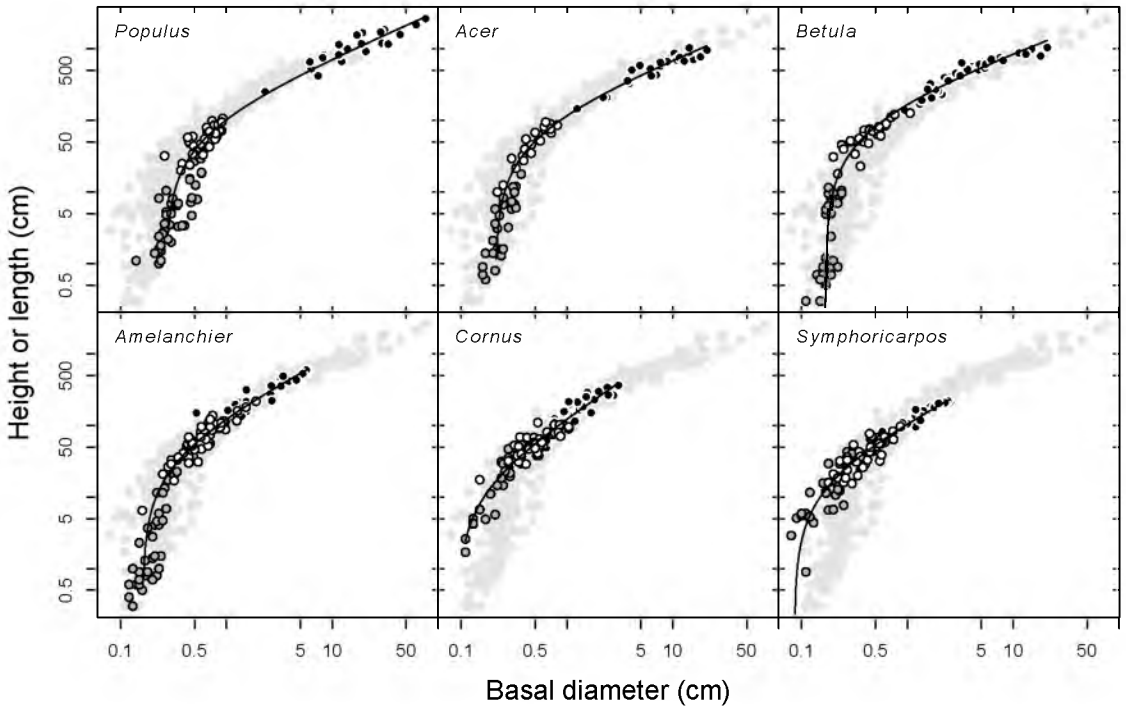

Figure S4.3. Height by diameter relationships for the six study species. Each data set includes twigs (dark grey) branches (open) and entire shoots (black). The combined data across species (light grey) are shown in each subplot for comparison. Regression lines follow the form: $H = aD^b - l_o$. Regression coefficients are given in Table 4.1. Species displayed in order of decreasing stature.

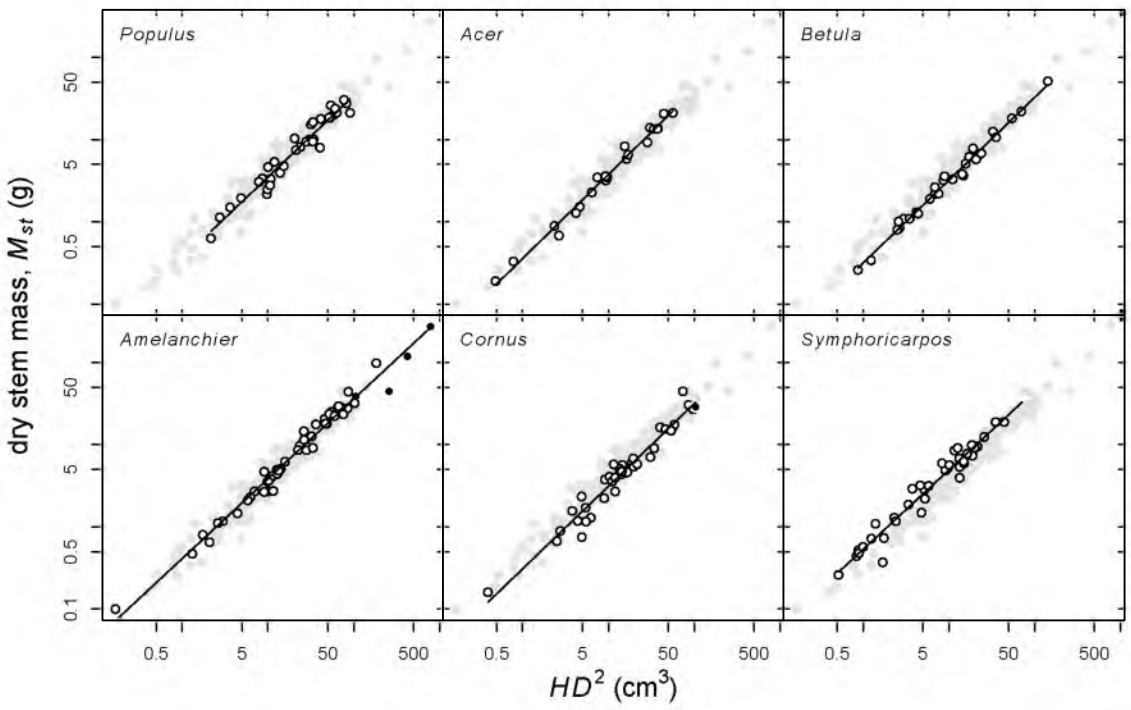

Figure S4.4. Dry stem mass scaling relationships obtained from branches (open) and entire individuals (black). The combined data across species (light grey) are shown in each subplot for comparison. Lines indicate OLS regressions whose coefficients are shown in Table 4.1. Species displayed in order of decreasing stature.

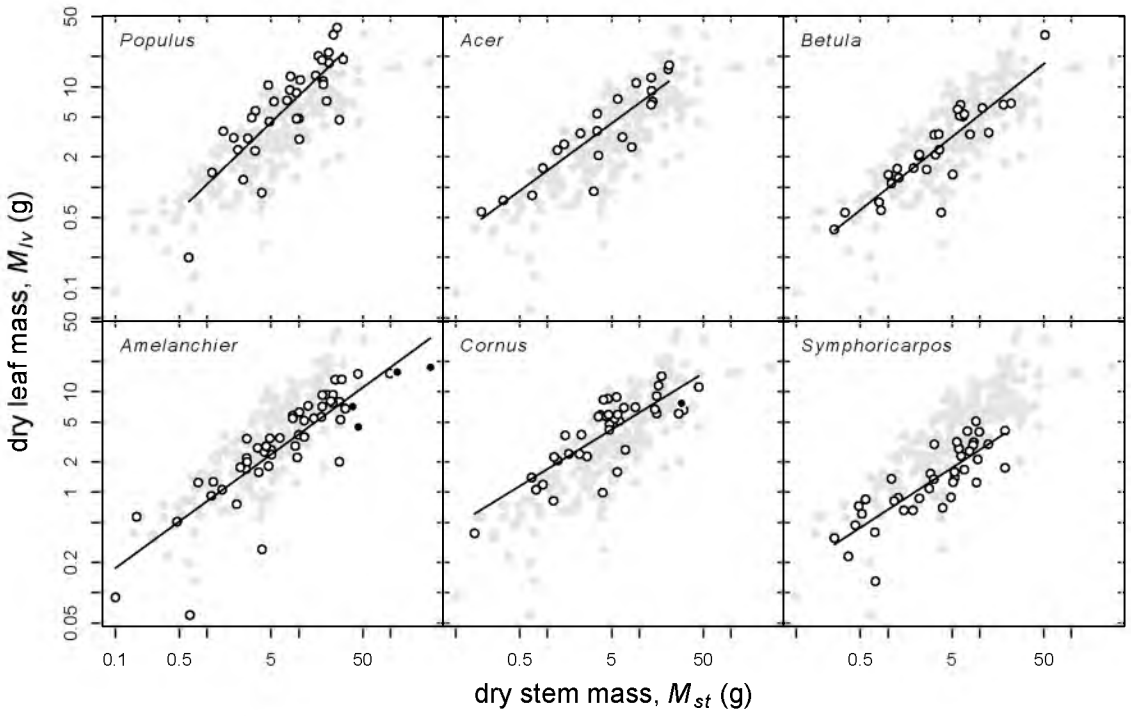

Figure S4.5. Dry leaf mass scaling relationships obtained from branches (open) and entire individuals (black). The combined data across species (light grey) are shown in each subplot for comparison. Lines indicate OLS regressions whose coefficients are shown in Table 4.1. Species displayed in order of decreasing stature.

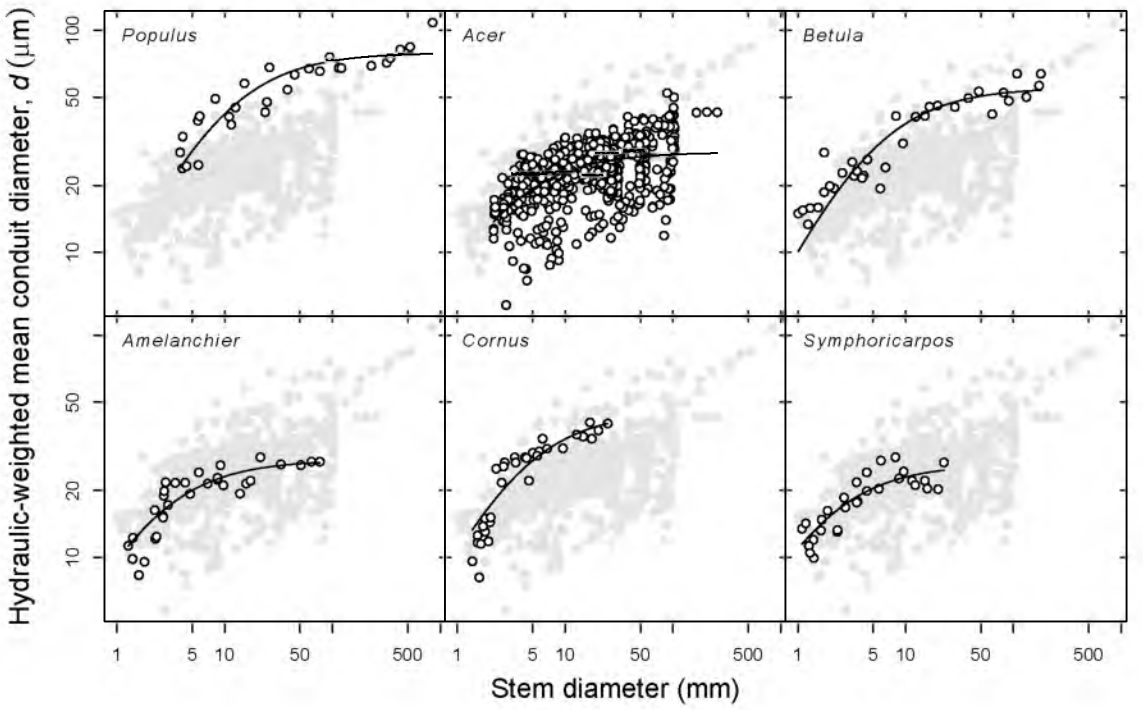

Figure S4.6. Conduit taper shown by area-weighted mean conduit diameter in multiple stems per species. For all species but *Acer*, data come from the outermost growth ring only. Points are fit with a rise to max function (parameters in Table 4.3). The combined data across species (light grey) are shown in each subplot for comparison. Species displayed in order of decreasing stature.

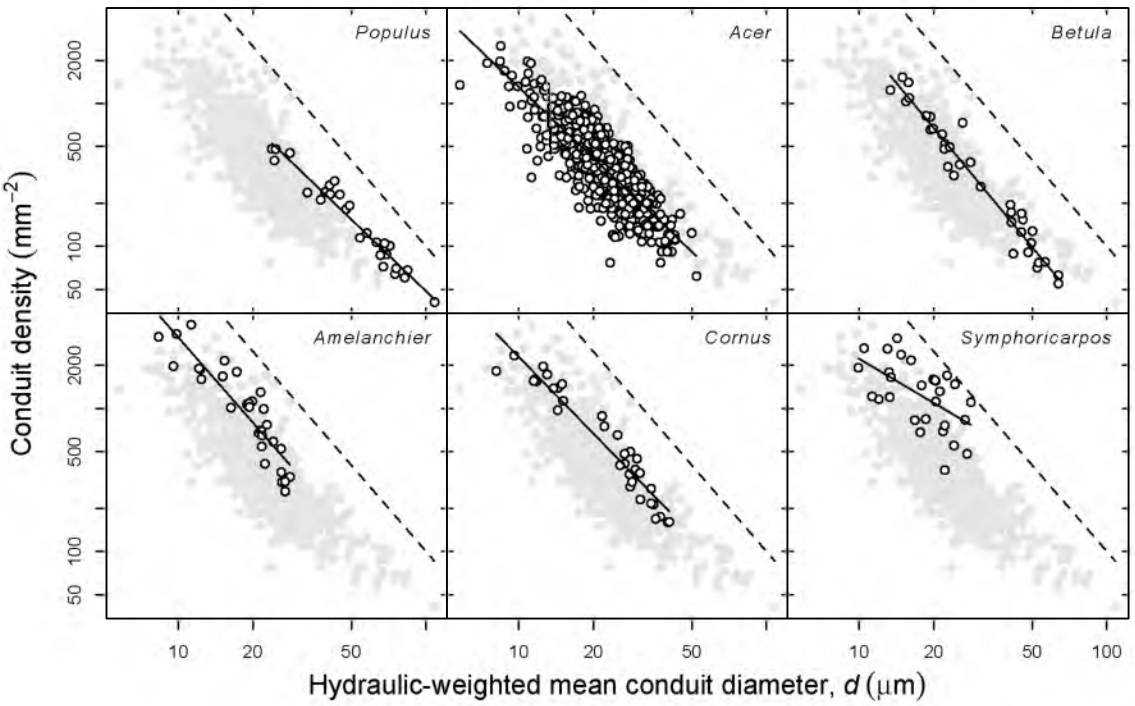

Figure S4.7. Conduit packing as shown by conduits per xylem area as a function of hydraulic-weighted conduit diameter. Parameters for solid OLS regression lines are shown in Table 4.3. The packing limits (dashed lines) give a sense of area occupied by conduits but are only strictly meaningful for area-weighted mean conduit diameters. The combined data across species (light grey) are shown in each subplot for comparison. Species displayed in order of decreasing stature.

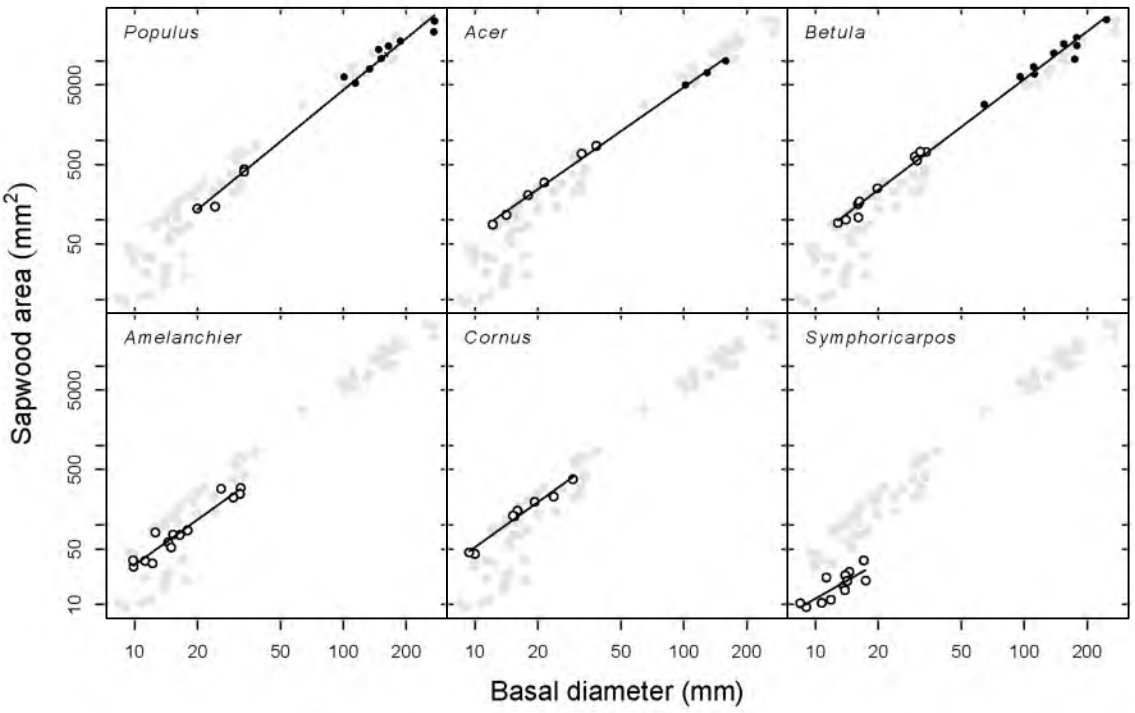

Figure S4.8. Sapwood area data determined from dye uptake is cross-sections (open) and cores (black). Lines indicate OLS regressions whose coefficients are shown in Table 4.3. The combined data across species (light grey) are shown in each subplot for comparison. Species displayed in order of decreasing stature.

CHAPTER 5

CONVERGENCE IN LEAF SIZE VS TWIG LEAF AREA SCALING: DO PLANTS OPTIMIZE LEAF AREA PARTITIONING?

5.1 Abstract

Corner's rule states that thicker twigs bear larger leaves. Since thicker twigs support greater total leaf area (A_t), the rule predicts that individual leaf size ($\bar{A}$) scales positively with A_t. How convergent is this scaling? To maximize detection of convergence, we compared co-occurring and functionally similar species. As predicted, $\bar{A}$ increased with A_t. The scaling was highly convergent; more so than the scaling of either $\bar{A}$ or A_t with other twig properties. A common $\bar{A}$ by A_t exponent of 0.6 meant that $\bar{A}$ and leaf number (n) on twigs increased in a specific coordination. Why? A model demonstrated that positive $\bar{A}$ by A_t scaling maximized the return on leaf investment in gap-filling twigs. The optimal exponent was near 1 (n = constant) for maximum self-shading. The exponent fell to 0.6 when self-shading decreased with larger gap size. Accordingly, Corner's rule and its specific quantitative form is consistent with an optimal leaf deployment that shifts predictably with canopy light environment.

5.2 Introduction

In 1949, Corner identified two basic properties of plant architecture: (1) larger leaves are borne on thicker stems and (2) plants with thicker stems are less densely branched. His claim led to numerous tests of "Corner's rules" across species and environments, and to explanations for why such rules would have evolved (e.g., White 1983a,b; Brouat *et al.* 1998; Westoby & Wright 2003; Olson *et al.* 2009; Yang *et al.* 2014). The second rule is easy to explain because it is a corollary of area-preserving branching (McMahon & Kronauer 1976; Sone *et al.* 2009; Eloy 2011). Cross-sectional stem area is approximately preserved

across branch junctions, so a given trunk area will support a similar total cross-sectional area of twigs. This means that a trunk could support many narrow twigs or a few thick ones. Fewer twigs require fewer branching junctions and, hence, Corner's second rule that thicker twigs show less dense branching.

At first glance, Corner's first rule seems equally simple to explain: bigger leaves require thicker twigs to support their greater transport and mechanical needs (White 1983b; Farnsworth & Van Gardingen 1995; Preston & Ackerly 2003; Wright *et al.* 2006). The complication is that twigs bear *multiple* leaves. So while it is obvious that twig dimensions must scale with *total* twig leaf area (A_t), it is not obvious why they should scale with *individual* leaf area ($\bar{A}$ = mean leaf area). Thicker twigs will have greater A_t, but this could be achieved regardless of whether $\bar{A}$ increases, decreases, or stays the same. Corner's first rule is peculiar in predicting that $\bar{A}$ increases with A_t. Therefore, we ask two questions: (1) how convergent is the positive scaling between individual and twig leaf area, and (2) can we explain why such scaling evolved? The "twig" is this context is defined as the current year's extension growth.

Surprisingly, in our review of the Corner's rule literature, the $\bar{A}$ vs A_t relationship is almost always overlooked (see Falster & Westoby 2003; Westoby & Wright 2003 for exceptions). Most studies assess relationships between leaf area ($\bar{A}$ or A_t) and twig size, but the positive $\bar{A}$ by A_t relationship is arguably the fundamental reason why thicker twigs have larger leaves.

Corner's first rule requires that $\bar{A}$ increases with A_t but it does not specify how. Suppose that $\bar{A}$ vs A_t can be described as a power function:

$$\bar{A} = a_1 A_t^{b_1} \tag{5.1}$$

where a_1 is a scaling multiplier and b_1 is a scaling exponent. Corner's rule only requires that $b_1 > 0$. Such positive scaling could be achieved in three general ways. If the number of leaves, n ($= A_t/\bar{A}$), is constant, any changes in A_t will be due to $\bar{A}$. Therefore, $\bar{A}$ vs A_t will be isometric ($b_1 = 1$ and $a_1 = 1/n$ in Eqn. 5.1). Alternatively, n could decrease with greater A_t, which requires $\bar{A}$ to increase faster than A_t so $b_1 > 1$. Finally, n could increase with $\bar{A}$ and A_t, making $0 < b_1 < 1$.

We assessed intraspecific $\bar{A}$ vs A_t scaling in six species to determine if species consistently followed one of these three scaling alternatives and whether the scaling was consistent across species. These results were compared to other scaling relationships involving twig diameter (d_t) and length (l_t), including Corner's first rule as usually stated: $\bar{A}$ vs d_t. Although nearly all analyses of Corner's rules have used interspecific data (but see Brouat *et al.*

1998; Preston & Ackerly 2003), we specifically chose to determine the scaling exponent b_1 intraspecifically. The intraspecific b_1 exponent is not confounded by species-specific shifts in the a_1 multiplier (Heusner 1982). The multiplier shifts because species can have inherently different $\bar{A}$ than others for the same A_t because of differences in habitat, natural history, phylogenetic affiliation, *etc.* (e.g., Givnish 1987; Cunningham *et al.* 1999). Our question is not why some species have different leaf sizes than others, but how and why leaf size varies with increasing twig leaf area within species. Recognizing that intraspecific b_1 could be sensitive to environment and plant functional type, we chose species that were co-occurring and functionally similar (deciduous angiosperm trees and shrubs with simple leaves and diffuse porous xylem) to test whether b_1 was convergent across species in ecologically and environmentally similar contexts.

The question of *how* $\bar{A}$ scales with A_t is simple to evaluate. Whereas, the question of *why* $\bar{A}$ should increase with A_t — much less why they may scale in a particular way — is more difficult to answer. We approached the "why" question from an economics standpoint with the hypothesis that twigs should exhibit the optimal $\bar{A}$ and n (and thereby A_t) that maximize the net gain from the twig's complement of leaves. The net gain is the benefit from the leaves minus their cost. The benefit stems from the light energy absorbed by the leaves while the cost is based on the energy required to construct and maintain leaves. We developed a model that computed optimal $\bar{A}$ and n for twigs with different degrees of self-shading and deployed in light gaps of different sizes. The model was used to predict how a twig's light environment influenced the optimal $\bar{A}$ by A_t scaling.

5.3 Materials and methods

5.3.1 Location and species

All material was collected in Red Butte Canyon Natural Research Area (40.78° N 111.81° W; 1640 to 1910 m.a.s.l.) located adjacent to the University of Utah in Salt Lake City. Data were collected for all species between July and September (after extension growth was complete) in 2011 and 2013. Six species were chosen from separate eudicot orders (Judd *et al.* 2008), including three shrubs (*Amelanchier alnifolia* Nutt., *Cornus sericea* L., and *Symphoricarpos oreophilus* A. Gray) and three trees (*Acer grandidentatum* Nutt., *Betula occidentalis* Hook. and *Populus fremontii* S. Watson). Hereafter, each will be referred to by its genus. These species were chosen due to their similarities. All are deciduous angiosperms with simple leaves and all grow within the riparian corridor. With the exception of *Symphoricarpos*, all have functionally diffuse porous xylem (Smith & Sperry 2014).

5.3.2 Twig architecture

Branches were collected from various individuals from each species. Trees sampled were generally < 15 m tall with shallow canopies and sampled twigs were at or near the canopy periphery. Material was transported in plastic bags to the lab and measured the same day. Twigs with obvious damage were excluded, as were branched (sylleptic) twigs, which occurred occasionally in *Cornus*. For each twig (n = 53 to 95 per species), we recorded twig leaf area (A_t), number of leaves (n), twig stem length (l_t) and twig basal diameter (d_t, measured at the bud scale scars at the base of the current year's growth). Leaf areas were measured with a Li-3100 (Li-Cor, Lincoln, NE). From A_t and n we calculated mean individual leaf area, $\bar{A}$. Scaling relationships between all twig properties were determined using SMA (standardized major axis) regression on logged data via the smatr package (Warton *et al.* 2012) for R 3.1.2 (R Core Team 2014). The smatr package was additionally used to test for common exponents, test for isometry, and perform pairwise comparisons between exponents. For pairwise comparisons, p-values were adjusted to avoid type I errors.

5.3.3 Economics model

The model assumes that a twig has a particular $\bar{A}$ and n (and hence A_t) because it maximizes net gain (benefit − cost). Benefit is a function of twig light absorption and cost is a function of twig leaf area. The model was written in R.

We created canopies of randomly placed circular leaves at 20 mean leaf area indices ($\overline{\text{LAI}}$) between 0.5 and 5 (see Fig. 5.1A-B). Within each random assemblage, there were areas of little or no coverage by leaves ("gaps") and areas with high coverage. Twigs were assumed to grow into the gaps, representing a "sun-leaf" light environment expected for the study species and their sampled twigs. To determine the spatial distribution of light penetration centered around the gaps (without twigs present), we discretized the simulation space and determined the canopy leaf coverage (LAI_c) in each pixel. For each pixel, the fraction of light penetrating the canopy, τ_c, was

$$\tau_c = (1 - f_l)^{\text{LAI}_c} \tag{5.2}$$

where f_l (= 0.5) is the fraction of incident light absorbed by each leaf in the canopy. The τ_c should be spatially autocorrelated, meaning pixels with high τ_c should be near other pixels with high τ_c. To represent the spatial autocorrelation statistically, we chose 1000 random pixels (0.8% of total) with the highest τ_c for each $\overline{\text{LAI}}$ (that is, pixels within light gaps). For each random pixel, we recorded τ_c at 20 discrete distances away and in random directions (see Fig. 5.1A,B, arrows). The mean τ_c vs distance, x, values were fit with the function:

$$\bar{\tau}_c = a_2 \exp(b_2 x) + \bar{\tau}_{c,min} \tag{5.3}$$

which was used to predict the light available in and around the gaps where the twig would be centered (see Fig. 5.1E,F). In Eqn. 5.3, $\bar{\tau}_{c,min}$ is the lower asymptote, which corresponds closely to the light penetration under a homogenous canopy with $\overline{\text{LAI}}$. The greater $\bar{\tau}_{c,min}$, the more open the canopy, and the larger its light gaps. For readability, $\bar{\tau}_{c,min}$ is referred to as "canopy openness" in subsequent text and figures.

Twigs populating canopy light gaps were modeled as vertically-oriented, unbranched stems (see Fig. 5.1C,D). Leaves were ellipses (aspect ratio = 3) arranged alternately with spiral phyllotaxy. The angle between leaves was centered on the golden angle (137.5°) with normally-distributed random variation (SD = 5.6°). We modeled leaf sizes and numbers based on observed ranges for the study species: $\bar{A} = 0.6$ to 83.9 cm^2 and $n = 1$ to 55. The $\bar{A}$ range was discretized into 55 logarithmically spaced values.

Light absorption by each leaf in each twig was calculated from $\bar{\tau}_c$ and leaf overlap within the twig. Leaf overlap was determined by discretizing the space and counting the leaves within the twig (LAI_t) above each pixel of each leaf. The fraction of total light incident on each pixel was

$$\tau_t = \bar{\tau}_c (1 - f_t)^{\text{LAI}_t} \tag{5.4}$$

where f_t is the fraction of attenuation by each leaf within the twig. The absorption, α, by each pixel in each leaf is

$$\alpha = \tau_t f_l dx^2 \tag{5.5}$$

where f_l (= 0.5) is the fraction of τ_t absorbed and dx is the side length of each pixel. The dx was 0.1 mm in the smallest leaves and increased with leaf size, which meant each leaf was composed of over 5600 pixels and all leaf sizes were represented with the same level of precision. Total absorption by each leaf (α_l) and the whole twig (α_t) were obtained by summing α.

The attenuation of light within the twig, f_t, was allowed to vary (Fig. 5.1C-F). If all light was collimated and incident parallel to the twig then self-shading would be maximized and the fraction of attenuation should equal the fraction of absorption ($f_t = f_l = 0.5$). However, in reality, self-shading will rarely be maximized because there is also diffuse light, leaves move, and the direction of collimated light moves relative to the twig. To simulate different degrees of self-shading, attenuation by leaves in the twig (f_t) was decoupled from absorption by the leaves (f_l). For example, in an open canopy with large gaps, leaves that are low on a twig may still have high integrated light absorption (i.e., μmol PAR m^{-2} day^{-1}) even if

each leaf above absorbs a large fraction of its incident light (e.g., Fig. 5.1, upper panels). Such a twig would have minimal self-shading. Under a denser canopy with smaller gaps, the light available to the same low-positioned leaf would be much more reduced by absorption of the leaves crowding around it (greater self-shading; e.g., Fig. 5.1, lower panels). Based on this logic, f_t (which defines the degree of self-shading) was a function of canopy openness ($\bar{\tau}_{c,min}$). We defined $f_{t,open}$ for the most open canopy with the largest gaps (greatest $\bar{\tau}_{c,min}$) and $f_{t,closed}$ for the densest canopy with the smallest gaps (lowest $\bar{\tau}_{c,min}$). The $f_{t,open}$ was assigned one of seven values from lowest to highest self-shading (0.01, 0.05, 0.1, 0.2, 0.3, 0.4, 0.5). The $f_{t,closed}$ either equaled $f_{t,open}$ (equal twig self-shading in all canopies) or was set to 0.5 (maximal self-shading in the densest canopy). When $f_{t,closed} = 0.5$, the f_t decreased either linearly or curvilinearly with increasing openness to $f_{t,open}$. For readability, we refer to f_t as "self shading" in subsequent text and figures.

We defined net gain as

$$\text{net} = \text{benefit} - \text{cost} = c_0\alpha_t - c_1 n\bar{A}^{\beta} \tag{5.6}$$

The multipliers c_0 and c_1 implicitly translate light absorption and leaf area into the same metabolic currency and the exponent β dictates how cost/area varies with $\bar{A}$. By default, cost/area was constant ($\beta = 1$) but we also considered increasing cost/area [$\beta > 1$; due to increasing LMA (Milla & Reich 2007) and/or proportionally greater structural investment in larger leaves (Niinemets *et al.* 2007; but see Villar & Merino 2001)].

Changing c_0 and c_1 changes net gains and can change which $\bar{A} : n$ pair is optimal. Because the relative benefit of any pair depends on the c_0/c_1 ratio, $c_1 = 1$ was generally maintained (but see next paragraph) while varying c_0. The range for the benefit coefficient, c_0, was selected by two criteria. (1) The c_0 must produce a positive maximum net gain within the modeled range of $\bar{A}$ and n. (2) The c_0 must produce this optimum across at least 15 of the 20 modeled canopies. Each modeled canopy typically produced a unique $\bar{A} : n : A_t$ optimum, so this second criterion ensured a robust sample of $\bar{A}$ and A_t optima from which to determine the b_1 scaling exponent. For each self-shading scenario, we ran the model with 500 c_0 values over the range predicted to satisfy the first criterion. The c_0 values were binned into 100 size classes and each c_0 was then filtered on the two criteria. Bins with fewer than four $\bar{A} : n$ pairs were excluded. From the remaining data, SMA regression was used to evaluate $\bar{A}$ vs A_t scaling in each c_0 bin.

We also modeled cost (via c_1) as a function of leaf light environment. Leaf mass/area and respiration/area (Posada *et al.* 2009) and N/area (Niinemets *et al.* 2015) have been

shown to increase asymptotically with light regime. This dependency was represented with a Michaelis-Menten-like function

$$c_1 = \frac{a_3 \alpha_l / \bar{A}}{b_3 + \alpha_l / \bar{A}} + 1 \tag{5.7}$$

where the minimum is 1, the maximum is $a_3 + 1$ and b_3 is the $\alpha_l / \bar{A}$ at which c_1 is halfway between the minimum and maximum. We varied a_3 and used $b_3 = 0.25$ because the maximum absorption per area was 0.5 ($= f_l$). Greater leaf thickness and N content should also increase leaf absorption, but Evans & Poorter (2001) showed the change in absorption is small. When c_1 varied, c_0 was chosen and regressions were performed as above.

5.4 Results

5.4.1 Twig architecture

The $\bar{A}$ and A_t were positively related within all six species (Fig. 5.2), as expected from Corner's first rule. SMA scaling exponents (b_1) were very similar, ranging from 0.56 to 0.66 (see Table 5.1) with support for a common exponent of 0.61 ($p = 0.072$). All exponents were significantly less than 1 ($p < 0.001$), meaning that n increased systematically with increasing $\bar{A}$ and A_t. Interspecific $\bar{A}$ by A_t scaling ($b_1 = 0.86$) was steeper than any intraspecific value due to variation in a_1 multipliers across species (see Fig. 5.2). $\bar{A}$ and A_t vs n scaling exponents were less convergent than $\bar{A}$ vs A_t (common exponent test $p = 0.005$ and 5.6e-4, respectively). This lack of support for a common exponent was attributable to *Betula*, which was significantly shallower than *Amelanchier* and *Symphoricarpos* in both cases (see Table 5.1).

No other relationship between twig properties showed the convergence observed for $\bar{A}$ by A_t (Fig. 5.3; Table 5.1). The more traditional assessment of Corner's first rule ($\bar{A}$ vs d_t) showed variable exponents (1.28 to 2.32) that were far from supporting a common exponent ($p = 1.8\text{e-}7$; five pairwise differences of 15 possible). The A_t by d_t data also showed a wide range in exponents (1.94 to 3.94) with no common exponent ($p = 4.4\text{e-}16$; eight pairwise differences). $\bar{A}$ and A_t scaled with length (Fig. 5.3C,D) similar to how they scaled with d_t due to the positive scaling between l_t and d_t. The $\bar{A}$ vs l_t exponents were somewhat convergent (range 0.35 to 0.61) but with four significant pairwise differences: *Cornus*, *Populus* and *Symphoricarpos* were steeper than *Betula* while *Populus* was also steeper than *Amelanchier*

5.4.2 Economics model

Across all scenarios of canopy structure and twig self-shading, $\bar{A}$ vs A_t exponents were positive, ranging from 0.52 to 1.31 overall. In other words, maximizing return on twig leaf investment predicted the Corner's rule corollary that greater A_t is achieved through greater $\bar{A}$. Before detailing the variation in exponents, it is necessary to describe the general behavior of the model.

Figure 5.4A illustrates that for a given light environment (i.e., canopy openness and twig self-shading) and constant n, the benefit (dashed line) and cost (grey line) increased with increasing $\bar{A}$. However, the benefit increased at a declining rate due to the loss of incident light as the larger leaf sizes extend beyond the canopy light gap. The cost increased isometrically with $\bar{A}$ (shown) or steeper depending on the value of exponent β. The result was that cost surpassed benefit at some $\bar{A}$. Before this point, net gain (Fig 5.4A, black line) was positive and there was some $\bar{A}$ that maximized net gain for this particular n and light environment. As n increased, the locally optimal $\bar{A}$ stayed the same or decreased (Fig. 5.4B) and maximum net increased to a peak and then declined. The $\bar{A} : n : A_t$ trio that maximized net was the optimal combination for this light environment.

The model predicted that as canopies became more open with larger gaps (higher $\bar{\tau}_{c,min}$), the optimal $\bar{A}$ and A_t increased (Fig. 5.4C; see also Fig. 5.1C). The scaling exponent was determined from SMA regressions across these $\bar{A}$ and A_t optima. All $\bar{A}$ by A_t regressions had $r^2 > 0.86$ (mean = 0.98). The c_0 values that met our criteria of producing optimal $\bar{A} : n : A_t$ under at least 15 of 20 canopies were narrowly distributed from 2.6 to 10.1 when $c_1 = 1$. The c_0 had a relatively minor effect on the $\bar{A}$ by A_t exponent, causing an average variation of 0.14 across 32 different scenarios.

The $\bar{A}$ by A_t exponent depended on the self-shading within the twig. When twig self-shading was constant across all canopy structures, exponents were near 1, indicating a relatively constant n. This was true regardless of the degree of self-shading (f_t values; Fig. 5.5A,B). Increasing the leaf cost exponent, β, from 1 to 1.1 (larger leaves are more expensive) slightly steepened the $\bar{A}$ by A_t scaling (Fig. 5.5B, open circles).

When self-shading decreased with more open canopies (e.g., as illustrated in Fig. 5.1C,D), the $\bar{A}$ by A_t exponent fell below one (Fig. 5.5C-F). The steeper the decrease, the lower the exponent, especially when self shading decreased curvilinearly (vs. linearly). Exponents fell to the observed common value of 0.61 and below (see grey bar in Fig. 5.5D,F). Increasing the cost of larger leaves (changing β from 1 to 1.1) tended to decrease the exponent but only markedly so when self-shading decreased linearly with canopy openness (Fig. 5.5D).

Making cost/area a function of light absorption had negligible effect on $\bar{A}$ vs A_t exponents. When leaves absorbing the maximum amount of light cost twice as much ($a_3 = 1$ in Eqn. 5.7), mean exponents increased or decreased (maximum change = +0.003) in the scenario represented by closed circles in Fig. 5.5D. Increasing to $a_3 = 3$ (up to 4x greater cost) had essentially no additional effect. Greater maximum cost did, however, result in higher selected c_0 range to compensate.

5.5 Discussion

We recast Corner's rule (1949) as the prediction that larger leaves correlate positively with greater twig leaf area. Not only was this prediction supported within measured species, but the $\bar{A}$ vs A_t scaling exponents (b_1) were more convergent across species than the scaling of other twig properties. In the six study species, all b_1 values were significantly less than one and they clustered around 0.6, indicating specific coordination between $\bar{A}$ and leaf number. Furthermore, our model supported Corner's rule and provided an answer to the question: why do thick twigs not support small leaves? The answer is: given that thicker twigs are necessary to support the hydraulic and mechanical demands of greater A_t, partitioning that larger A_t into few, large leaves produces a better return on investment than many, small leaves.

The model predicted that exponent b_1 is a function of twig self-shading and leaf cost/area. When twig self-shading was constant across all modeled canopy structures, the model generally predicted b_1 at or near isometry (i.e., constant n; Fig. 5.5B). The tendency for constant n can be explained by the geometry of spiral phyllotaxy. When divergence between leaves is the exact golden angle, leaves will never perfectly overlap but once the leaves have covered one rotation, additional leaves fill increasingly small gaps left by the leaves above. When the potential benefit increases (via greater c_0 or a more open canopy with larger gaps) it is generally more beneficial to fill the gap by increasing $\bar{A}$ than it is to increase n. This results in nearly constant n and, therefore, $b_1 \approx 1$. Reducing twig self-shading under all canopies allowed more light to reach these lower leaves and favor greater n, but the effect was the same across environments, which maintained b_1 near isometry.

There was a tendency for the model to predict b_1 somewhat greater than 1 when twig self-shading was the same under all canopies (Fig. 5.5B). This corresponds to fewer, larger leaves in more open canopies. The reason for this is related to the rate of decline in available light away from the twig center (i.e., $\bar{\tau}_c$ in Eqn. 5.3, Fig. 5.1E,F). Suppose the most open canopy favors a particular $\bar{A} : n$ pair. This canopy has a gradual decline in $\bar{\tau}_c$ moving away

from the center of its large gaps (see Fig. 5.1E), so large $\bar{A}$ is favored over large n. For the closed canopy with smaller gaps, however, $\bar{\tau}_c$ drops quickly to its minimum (see Fig. 5.1F). This curve is likely steep enough to make increasing n more beneficial than increasing $\bar{A}$, resulting in more leaves in the closed vs open canopy and $b_1 > 1$. When larger leaves cost more per area (i.e., $\beta > 1$), b_1 became even steeper (see Fig. 5.5B). Increasing β from 1 to 1.1 favored more leaves under all canopies but more so under denser canopies. It is likely that the constraint on leaf size in low light leads these twigs to favor even more small leaves when they are cheaper.

Altering self-shading across canopy structures was necessary to favor $b_1 < 1$, as observed in the study species. Selectively reducing twig self-shading under more open canopies allowed these high light environments that already favor larger $\bar{A}$ to also favor greater n. Keeping self-shading high in closed canopies maintained smaller n with smaller $\bar{A}$. The exponent b_1 was further reduced when $\beta > 1$ (see Fig. 5.5D,F). Making larger leaves more expensive favors smaller $\bar{A}$ and greater n. This was especially true under more open canopies with low self-shading and large leaves. According to the model, our observed common exponent of $b_1 = 0.61$ should be associated with less self-shading in larger vs smaller twigs across all the study species, perhaps in combination with a greater specific cost of larger leaves. Although beyond the scope of the present study, this very specific hypothesis is testable with measurements of twig and canopy light distribution and specific leaf areas.

The traditional assessment of Corner rule ($\bar{A}$ vs d_t) produced much more varied exponents than $\bar{A}$ by A_t scaling. Interestingly, $\bar{A}$ by d_t exponents covaried with A_t by d_t exponents. The $\bar{A}$ by A_t exponent can be represented by how $\bar{A}$ and A_t scale with d_t. For example, in *Acer*, we observed $\bar{A} \propto d_t^{2.09}$ and $A_t \propto d_t^{3.54}$, making $\bar{A} \propto A_t^{0.59=2.09/3.54}$. This mathematical relationship makes it apparent that although $\bar{A}$ by d_t and A_t by d_t scaling exponents seemed to vary widely (1.28 to 2.32 and 1.94 to 3.94, respectively), their ratios remained around 0.6. This apparent coordination to produce $b_1 \approx 0.6$ supports our hypothesis that $\bar{A}$ vs A_t scaling is more fundamental to Corner's rule than the scaling of either leaf area with twig size.

Our data only represent species from one functional type and one environment. Additional studies will reveal if other functional groups in other environments share an $\bar{A}$ vs A_t exponent and whether it equals 0.6 or varies systematically and with light environment as predicted by our model. We were unable to find any other study that reported $\bar{A}$ by A_t scaling intraspecifically. It seems that this more fundamental basis for Corner's rule has

been largely overlooked.

We did find a single intraspecific study, however, where we could deduce $\bar{A}$ by A_t scaling from the reported SMA scaling of both areas with d_t^2. Preston & Ackerly (2003) reported individual A_t by d_t^2 exponents and a common $\bar{A}$ by d_t^2 exponent for 12 California species from three genera and contrasting environments. From these data, we calculated b_1 between 0.64 to 0.90 (mean = 0.76) with steeper slopes slightly favored by xeric (vs mesic) species. All of these exponents fall within the range predicted by the model, but it is difficult to infer how the canopy light environment varied across these species.

There are several interspecific studies where $\bar{A}$ by A_t scaling could be deduced by the same approach or from reported $\bar{A}$ and A_t species means. These data are difficult to interpret because as our study demonstrated, the a_1 multiplier can vary across species causing inter- and intraspecific exponents to differ. Similar inter- vs. intraspecific discrepancies in leaf scaling were found by Dombroskie & Aarssen (2012). Nevertheless, many of these interspecific inferences are broadly consistent with the trends suggested by our model. Data from White (1983a) indicate b_1 was steeper among shade-tolerant species ($b_1 = 1.33$) where denser canopies could reduce variation in self-shading, than among intermediate (1.05) and intolerant (0.85) species where self-shading could be more variable. White's (1983b) other study was consistent with a markedly steeper scaling in evergreen angiosperms ($b_1 = 1.14$), whose broader leaves may cause more consistent self-shading than the needle leaves of evergreen gymnosperms ($b_1 = 0.68$). Falster & Westoby's (2003) data also indicate steeper scaling under higher leaf cover ($b_1 = 1.53$) vs low (1.37), but the difference was not significant. Other interspecific studies were less obviously relatable to light environments (Westoby & Wright 2003; Yang *et al.* 2009; Liu *et al.* 2010). Interspecific SMA exponents are likely to be steeper than intraspecific ones because of lower r values that result from differing a_1 multipliers. As in our study, the interspecific data tended to show more variation in $\bar{A}$ by d_t and A_t by d_t exponents than in b_1.

The model results were encouraging and suggestive that optimizing the investment in leaves, as we have defined it, is an important control on leaf size and number. However, the model could be extended to broaden its applicability. The model consistently predicts larger leaves in larger gaps, a trend that ignores potential energy-balance problems of large leaves in too much light (Givnish 1987; Long *et al.* 1994). Furthermore, the assumption that twigs always target light gaps biases the analysis towards twigs growing into the canopy periphery, or growing in relatively open canopies (typical "sun" leaves). Hence, the model fails to predict the general observation of larger "shade" leaves found in the more uniform

shade beneath dense canopies (Sack *et al.* 2003, 2006; Nardini *et al.* 2012) and across species (Niinemets & Kull 1994; Bragg & Westoby 2002). Running the model for uniform light does increase optimal leaf size (not shown); and adding energy-balance penalties would extend the model to the qualitative differences in light environments of classic "sun" vs "shade" leaves (Hanson 1917; Sack *et al.* 2006). Additionally, the model as applied here does not predict changes in leaf size across environments with contrasting water supply or soil fertility (Givnish 1987; Cunningham *et al.* 1999). These shortcomings could specifically be addressed by extending the model to more explicitly define multipliers c_0 and c_1 in terms of structural and physiological characteristics of leaves.

We have identified a fundamental corollary of Corner's rule that is supported empirically and theoretically. The specific predictions of the economics model are eminently testable, because the driving variables of canopy openness and twig self-shading (Figs. 5.1,5.5) can be measured with arrays of light sensors within twigs and canopies. The simplicity of the question and the minimal data requirements should inspire further evaluation of why thick twigs should support large leaves.

5.6 Acknowledgements

Jon Seger provided input that led to the economics model concept. David Love assisted with data collection in 2011. Duncan D. Smith and John S. Sperry were supported by NSF IBN-0743148.

5.7 References

Bragg, J.G. & Westoby, M. (2002). Leaf size and foraging for light in a sclerophyll woodland. *Functional Ecology*, 16, 633–639.

Brouat, C., Gibernau, M., Amsellem, L. & McKey, D. (1998). Corner's rules revisited: ontogenetic and interspecific patterns in leaf-stem allometry. *New Phytologist*, 139, 459–470.

Corner, E.J.H. (1949). The durian theory of the origin of the modern tree. *Annals of Botany*, 13, 368–414.

Cunningham, S.A., Summerhayes, B. & Westoby, M. (1999). Evolutionary divergences in leaf structure and chemistry, comparing rainfall and soil nutrient gradients. *Ecological Monographs*, 69, 569–588.

Dombroskie, S.L. & Aarssen, L.W. (2012). The leaf size/number trade-off within species and within plants for woody angiosperms. *Plant Ecology and Evolution*, 145, 38–45.

Eloy, C. (2011). Leonardo's rule, self-similarity, and wind-induced stresses in trees. *Physical Review Letters*, 107, 1–5.

Evans, J.R. & Poorter, H. (2001). Photosynthetic acclimation of plants to growth irradiance: the relative importance of specific leaf area and nitrogen partitioning in maximizing carbon gain. *Plant, Cell and Environment*, 24, 755–767.

Falster, D.S. & Westoby, M. (2003). Leaf size and angle vary widely across species: what consequences for light interception? *New Phytologist*, 158, 509–525.

Farnsworth, K.D. & Van Gardingen, P.R. (1995). Allometric analysis of Sitka spruce branches: mechanical versus hydraulic design principles. *Trees - Structure and Function*, 10, 1–12.

Givnish, T.J. (1987). Comparative studies of leaf form: assessing the relative roles of selective pressures and phylogenetic constraints. *New Phytologist*, 106, 131–160.

Hanson, H.C. (1917). Leaf-structure as related to environment. *American Journal of Botany*, 4, 533–560.

Heusner, A.A. (1982). Energy and metabolism I. Is the 0.75 mass exponent of Kleiber's equation a statistical artifact? *Respiration Physiology*, 48, 1–12.

Judd, W.S., Campbell, C.S., Kellogg, E.A., Stevens, P.F. & Donoghue, M.J. (2008). *Plant Systematics: a Phylogenetic Approach*. 3rd edn., Sinauer Associates, Inc., Massachusetts, MA.

Liu, Z., Cai, Y., Li, K. & Guo, J. (2010). The leaf size-twig size spectrum in evergreen broadleaved forest of subtropical China. *African Journal of Biotechnology*, 9, 3382–3387.

Long, S.P., Humphries, S. & Falkowski, P.G. (1994). Photoinhibition of photosynthesis in nature. *Annual Review of Plant Physiology and Plant Molecular Biology*, 45, 633–662.

McMahon, T.A. & Kronauer, R.E. (1976). Tree structures: deducing the principle of mechanical design. *Journal of Theoretical Biology*, 59, 443–466.

Milla, R. & Reich, P.B. (2007). The scaling of leaf area and mass: the cost of light interception increases with leaf size. *Proceedings of the Royal Society B: Biological Sciences*, 274, 2109–2114.

Nardini, A., Pedá, G. & Salleo, S. (2012). Alternative methods for scaling leaf hydraulic conductance offer new insights into the structure-function relationships of sun and shade leaves. *Functional Plant Biology*, 39, 394–401.

Niinemets, Ü., Keenan, T.F. & Hallik, L. (2015). A worldwide analysis of within-canopy variations in leaf structural, chemical and physiological traits across plant functional types. *New Phytologist*, 205, 973–993.

Niinemets, Ü. & Kull, K. (1994). Leaf weight per area and leaf size of 85 Estonian woody species in relation to shade tolerance and light availability. *Forest Ecology and Management*, 70, 1–10.

Niinemets, Ü., Portsmuth, A., Tena, D., Tobias, M., Matesanz, S. & Valladares, F. (2007). Do we underestimate the importance of leaf size in plant economics? Disproportional scaling of support costs within the spectrum of leaf physiognomy. *Annals of Botany*, 100, 283–303.

Olson, M.E., Aguirre-Hernández, R. & Rosell, J.A. (2009). Universal foliage-stem scaling across environments and species in dicot trees: plasticity, biomechanics and corner's rules. *Ecology Letters*, 12, 210–219.

Posada, J.M., Lechowicz, M.J. & Kitajima, K. (2009). Optimal photosynthetic use of light by tropical tree crowns achieved by adjustment of individual leaf angles and nitrogen content. *Annals of Botany*, 103, 795–805.

Preston, K.A. & Ackerly, D.D. (2003). Hydraulic architecture and the evolution of shoot allometry in contrasting climates. *American Journal of Botany*, 90, 1502–1512.

R Core Team (2014). *R: A Language and Environment for Statistical Computing*. R Foundation for Statistical Computing, Vienna, Austria, URL http://www.R-project.org/.

Sack, L., Cowan, P.D., Jaikumar, N. & Holbrook, N.M. (2003). The 'hydrology' of leaves: co-ordination of structure and function in temperate woody species. *Plant, Cell and Environment*, 26, 1343–1356.

Sack, L., Melcher, P.J., Liu, W.H., Middleton, E. & Pardee, T. (2006). How strong is intracanopy leaf plasticity in temperate deciduous trees? *American Journal of Botany*, 93, 829–839.

Smith, D.D. & Sperry, J.S. (2014). Coordination between water transport capacity, biomass growth, metabolic scaling and species stature in co-occurring shrub and tree species. *Plant, Cell and Environment*, 37, 2679–2690.

Sone, K., Suzuki, A.A., Miyazawa, S., Noguchi, K. & Terashima, I. (2009). Maintenance mechanisms of the pipe model relationship and Leonardo da Vinci's rule in the branching architecture of *Acer rufinerve* trees. *Journal of Plant Research*, 122, 41–52.

Villar, R. & Merino, J. (2001). Comparison of leaf construction costs in woody species with differing leaf life-spans in contrasting ecosystems. *New Phytologist*, 151, 213–226.

Warton, D.I., Duursma, R.A., Falster, D.S. & Taskinen, S. (2012). smatr 3 — an r package for estimation and inference about allometric lines. *Methods in Ecology and Evolution*, 3, 257–259.

Westoby, M. & Wright, I.J. (2003). The leaf size — twig size spectrum and its relationship to other important spectra of variation among species. *Oecologia*, 135, 621–628.

White, P.S. (1983a). Corner's rules in eastern deciduous trees: allometry and its implications for the adaptive architecture of trees. *Bulletin — Torrey Botanical Club*, 110, 203–212.

White, P.S. (1983b). Evidence that temperate east North American evergreen woody plants follow Corner's rules. *New Phytologist*, 95, 139–145.

Wright, I.J., Falster, D.S., Pickup, M. & Westoby, M. (2006). Cross-species patterns in the coordination between leaf and stem traits, and their implications for plant hydraulics. *Physiologia Plantarum*, 127, 445–456.

Yang, D., Li, G. & Sun, S. (2009). The effects of leaf size, leaf habit, and leaf form on leaf/stem relationships in plant twigs of temperate woody species. *Journal of Vegetation Science*, 20, 359–366.

Yang, X., Yan, E., Chang, S.X., Wang, X., Zhao, Y. & Shi, Q. (2014). Twig-leaf size relationships in woody plants vary intraspecifically along a soil moisture gradient. *Acta Oecologica*, 60, 17–25.

Table 5.1. SMA regressions between all measured twig structure parameters in each species and results from common exponent tests. Table sorted by test p-value. Pairwise differences were evaluated using p=0.05 as a threshold for adjusted p-values. Note that adjusting pairwise p-values leads to a discrepancy between the common exponent test and pairwise differences in $\bar{A}$ vs A_t. Units: areas in cm^2; diameters in mm; lengths in cm.

y	x	SMA coef.	*Acer grand.*	*Amel. alnifolia*	*Betula occidentalis*	*Cornus sericea*	*Populus fremontii*	*Symphor. oreophilus*	common exp p-value	pairwise differences
$\bar{A}$	A_t	mult	1.69	0.89	1.33	0.88	1.18	0.26		
		exp	0.59	0.65	0.59	0.60	0.56	0.66	0.072	0
$\bar{A}$	n	mult	5.43	1.52	3.78	1.68	2.26	0.061		
		exp	1.13	1.35	0.91	1.09	1.08	1.46	0.005	2
A_t	n	mult	7.21	2.26	5.84	2.93	3.15	0.11		
		exp	1.91	2.08	1.53	1.81	1.90	2.21	5.6e-4	2
$\bar{A}$	l_t	mult	15.3	7.99	8.58	4.27	7.86	0.73		
		exp	0.51	0.42	0.35	0.54	0.61	0.54	4.6e-5	4
$\bar{A}$	d_t	mult	4.37	4.11	2.58	4.49	2.87	1.51		
		exp	2.09	1.71	2.32	1.60	1.67	1.28	1.8e-7	5
n	l_t	mult	2.51	3.41	2.48	2.35	3.19	5.48		
		exp	0.45	0.31	0.39	0.49	0.57	0.37	8.8e-13	6
A_t	l_t	mult	41.6	29.1	23.5	13.8	28.6	4.76		
		exp	0.87	0.64	0.60	0.89	1.08	0.83	6.1e-13	9
A_t	d_t	mult	4.99	10.4	3.06	14.9	4.80	14.3		
		exp	3.54	2.63	3.94	2.66	2.96	1.94	4.4e-16	8
n	d_t	mult	0.82	2.08	0.66	2.45	1.25	9.02		
		exp	1.86	1.26	2.57	1.47	1.56	0.88	0	9
l_t	d_t	mult	0.087	0.20	0.033	1.09	0.19	3.81		
		exp	4.09	4.09	6.62	2.97	2.73	2.36	0	10

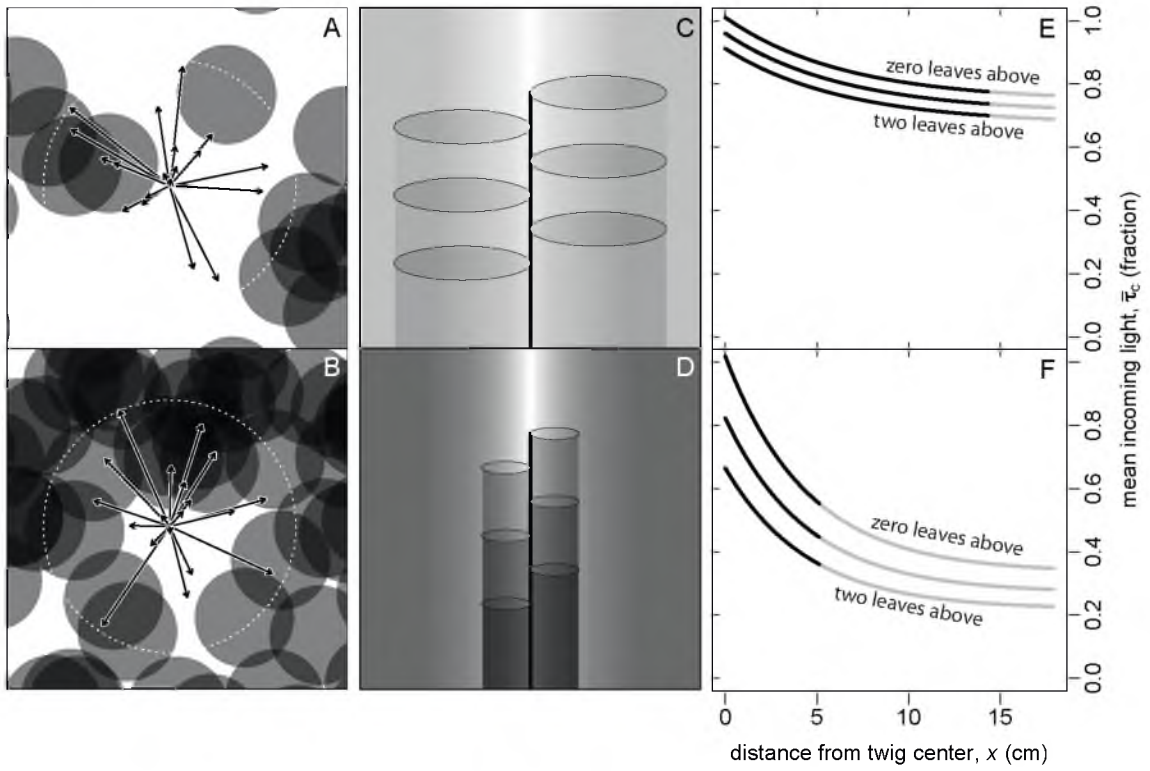

Figure 5.1. Key components of the light interception model illustrated by an open canopy with low self-shading (top row) and a denser canopy with higher self-shading. The incoming light environment was modeled as randomly placed leaves at different densities (**A-B**). Light gaps were quantified from incoming light in random directions at distances from points with high light (arrows) up to the maximum leaf length (dotted white circles). Under these canopies, mean incoming light decreased exponentially with distance from highest light (see horizontal gradients in **C-D** and "zero leaves" curves in **E-F**). Twig self-shading reduced available light to leaves lower on the twig and the amount of reduction was a function of canopy openness (see vertical gradients in **C-D** and "leaves above" curves in **E-F**). Curves in **E-F** indicate available light to three uppermost leaves; black portions correspond to optimal leaf size. For illustration, curves reflect perfect leaf overlap.

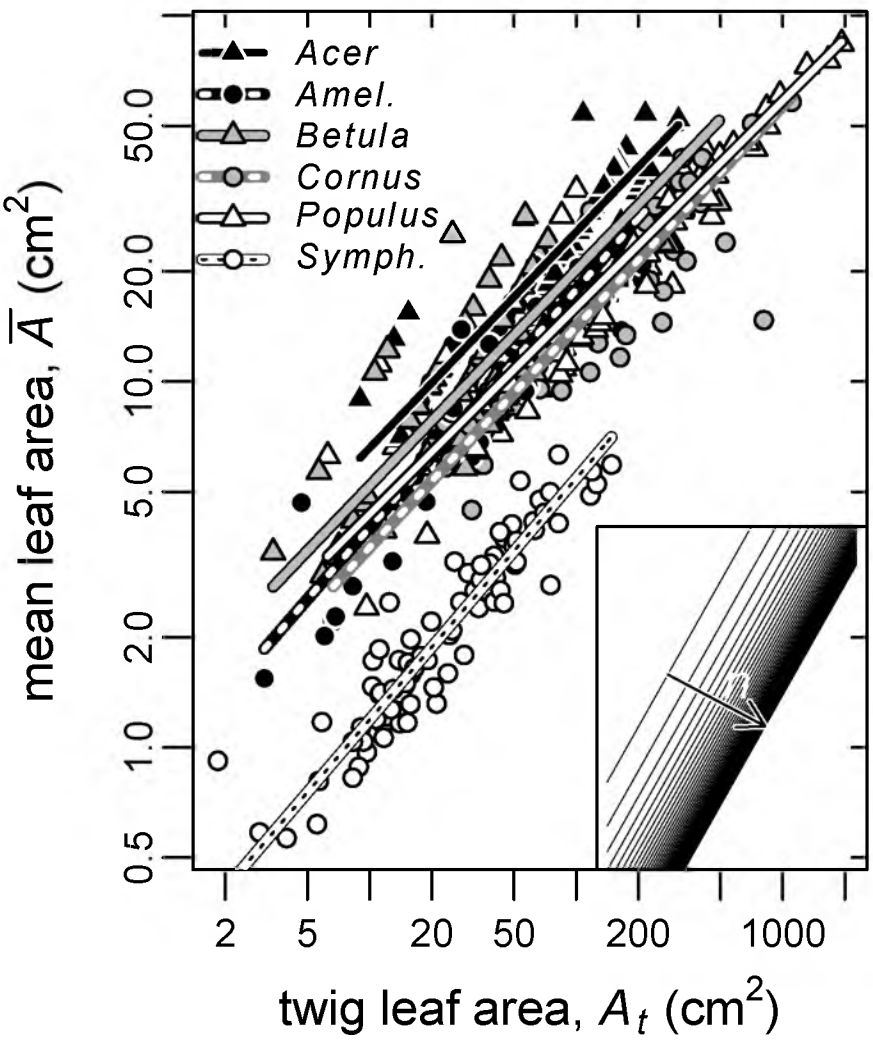

Figure 5.2. Mean vs twig leaf area ($\bar{A}$ vs A_t) relationships. SMA scaling exponents were very similar across species and all less than isometric. Scaling coefficients given in Table 5.1. Inset shows iso-n lines, which correspond to $\bar{A}$ vs A_t isometry. Triangles correspond to trees and circles to shrubs.

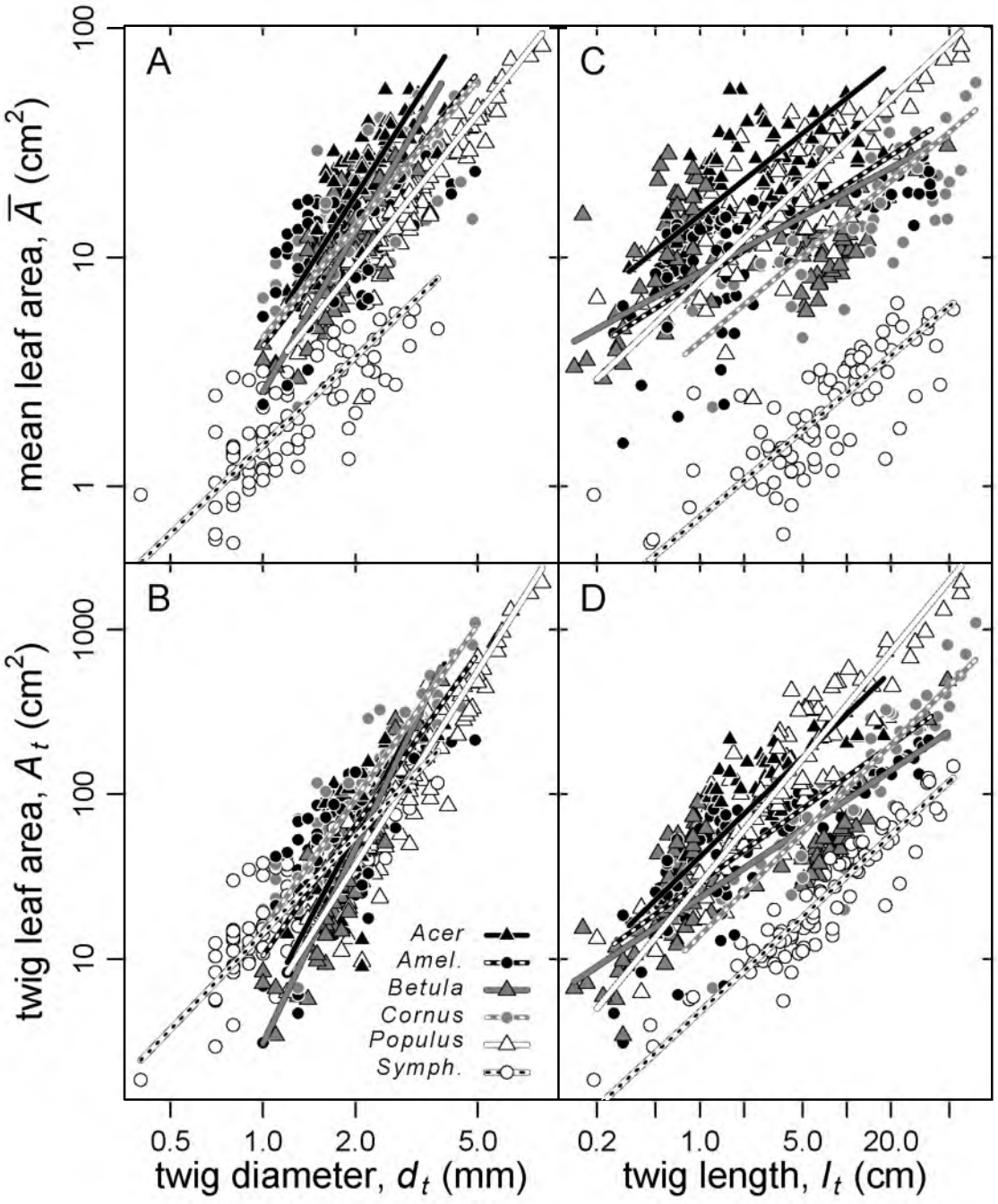

Figure 5.3. Mean leaf area and twig leaf area were well correlated with twig diameter and length within species. However, the SMA regressions (shown) had very different exponents. Scaling coefficients and common exponent tests in Table 5.1. Triangles indicate tree species. Circles are shrubs.

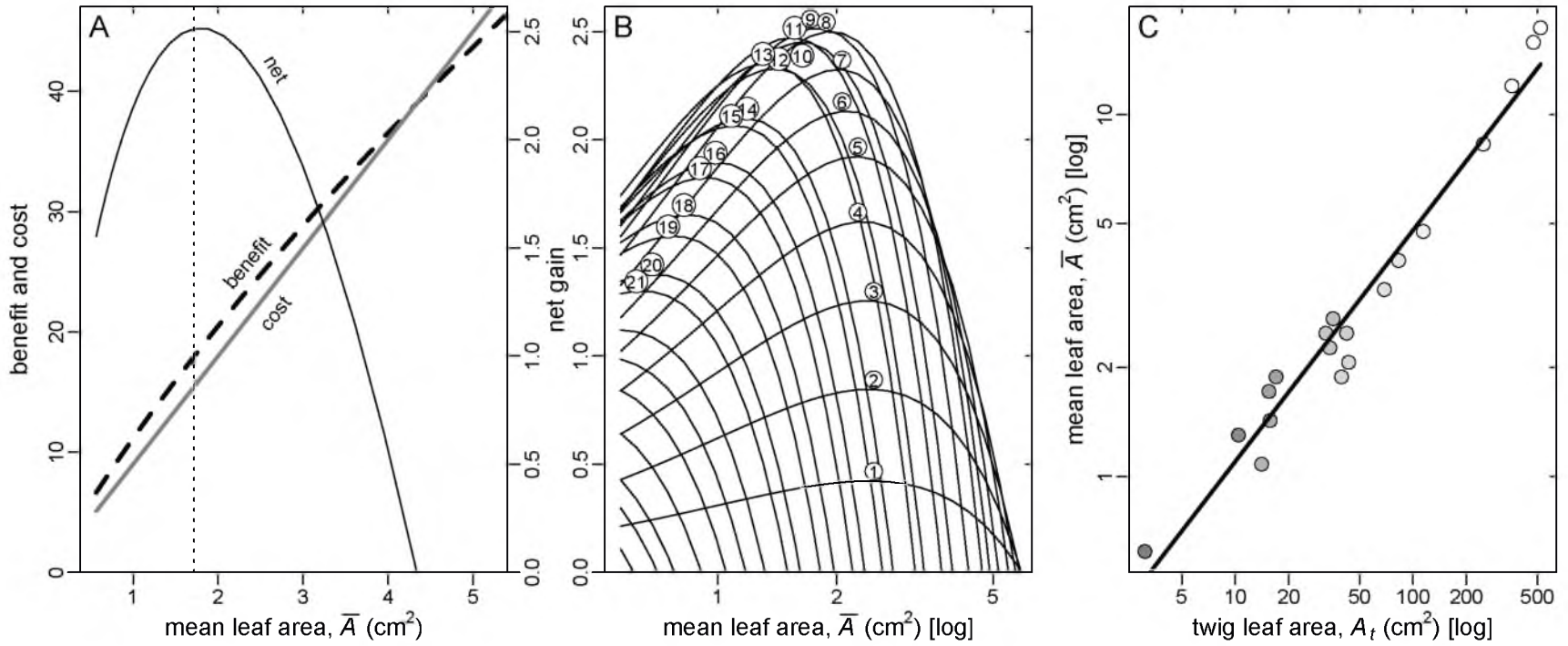

Figure 5.4. Example of optimal $\bar{A}$, n and A_t selection and $\bar{A}$ vs A_t scaling. **A**: With constant twig leaf number ($n = 9$) and increasing mean leaf area, the total benefit (dashed line) increases faster and then slower than total cost (grey line), leading to an optimal $\bar{A}$ (vertical line) which maximizes net gain (solid black line). Shown are model data for twigs under a canopy with $\overline{\mathrm{LAI}} = 3.8$, $f_t = 24\%$, $c_0 = 3.1$, and $\beta = 1$. **B**: For increasing n (numbers at peaks) each n has an optimal $\bar{A}$ and across n there is an optimal $\bar{A} : n$ pair ($1.7 : 9$, here). Model conditions as above. **C**: The optimal $\bar{A}$ and n (and hence A_t) increased with increasing canopy openness (lighter symbol shades denote greater openness). Model conditions as above but twig self-shading varied curvilinearly from $f_{t,open} = 0.05$ to $f_{t,closed} = 0.5$, which produced $b_1 = 0.64$.

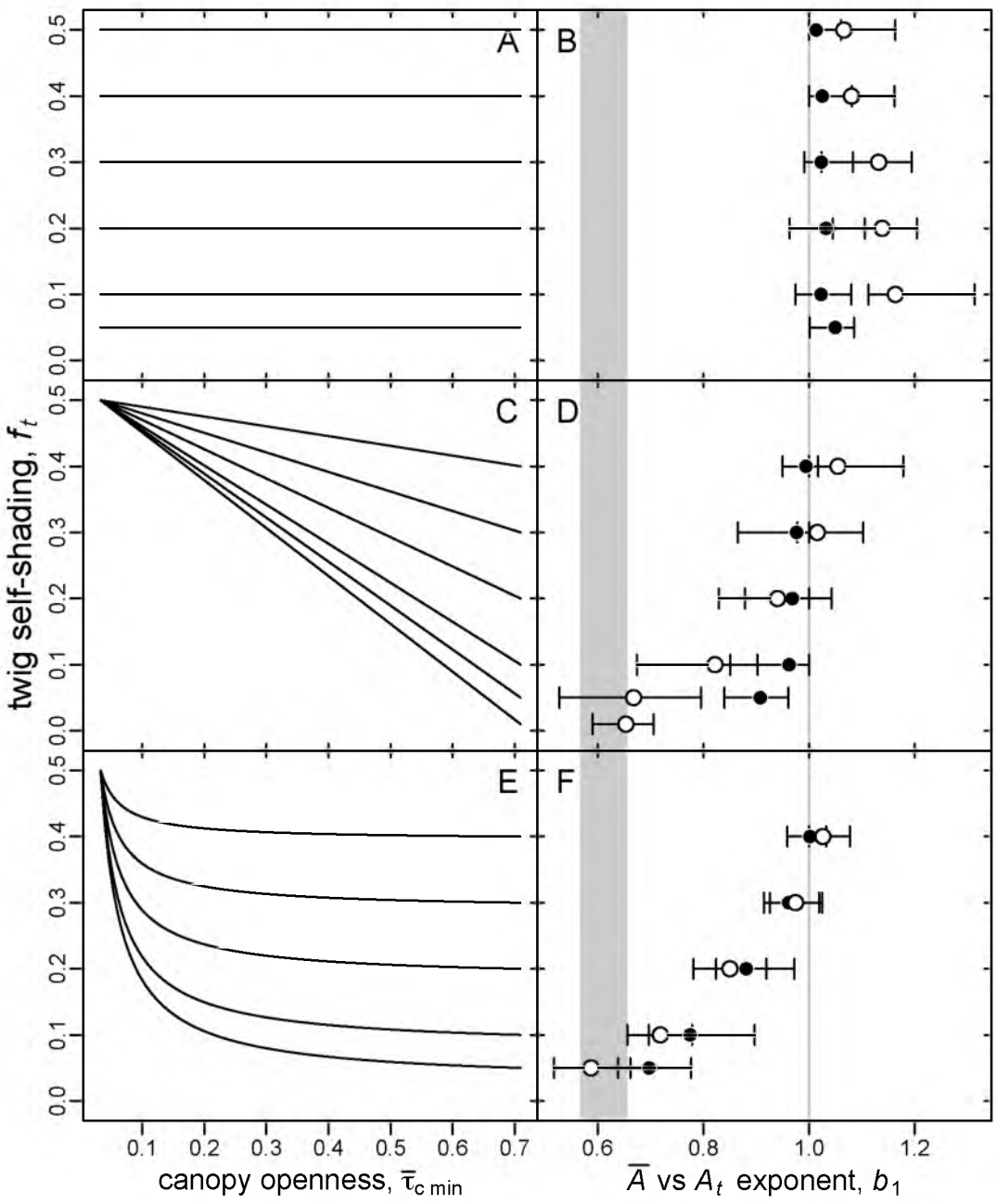

Figure 5.5. Self-shading vs canopy openness scenarios (**A**, **C**, **E**) next to corresponding $\bar{A}$ vs A_t scaling exponents (**B**, **D**, **F**). Symbols = mean; bars = range. Exponents shown relative to isometry (grey line) and the observed range (grey bar). Leaf cost per area was either constant ($\beta = 1$; closed circles) or increased with size ($\beta = 1.1$; open circles). Constant self-shading across canopies (**A**) generally produced exponents at or above one (**B**). Selectively reducing self-shading either linearly (**C**) or curvilinearly (**E**) in more open canopies was necessary to predict the observed exponents (**D** and **F**).